Forest-atmosphere exchange of reactive nitrogen in a low polluted area – Part I: Measuring temporal dynamics ~~and annual budgets~~

Pascal Wintjen[1], Frederik Schrader[1], Martijn Schaap[2,3], Burkhard Beudert[4], and Christian Brümmer[1]

[1]Thünen Institute of Climate-Smart Agriculture, Bundesallee 68, 38116, Braunschweig, Germany
[2]TNO, Climate Air and Sustainability, Utrecht, 3584 CB, ~~t~~The Netherlands
[3]Institute of Meteorology, Freie Universität Berlin, 12165 Berlin, Germany
[4]Bavarian Forest National Park, 94481, Grafenau, Germany

Correspondence: Pascal Wintjen (pascal.wintjen@thuenen.de)

Abstract. ~~Accurate modeling of nitrogen deposition is essential for identifying exceedances of critical loads and designing effective mitigation strategies. However, there are still uncertainties in modern deposition routines due to a limited availability of long-term flux measurements of reactive nitrogen compounds for model development and validation.~~ Understanding the biosphere-atmosphere exchange characteristics of nitrogen is essential for the parameterization of modern deposition routines. For investigating temporal dynamics and responses of reactive nitrogen compounds to micrometeorology and biophysical factors, long-term flux measurements are needed. In this study, we investigate ~~the performance of dry deposition inferential models with regard to annual budgets and~~ the exchange patterns of total reactive nitrogen (ΣN_r) and determine annual dry deposition budgets based on measured data at a low-polluted mixed forest located in the Bavarian Forest National Park (NPBW), Germany. Flux measurements of ΣN_r were carried out with a Total Reactive Atmospheric Nitrogen Converter (TRANC) coupled to a chemiluminescence dectector (CLD) for 2.5 years.

The average ΣN_r concentration was ~~approximately 5.2 ppb~~ 3.1 μg N m^{-3}. Denuder measurements with DELTA samplers and chemiluminescence measurements of nitrogen oxides (NO_x) have shown that NO_x has the highest contribution to ΣN_r ($\sim$ 521%), followed by ammonia (NH_3) ($\sim$ 221%), ammonium (NH_4^+) ($\sim$ 145%), nitrate NO_3^- ($\sim$ 7%), and nitric acid (HNO_3) ($\sim$ 6%). Only slight seasonal changes were found in the ΣN_r concentration level whereas a seasonal pattern was observed for NH_3 and NO_x. NH_3 showed highest contributions to ΣN_r in spring and summer, NO_x in autumn and winter.

We observed mostly deposition fluxes at the measurement site with median fluxes ranging from -15 ~~ng N m^{-2} s^{-1}~~ to -5 ng N m^{-2} s^{-1} (negative fluxes indicate deposition). Median deposition velocities ranged from 0.2 to 0.5 cm s^{-1}. In general, highest deposition velocities ~~was~~ were recorded during high incident radiation, in particular from May to September. ~~ΣN_r deposition was enhanced by higher temperatures, lower relative humidity, high ΣN_r concentration, and dry leaf surfaces.~~ Our results suggest that seasonal changes in concentrations of the ΣN_r compounds and radiation were most likely influencing the deposition velocity (v_d). ~~dry conditions seem to favour nitrogen dry deposition at natural ecosystems.~~ We found that from May to September higher temperatures, lower relative humidity, dry leaf surfaces, and no precipitation increase v_d. The effective canopy resistance ($R_{c,eff}$) was slightly lower at low relative humidity and higher ΣN_r concentrations. Aerodynamic (R_a) and boundary-layer resistance (R_b) showed a negligible contribution to v_d in comparison to $R_{c,eff}$ highlighting the importance of

the surface resistance to the uptake of ΣN_r. Presumably, stomatal uptake seemed to be most responsible for ΣN_r during those months.

During rain and in periods of lower radiation, v_d was significantly lower and sometimes even negative indicating emission phases of ΣN_r. In those times, $R_{c,eff}$ increased, and R_a and R_b were in same order of magnitude as $R_{c,eff}$, and thus atmospheric resistances seemed to be as important as the surface resistance for the ΣN_r exchange. In periods of lower radiation and rain, cuticular or soil processes appeared to be relevant for the ΣN_r exchange.

~~For determining annual dry deposition budgets we used the bidirectional inferential scheme DEPAC (DEPosition of Acidifying Compounds) with locally measured input parameters, called DEPAC-1D, as gap-filling strategy for TRANC measurements. In a second approach, the mean-diurnal-variation method (MDV) was applied to gaps of up to five days whereas DEPAC-1D was used for remaining gaps. We compared them to results from the chemical transport model LOTOS-EUROS (LOng Term Ozone Simulation – EURopean Operational Smog) v2.0 and from the canopy budget technique conducted at the measurement site. After 2.5 years, dry deposition based on TRANC measurements resulted in (11.1 ± 3.4) kg N ha^{-1} with DEPAC-1D as gap-filling method and (10.9 ± 3.8) kg N ha^{-1} with MDV and DEPAC-1D as gap-filling methods. Both values are close to dry deposition by DEPAC-1D (13.6 kg N ha^{-1}) considering the uncertainties of measured fluxes and possible uncertainty sources of DEPAC-1D. The difference of DEPAC-1D to TRANC can be related to parameterizations of reactive gases or the missing exchange path with soil. 16.8 kg N ha^{-1} deposition were calculated by LOTOS-EUROS for considering land-use class weighting. We further showed that predicted NH_3 concentrations, an input parameter of LOTOS-EUROS, were the main reason for the discrepancy in dry deposition budgets between the different methods. On average, annual TRANC dry deposition was 4.5 kg N ha^{-1} a^{-1} for both gap-filling approaches, DEPAC-1D showed 5.3 kg N ha^{-1} a^{-1}, and LOTOS-EUROS modeled 5.2 kg N ha^{-1} a^{-1} to 6.9 kg N ha^{-1} a^{-1} depending on the weighting of land-use classes within the site's grid cell. 7.5 kg N ha^{-1} a^{-1} was estimated with the canopy budget technique for the period from 2016 to 2018 as upper estimate and 4.6 kg N ha^{-1} a^{-1} as lower estimate.~~

No significant influence of temperature, humidity, friction velocity, or precipitation on ΣN_r dry deposition sums were found with differences between deposition estimates being within their uncertainty ranges. We used the Mean-Diurnal-Variation (MDV) approach for filling gaps of up to five days. Remaining gaps were replaced by a monthly average of the specific half-hour value. From June 2016 to May 2017 and June 2017 to May 2018, we estimated dry deposition sums of 3.8 ± 0.8 kg N ha^{-1} and 4.1 ± 1.1 kg N ha^{-1}, respectively. Mean total wet depositions were 8.0 kg N ha^{-1} and 6.8 kg N ha^{-1} for the timeframes 2016/2017 and 2017/2018, respectively. Adding results from the wet deposition measurements to the measurement years, we determined 11.8 kg N ha^{-1} and 10.9 kg N ha^{-1} as total nitrogen deposition, respectively.

Our findings provide a better understanding of exchange dynamics at low-polluted, natural ecosystems ~~and show~~ , thereby providing opportunities for further development of deposition models.

1 Introduction

Reactive nitrogen (N_r) compounds are essential nutrients for plants. However, an intensive supply of nitrogen by fertilisation or atmospheric deposition is harmful for natural ecosystems and leads to a loss of biodiversity through soil acidification and eutrophication (Krupa, 2003; Galloway et al., 2003) and may also threaten human health by acting as precoursors for ozone (O_3) and PM2.5 ~~(Krupa, 2003; Galloway et al., 2003)~~ (Erisman et al., 2013). Atmospheric nitrogen load increased significantly during the last century due to intensive crop production and livestock farming (Sutton et al., 2011; Flechard et al., 2011, 2013; Sutton et al., 2013) (mainly through ammonia) and fossil fuel combustion by traffic and industry (mainly through nitrogen dioxide and nitrogen oxide). The additional amount of N_r enhances biosphere-atmosphere exchange of N_r (Flechard et al., 2011), affects plant health (Sutton et al., 2011) and influences the carbon sequestration of ecosystems such as forests (Magnani et al., 2007; Högberg, 2007; Sutton et al., 2008; Flechard et al., 2020), although the impact of increasing nitrogen deposition on forests carbon sequestration is still under investigation.

For estimating the biosphere-atmosphere exchange of N_r compounds such as nitrogen monoxide (NO), nitrogen dioxide (NO_2), ammonia (NH_3), nitrous acid (HONO), nitric acid (HNO_3) and particulate ammonium nitrate (NH_4NO_3), the eddy-covariance (EC) approach has proven its applicability on various ecosystems. The sum of these compounds is called total reactive nitrogen (ΣN_r) throughout this manuscript. For evaluating fluxes of NO and NO_2 the EC technique has been tested in earlier studies (Delany et al., 1986; Eugster and Hesterberg, 1996; Civerolo and Dickerson, 1998; Li et al., 1997; Rummel et al., 2002; Horii et al., 2004; Stella et al., 2013; Min et al., 2014). In recent years, progress has been made in EC measurements of NH_3 (Famulari et al., 2004; Whitehead et al., 2008; Ferrara et al., 2012; Zöll et al., 2016; Moravek et al., 2019). First attempts in applying EC had been made on HNO_3, organic nitrogen molecules, nitrate (NO_3^-), and ammonium aerosols (NH_4^+) (Farmer et al., 2006; Nemitz et al., 2008; Farmer and Cohen, 2008; Farmer et al., 2011). Due to typically low concentrations, high reactivity, and water solubility, measuring fluxes of N_r compounds is still challenging since instruments need a low detection limit and a response time of $< 1\,s$ (Ammann et al., 2012). Thus, fast-response instruments for measuring N_r compounds like HNO_3 or NH_3 are equipped with a special inlet and short heated tubes to prevent interaction with tube walls (see Farmer et al., 2006; Zöll et al., 2016). However, these instruments need regular maintenance, have a high power consumption, and need a climate controlled environment for a stable performance. Considering the high technical requirements of these instruments, measuring fluxes of HNO_3 or NH_3 with these instrument is still challenging.

The Total Reactive Atmospheric Nitrogen Converter (TRANC) (Marx et al., 2012) converts all above mentioned N_r compounds to NO. In combination with a fast-response chemiluminescence detector (CLD), the system allows measurements of ΣN_r with a high sampling frequency. Due to a low detection limit and a response time of about 0.3 s, the TRANC-CLD system can be used for flux calculation based on the eddy-covariance (EC) technique. The TRANC-CLD system has been shown to be suitable for EC measurements above a number of different ecosystems (see Ammann et al., 2012; Brümmer et al., 2013; Zöll et al., 2019; Wintjen et al., 2020).

~~Most of the mentioned~~ Prior EC studies ~~about~~of ΣN_r or its compounds were carried out above managed field sites or close to agricultural or industrial emission hotspots, in order to focus on measuring the impact of environmental pollution or

fertilization on (crop) plants. Only a few studies were conducted at remote locations, but were mainly focusing only on single N_r compounds (e.g., Wyers and Erisman, 1998; Horii et al., 2004, 2006; Wolff et al., 2010; Min et al., 2014; Geddes and Murphy, 2014; Hansen et al., 2015). At remote sites, concentrations of reactive N_r compounds are typically low and close to the detection limit of the deployed instruments. Zöll et al. (2019) demonstrated that the TRANC-CLD system is able to detect concentrations and fluctuations of ΣN_r accurately even at low ambient levels ~~concentrations of air pollutants~~. It was the first study presenting short-term flux measurements of ΣN_r ~~at that site~~ conducted with the same instrumentation at the measurement site with a focus on establishing a link between the drivers of both ΣN_r and CO_2. ~~For a reliable prediction of ΣN_r fluxes and annual budgets through the use of dry deposition (inferential) models, long-term flux measurements are needed to verify the background nitrogen load and examine natural exchange characteristics at low concentrations of N_r compounds. Therefore, flux measurements at remote locations are required to improve deposition models and increase knowledge about the exchange behaviour of ΣN_r under various environmental conditions.~~ The authors identified incident radiation as primary driver for ΣN_r and CO_2 fluxes. Investigations on light response curves exhibited a reversal point for ΣN_r highlighting the existence of a canopy compensation point. The overall concentration of ΣN_r was identified as secondary driver for the ΣN_r exchange showing that processes affecting the physical and chemical properties of ΣN_r are more relevant than other micrometeorological drivers for the ΣN_r fluxes. Further analyses on deposition velocities and corresponding aerodynamic, boundary layer, and canopy resistances of ΣN_r allow to examine if the exchange is driven by turbulent or canopy processes. These investigations were formerly made for individual components of ΣN_r. For example, Wolff et al. (2010) found that aerosol fluxes of total ammonium and total nitrate were driven by aerodynamic processes. NH_3 features bidirectional exchange through stomata and cuticles (e.g., Farquhar et al., 1980; Sutton et al., 1995, 1998; Wyers and Erisman, 1998; Flechard et al., 1999; Milford et al., 2001; Nemitz et al., 2001; van Zanten et al., 2010; Wichink Kruit et al., 2010, 2017). NO_2 exhibits mainly stomatal and insignificant cuticular deposition (e.g., Rondon et al., 1993; Alberto Rondón and Granat, 1994; Thoene et al., 1991, 1996; Gessler et al., 2000, 2002; Sparks et al., 2001; Teklemmariam and Sparks, 2006; I.G. Chaparro-Suarez et al., 2011; Breuninger et al., 2013; Stella et al., 2013) whereas NO emissions are driven by soil microbial activities, which are influenced by soil temperature, soil moisture, and soil nitrogen (e.g., A. Remde et al., 1989; Remde and Conrad, 1993; David Fowler et al., 1998; Ludwig et al., 2001; Schindlbacher et al., 2004; Behrendt et al., 2014; Medinets et al., 2016). Since N_r species exhibit an interannual variability and various reaction pathways, the exchange mechanisms of ΣN_r change through the seasons. With the availability of long-term flux measurements at a remote location, we were able to investigate seasonal changes in deposition velocities and resistances at low concentrations of ΣN_r and its components. An evaluation could be important for inferential deposition models in order to validate bidirectional resistance schemes.

During a measurement campaign instrumental performance issues and/or periods of insufficient turbulence arise, which require a quality flagging of processed fluxes. Afterwards, the resulting gaps in the measured time-series need to be filled in order to properly estimate long-term deposition budgets. Known gap-filling strategies include the Mean-Diurnal-Variation (MDV) method (Falge et al., 2001), look-up tables (LUT) (Falge et al., 2001), non-linear regression (NLR) (Falge et al., 2001), marginal distribution sampling (MDS) (Reichstein et al., 2005), and artificial neural networks (Moffat et al., 2007). However, most of these methods have in common that they were originally designed for carbon dioxide (CO_2) or other inert gases.

~~Applying the MDS method to ΣN_r is not recommended, since exchange characteristics during night-time, the light-response curve, and controlling factors of ΣN_r differ from those of CO_2 (Zöll et al., 2019)~~ MDS requires a short-term stability of fluxes and micrometeorological parameters. This condition is not necessarily fulfilled for ΣN_r and its components. Their exchange patterns are characterized by a higher variability for different time scales leading to a lower autocorrelation and non-stationarities in flux time series compared to inert gases like CO_2. It is, on the other hand, possible to use statistical methods like MDV or linear interpolation to fill short gaps in flux time series. This was done by Brümmer et al. (2013), but filling long gaps with this technique is not recommended. Since exchange patterns of ΣN_r can substantially vary each day depending on the composition of ΣN_r and micrometeorology, it is questionable if statistical methods are suitable for ΣN_r considering the high reactivity and chemical properties of its compounds. ~~Up to now, no common gap-filling procedure exists for N_r compounds.~~

~~For nitrogen deposition assessments over large regions modeling approaches are needed due to low number of measurements. Chemical transport models (CTM) like LOTOS-EUROS (LOng Term Ozone Simulation (LOTOS) – EURopean Operational Smog (EUROS)) (Schaap, M. and Timmermans, R. M. A. and Roemer, M. and Boersen, G. A. C. and Builtjes, P. J. H. and Sauter, F. J. and~~

~~(Manders, Astrid M. M. and Builtjes, Peter J. H. and Curier, Lyana and Denier van der Gon, Hugo A. C. and Hendriks, Carlijn and Jonker~~ ~~and the Operational Priority Substance (OPS) model (J. A. van Jaarsveld, 2004) are the method of choice. LOTOS-EUROS predicts the dry deposition of various N_r compounds in a grid cell by utilizing meteorological data from the European Centre for Medium-Range Weather Forecasts (ECMWF) and information about the land-use class of the grid cell. Both CTMs use the deposition module DEPAC (DEPosition of Acidifying Components) (Erisman et al., 1994) for calculating deposition velocities. DEPAC is a dry deposition inferential scheme featuring bidirectional NH_3 exchange (van Zanten et al., 2010). However, calculated budgets from CTM are affected by uncertainties in the emission of several N_r compounds, transport range, (atmospheric) chemistry, and deposition processes. For improving models in these aspects, a validation to flux measurements is required. Such comparisons with novel measurement techniques are sparse and only available from few field campaigns.~~

~~It is also possible to use DEPAC as a stand-alone model for estimating dry deposition of N_r compounds. For site-based modeling with DEPAC, decoupled from a CTM and henceforth called DEPAC-1D, only measurements of common micrometeorological variables and concentrations of the individual N_r compounds are needed. Since all of these requirements were measured at the study site, DEPAC-1D results can be used as a further gap-filling option. Hence, an estimation of the ΣN_r dry deposition from flux measurements can be performed and a comparison of complete flux time series against DEPAC-1D and LOTOS-EUROS can be carried out for the measurement site.~~

~~Additionally, deposition measurements using the so-called "canopy budget method" of the forested and open land portion of the site were conducted close to the flux tower. These measurements were taken after the International Co-operative Programme on Assessment and Monitoring of Air Pollution Effects on Forests (ICP Forests) (Clarke, N. and Zlindra, D. and Ulrich, E. and Mosello, R.~~ ~~established by the United Nations Economic Commission for Europe (UNECE). Measurements of the canopy outflow allow the calculation of the nitrogen deposition after canopy budgets technique (CBT) (Draaijers, G. P. J. and Erisman, J. W., 1995; de Vries, W. and~~ ~~Thus, we had the opportunity to compare four independent techniques for estimating the nitrogen dry deposition.~~

The study presented here is the first one showing long-term flux measurements of ΣN_r above a remote forest ~~and conducting comparison to different methods used for estimating nitrogen dry deposition~~ focusing on the impact of environmental controls on fluxes, deposition velocities, and resistances. We discuss the observed flux pattern of ΣN_r (1), investigate the influence of micrometeorology on ~~the estimated fluxes~~ determined deposition velocities and (canopy) resistances (2), ~~and compare the nitrogen dry deposition of LOTOS-EUROS with DEPAC-1D, flux measurements, and nitrogen outflow measurements based on CBT~~ and show the influence of micrometeorological parameters on dry deposition sums estimated with the MDV approach (3). Wet deposition results obtained from bulk and wet-only sampler measurements are complementarily used to estimate total deposition.

Part II of the paper will present the usage of the acquired dataset in a modeling framework to estimate annual N budgets. Modeled fluxes and deposition velocities of the ΣN_r components will be compared to values reported in literature. Similar to Part I, the influence of micrometeorology on modeled fluxes, deposition velocities, and resistance will be investigated. Dry depositions estimated with the EC method will be compared to results from modeling approaches using in-situ and modeled input parameters and to canopy outflow measurements. We will discuss the ecological impact of nitrogen deposition on forest ecosystems. A comparison to annual N budgets reported for other forest ecosystems will be carried out.

2 Materials and Methods

2.1 Site and meteorological conditions

Measurements were ~~carried~~ made in the Bavarian Forest National Park (NPBW) (48°56'N 13°25'E, 807 m a.s.l) in southeast Germany. The unmanaged site is located in the Forellenbach catchment ($\sim 0.69\,km^2$ (Beudert and Breit, 2010)) ~~and~~, is surrounded by a natural, mixed forest, and is about 3 km away from the Czech border. Due to the absence of emission sources of N_r in the surroundings of the measurement site, mean annual concentrations of NO_2 (~~1.9-4.4~~ 2.1-4.8 ppb), NO (0.4-1.~~5~~6 ppb) and NH_3 (1.~~3~~4 ppb) are low (Beudert and Breit, 2010). The site is characterized by low annual temperatures (6.1°C) and high annual precipitation (1327 mm) measured at 945 m a.s.l ~~(Beudert pers. Comm.)~~. Annual temperature in 2016, 2017, and 2018 was 6.8°C, 6.9°C, and 8.0°C and precipitation was 1208 mm, 1345 mm, and 1114 mm, respectively. There are no industries or power plants nearby, only small villages with moderate animal housing and farming (Beudert et al., 2018). Due to these site characteristics, measurements of the ΣN_r background deposition are possible. For monitoring air quality and micrometeorology a 50 m tower was installed in the 1980s. Measurements of ozone, sulphur dioxide, and NO_x, the sum of NO and NO_2, have been conducted since 1990 (Beudert and Breit, 2010). The Forellenbach site is part of the International Cooperative Program on Integrated Monitoring of Air pollution Effects on Ecosystems (ICP IM) within the framework of the Geneva Convention on Long-Range Transboundary Air Pollution (UNECE, 2020) and belongs to the Long Term Ecological Research (LTER) network (LTER, 2020). The Federal Environment Agency (UBA) and NPBW Administration have been carrying out this monitoring program in the Forellenbach catchment~~, which is remote from significant sources of emission~~. The flux footprint consists of Norway spruce (*Picea abies*) and European beech (*Fagus sylvatica*) covering approximately 80% and 20% of the footprint,

respectively (Zöll et al., 2019). During the study period, maximum stand height was less than 20 m since dominating Norway spruce are recovering from a complete dieback by bark beetle in the mid-1990s and 2000s (Beudert and Breit, 2014).

2.2 Experimental setup

Flux measurements of ΣN_r were ~~carried out~~ made from January 2016 until end of June 2018 at a height of 30 m above ground. A custom-built ΣN_r converter (total reactive atmospheric nitrogen converter, TRANC) after Marx et al. (2012) and a 3-D ultrasonic anemometer (GILL-R3, Gill Instruments, Lymington, UK) were attached on different booms close to each other at 30 m height. The TRANC was connected via a 45 m opaque PTFE tube to a fast-response chemiluminescence detector (CLD 780 TR, ECO PHYSICS AG, Dürnten, Switzerland), which was ~~set~~ housed in an air-conditioned box at the bottom of the tower. The CLD was coupled to a dry vacuum scroll pump (BOC Edwards XDS10, Sussex, UK), which was placed at ground level, too. The inlet of the TRANC is designed after Marx et al. (2012) and Ammann et al. (2012). The conversion of ΣN_r to NO is split in two steps. Firstly, a thermal conversion occurs in an iron-nickel-chrome tube at 870°C ~~resulting in an oxidization of reduced N_r compounds~~. The thermal conversion of NH_4NO_3 leads to gaseous NH_3 and HNO_3. The latter is split up into to NO_2, H_2O, and O_2. NH_3 oxidized by O_2 at a platinum gauze to NO. HONO is split up to NO and a hydroxyl radical (OH). ~~Afterwards, a catalytic conversion takes place in a passively heated gold tube at 300°C while remaining oxidized N_r species are further reduced to NO.~~ In a second step, a gold tube passively heated to 300°C catalytically converts the remaining oxidized N_r species to NO. In this process, carbon monoxide (CO) is acting as a reducing agent. More details about the chemical conversion steps can be found in Marx et al. (2012). A critical orifice was mounted at the TRANC's outlet and restricted the mass flow to 2.1 $L\,min^{-1}$ after the critical orifice assuring low pressure along the tube. The mass flow rate before the critical orifice was the same as after the critical orifice. Since mass flow was equal to both sides of the critical orifice, a difference in flow velocity was induced due to the reduction in pressure. Flow velocities were not measured for the different sections.

The conversion efficiency of the TRANC had been investigated by Marx et al. (2012). They found 99% for NO_2, 95% for NH_3, and 97% for a gas mixture of NO_2 and NH_3. Conversion efficiencies for sodium nitrate ($NaNO_3$), ammonium nitrate (NH_4NO_3), and ammonium sulfate ($(NH_4)_2SO_4$) were 78%, 142%, and 91%, respectively. Overall, the results indicate that the TRANC is able to convert aerosols and gases efficiently to NO. For further details we refer to the publication of Marx et al. (2012).

For determining local turbulence - wind speed, wind direction, friction velocity (u_*) - measurements of the wind components (u, v, and w) were conducted using the sonic anemometer. Close to the sonic, an open-path LI-7500 infrared gas analyzer (IRGA) for measuring CO_2 and H_2O concentrations was installed.

For investigating the local meteorology, air temperature and relative humidity sensors (HC2S3, Campbell Scientific, Logan, Utah, USA) were mounted at four different heights (10, 20, 40, and 50 m above ground). At the same levels, wind propeller anemometers (R.M. Young, Wind Monitor Model 05103VM-45, Traverse City, Michigan, USA) were mounted on booms. Leaf wetness sensors designed after the shape of a leaf (Decagon, LWS, n=6, Pullman, Washington, USA) were attached to branches of a spruce and a beech tree near the tower. ~~The branches~~ Sensors of the beech tree were at heights of approximately 2.1 m, 5.6 m, and 6.1 m, ~~the branches~~ sensors of the spruce tree were at heights of 2.1 m, 4.6 m, and 6.9 m. These measurements

started in April 2016. Due to a wetting of the sensor's surface, the electric conductivity of the material changes. This signal, the leaf wetness, was converted by the instrument to dimensionless counts. Based on the number and range of counts, different wetness states could be defined. Half-hourly leaf wetness values were in the range from 0 to 270. In this study, we defined the wetness states "dry" and "wet". The condition wet can be induced by the accumulation of hygroscopic particles extending the duration of the wetness state or water droplets. In order to classify a leaf as dry or wet, we determined a threshold value based on the medians of leaf wetness values. ~~For calculating the leaf wetness value, the following calculation scheme was conducted.~~ During daylight (global radiation $> 20\,\mathrm{W\ m^{-2}}$), medians ranged from 1.1 to 2.0 and were between 4.1 and 9.4 during nighttime. During nighttime, medians are higher due to dew formation. According to the values determined during daylight, we set the threshold value to 1.5 for all sensors. If the leave wetness value~~, an arbitrary unit,~~ was lower than ~~10~~ 1.5, the leaf was considered as dry. Otherwise, the leaf ~~area~~ surface was considered as wet. To take differences between the sensors into account, all sensors were used to derive a common wetness Boolean. Therefore, the number of dry sensors were counted for each half-hour: ~~I~~if at least three sensors were considered as dry, the corresponding half-hour was considered as mostly dry. A cleaning of sensors was not conducted because contamination effects could be corrected by implemented algorithms. The derived wetness Boolean was used in the analysis of deposition velocities and resistances (Sec. 3.2).

~~Measurements of~~ Ambient NH_3 ~~were carried out~~ was collected by passive samplers at ground level (1.5), 10, 20, ~~40~~30, and 50 m from January 2016 to June 2018. Measurements at 40 m started in July 2016. The collector at ground level was moved to 40 m. Passive samplers of the IVL type (Ferm, 1991) were used for NH_3, and the exposition duration was approximately one month at a time. DELTA measurements (DEnuder for Long-Term Atmospheric sampling (e.g., Sutton et al., 2001; Tang et al., 2009)) of NH_3, HNO_3, SO_2, NO_3^-, and NH_4^+ were taken at the 30-m platform. The DELTA measurements had the same sampling duration as the passive samplers. The denuder preparation and subsequent analyzing of the samples was identical to the procedure for KAPS denuders (Kananaskis Atmospheric Pollutant Sampler, (Peake, 1985; Peake and Legge, 1987)) given in Dämmgen et al. (2010) and Hurkuck et al. (2014). We controlled the pump to keep flow at a constant level and checked the pipes for contamination effects before analyzing. Blank values were used as additional quality control.

Fast-response measurements of NH_3 were performed with a~~n~~ NH_3 Quantum Cascade Laser (QCL) (model mini QC-TILDAS-76 from Aerodyne Research, Inc. (ARI, Billerica, MA, USA)) at 30 m height, too. The setup of the QCL was the same as described in Zöll et al. (2016). ~~These measurements were used for inferential modeling of reactive nitrogen dry deposition~~. Further details about the location and specifications of the installed instruments can be found in Zöll et al. (2019) and Wintjen et al. (2020).

At the top of the tower (50-m platform), measurements of NO and NO_2 were conducted by the NPBW using a chemiluminescence detector (APNA - 360, HORIBA, Tokyo, Japan). Measurements of global radiation and atmospheric pressure were also conducted at 50 m. Precipitation was measured at a location in 1 km southwest distance from the tower according to WMO (World Meteorological Organization) guidelines (Jarraud, 2008), and data were quality-checked by the NPBW (Beudert and Breit, 2008, 2010). Wet ~~D~~deposition was collected as bulk and wet-only samples in weekly intervals in close vicinity to the tower using ~~three~~ four samplers, three bulk samplers and one wet-only sampler, at an open site ~~(bulk deposition) and 15 and 10~~

samplers beneath the canopy of a mature European beech and Norway Spruce stand (throughfall), respectively. This procedure is in common with the guidelines proposed by Clarke, N. and Zlindra, D. and Ulrich, E. and Mosello, R. and Derome, J. and Derome, K. an

The canopy budget technique (CBT) is the most common method for estimating total and dry nitrogen deposition in ecological field research based on inorganic nitrogen fluxes (NO_3^-, NH_4^+) only (see Staelens, J. and Houle, D.and De Schrijver, A. and Neir Total deposition of dissolved inorganic nitrogen (DIN_t) was estimated on yearly basis after the CBT approach of Draaijers, G. P. J. and Erisn and de Vries, W. and Reinds, G. J. and Vel, E. (2003) whose results differed only marginally and were therefore averaged. The biological conversion of deposited inorganic nitrogen into dissolved organic nitrogen (DON) in the canopy which is not addressed in CBT was estimated by the difference of DON fluxes between throughfall and bulk deposition (ΔDON). Adding ΔDON to throughfall DIN or to DIN_t reveals a frame of minimum and maximum estimates of total nitrogen deposition N_t and, by subtracting DIN deposition at open site from these N_t, of minimum and maximum estimates of dry deposition (Beudert and Breit, 2014) .

2.3 Flux calculation and post processing

The software package EddyMeas, included in EddySoft (Kolle and Rebmann, 2007), was used to record the data with a time resolution of 10 Hz. Analog signals from CLD, LI-7500, and the sonic anemometer were collected at the interface of the anemometer and joined to a common data stream. Flux determination covered the period from 1 January 2016 to 30 June 2018. Half-hourly fluxes were calculated by the software EddyPro 7.0.4 (LI-COR Biosciences, 2019). For flux calculation a 2-D coordinate rotation of the wind vector was selected (Wilczak et al., 2001), spikes were detected and removed from time series after Vickers and Mahrt (1997), and block averaging was applied. Due to the distance the from inlet of TRANC to the CLD, a time lag between concentration and sonic data was inevitable. The covariance maximization method allows to estimate the time lag via shifting the time series of vertical wind and concentration against each other until the covariance is maximized (Aubinet et al., 2012; Burba, 2013). The time lag was found to be about approximately 20 s (see Fig. A1 Fig. S1). Figures with the notation Sn where n=1...9 can be found in the supplemental material. We instructed EddyPro to compute the time lag after covariance maximization with default setting while using 20 s as default value and set the range from 15 s to 25 s (for details see Wintjen et al., 2020). For correcting flux losses in the high-frequency range we used an empirical method suggested by Wintjen et al. (2020), which uses measured cospectra of sensible heat ($\mathrm{Co}(w,T)$) and $\Sigma\mathrm{N_r}$ flux ($\mathrm{Co}(w,\Sigma\mathrm{N_r})$) and an empirical transfer function. We followed their findings and used bimonthly medians of the damping factors for correcting calculated fluxes since the chemical composition of $\Sigma\mathrm{N_r}$ exhibits seasonal differences (see Fig. 4 and Brümmer et al., 2013). On average, the damping factor was 0.78, which corresponds to flux loss of 22% (Wintjen et al., 2020). The authors determined flux loss factors for two different ecosystems, which are different, for example, in the composition of $\Sigma\mathrm{N_r}$. They assumed that the differences in flux losses are also related to the chemical composition of $\Sigma\mathrm{N_r}$. The low-frequency flux loss correction was done with the method of Moncrieff et al. (2004), and the random flux error was calculated after Finkelstein and Sims (2001).

Previous measurements with the same CLD model by Ammann et al. (2012) and Brümmer et al. (2013) revealed that the device is affected by ambient water vapour due to quantum mechanical quenching. Excited NO_2 molecules can reach ground state without emitting a photon by colliding with a H_2O molecule, thereby no photon is detected by the photo cell. It results

in a sensitivity reduction of 0.19% per 1 $\mathrm{mmol\,mol^{-1}}$ water vapour increase. Thus, calculated fluxes were corrected after the approach by Ammann et al. (2012) and Brümmer et al. (2013) using the following equation:

$$F_{\mathrm{NO,int}} = -0.0019 \cdot c_{\Sigma \mathrm{N_r}} \cdot F_{\mathrm{H_2O}} \quad (1)$$

The NO interference flux $F_{\mathrm{NO,int}}$ has to be added to every estimated flux value. $c_{\Sigma \mathrm{N_r}}$ is the measured concentration of the CLD and $F_{\mathrm{H_2O}}$ the estimated H_2O flux from the LI-7500 eddy-covariance system. The correction contributed approximately 132 g N $\mathrm{ha^{-1}}$ to two years of TRANC flux measurements if the Mean-Diurnal-Variation (MDV) approach was used as gap-filling approach. Half-hourly interference fluxes were between -3 and +0.3 ng N $\mathrm{m^{-2}\ s^{-1}}$. Their random flux uncertainty ranged between 0.0 and 0.5 ng N $\mathrm{m^{-2}\ s^{-1}}$

After flux calculation, we applied different criteria to identify low-quality fluxes. We removed fluxes, which were outside the range of -4520 ~~ngNm^{-2}s^{-1}~~ng N $\mathrm{m^{-2}\ s^{-1}}$ to 2420 ~~ngNm^{-2}s^{-1}~~ng N $\mathrm{m^{-2}\ s^{-1}}$, discarded periods with insufficient turbulence ($u_* < 0.1$ ~~ms^{-1}~~m $\mathrm{s^{-1}}$) (see Zöll et al., 2019), and fluxes with a quality flag of "2" (Mauder and Foken, 2006)~~., and variances of T, w, and $\Sigma \mathrm{N_r}$ exceeding a threshold of two times 1.96σ.~~ These criteria ensure the quality of the fluxes, but lead to systematic data gaps in flux time series. Instrumental performance problems led to further gaps in the time series. Most of them were related to maintaining and repairing of the TRANC and/or CLD, for example, heating and pump issues, broken tubes, empty O_2 gas tanks (O_2 is required for CLD operation), power failure, or a reduced sensitivity of the CLD. The reduction in sensitivity may be caused by reduced pump performance leading to an increase in sample cell pressure. If pressure in the sampling cell is outside the regular operating range, low pressure conditions needed for the detection of photons emitted by excited NO_2 molecules may not hold. Pump efficiency was controlled at least monthly, and tip seals were replaced if necessary. The sensitivity of the CLD could also be reduced by changes in the O_2 supply from gas tanks to ambient, dried box air if O_2 gas tanks were empty. Issues in the air-conditioning system of the box could also affect the sensitivity of the CLD. An influence of aging on the inlet, tubes, and filters may also affect the measurements. In order to minimize an impact on the measurements, half-hourly raw concentrations were carefully checked for irregularities like spikes or drop-outs by visual screening. Considering the time period of ongoing measurements from the beginning of January 2016 till June 2018, the quality flagging resulted in 52.2% missing data. The loss in flux data is higher than values reported by Brümmer et al. (2013). They reported ~~only a u_* filter, which caused~~ a flux loss of 24% caused by u_* filtering. In this study, the same u_* threshold caused a flux loss of approximately ~~14.8~~15.5%. ~~21~~32.7% data loss from January 2016 to June 2018 ~~is~~was caused by instrumental performance problems showing that TRANC-CLD system was overall operating moderately stable. ~~For gap-filling we used DEPAC with locally measured input variables, here called DEPAC-1D. This procedure is described in Sect. 2.3.~~ For gap-filling we applied the MDV approach to gaps in the $\Sigma \mathrm{N_r}$ flux time series. The window for filling each gap was set to $\pm$5 days. Remaining, long-term gaps were filled by a monthly average of the specific half-hour value estimated from non-gap-filled fluxes (Fig. 6) in order to estimate $\Sigma \mathrm{N_r}$ dry deposition sums from June 2016 to May 2017 and from June 2017 to May 2018. Uncertainties of the gap-filled fluxes are estimated by the standard error of the mean.

As outlined in Sec. 2.2, measurements of NH_3 were made with a QCL at high temporal resolution. In combination with the sonic anemometer, it gives the opportunity to determine NH_3 fluxes and to further investigate the non-NH_3 component of

the ΣN_r flux. However, a calculation of the NH_3 fluxes with the EC method was not possible in this study. No consistent NH_3 time lag was found making flux evaluation impossible. Due to regular pump maintenance, cleaning of the inlet and absorption cell, issues related to the setup of the QCL were unlikely to be the cause. We suppose that the variability in the measured NH_3 concentrations was not sufficiently detectable by the instrument. Significant short-term variability in the ΣN_r raw concentrations were not found in the NH_3 signal even in spring or summer. Thus, no robust time lag estimation could be applied to the vertical wind component of the sonic anemometer and the NH_3 concentration. Recently, Ferrara et al. (2021) found large uncertainties for low NH_3 fluxes measured with the same QCL model. Cross-covariance functions had a low signal-to noise ratio indicating that most of the fluxes were close to the detection limit.

2.4 Determining deposition velocity and canopy resistance of ΣN_r from measurements

In surface-atmosphere exchange models of N_r species like NO_2, NO, NH_3, HNO_3, or nitrogen aerosols, the flux (F_t) is calculated by multiplying concentrations of a trace gas modeled or measured at a reference height ($\chi_a(z-d)$) with a so-called deposition velocity ($v_d(z-d)$) where z is measurement height and d the zero-plane displacement height (van Zanten et al., 2010). The deposition velocity can be described by an electrical analogy and is defined as the inverse of the sum of three resistances (Wesely, 1989; Erisman and Wyers, 1993). According to its definition a positive v_d indicates deposition, a negative v_d emission. Note that, strictly speaking, for bidirectional exchange v_d needs to be interpreted as an "exchange velocity", i.e. it can technically become negative during emission phases. Equations are the same as for v_d (van Zanten et al., 2010).

$$F_t = -v_d(z-d) \cdot \chi_a(z-d) \quad \text{with } v_d = (R_a(z-d) + R_b + R_{c,eff})^{-1} \tag{2}$$

R_a is the aerodynamic resistance, R_b is the quasi-laminar boundary layer resistance, and $R_{c,eff}$ is the (effective) canopy resistance (i.e., including the effects of compensation points for some species). R_a is adapted from Garland (1977) and R_b based on Jensen and Hummelshøj (1995, 1997). They are influenced by micrometeorological parameters, surface conditions, and chemical properties of the N_r species of interest. R_a is defined as

$$R_a(z-d) = \frac{u(z-d)}{u_*^2} - \frac{\Psi_H(\frac{z-d}{L}) - \Psi_M(\frac{z-d}{L})}{u_* \cdot \kappa} \tag{3}$$

where u_* is the friction velocity, $u(z-d)$ is the wind speed at the reference height, κ is the von Kàrmàn Constant (≈ 0.41), L is the Obukhov length, and Ψ_H and Ψ_M are the integrated stability corrections for entrained scalars and momentum following Webb (1970) and Paulson (1970), respectively. R_b is given as

$$R_b = \frac{\nu_{air}}{D_{cp}} \cdot \left(\frac{c}{LAI^2} \cdot \frac{l \cdot u_*}{\nu_{air}} \right)^{\frac{1}{3}} \cdot \frac{1}{u_*} \tag{4}$$

where ν_{air} is the kinematic viscosity of air, D_{cp} is the molecular diffusivity of the N_r species, LAI is the leaf area index, c an empirically determined constant, which is set to 100 according to Jensen and Hummelshøj (1997), and l represents a typical leaf width (Jensen and Hummelshøj, 1995), which is set to 0.01 m. We determined the molecular diffusion coefficient for ΣN_r as

the weighted average of the campaign-wise averages of HNO_3, NH_3, NO, and NO_2 multiplied with their individual molecular diffusivities adapted from Massman (1998) and J.L. Durham and Stockburger (1986). It should be noted that particles are mostly not affected by a boundary-layer resistance compared to gases. However, the analysis of DELTA measurements showed that the mean particle contribution to the ΣN_r concentrations is only 22%. LAI was estimated after the same scheme used for the depostion module DEPAC (DEPosition of Acidifying Components) (Erisman et al., 1994) (see Appendix B of van Zanten et al., 2010). A linear increase of the LAI was calculated from mid of April to begin of May, a linear decrease from October to begin of November. Values ranged between 4.1 and 4.8. Fig. 1 shows the LAI for measured fractions of spruce and beech forest.

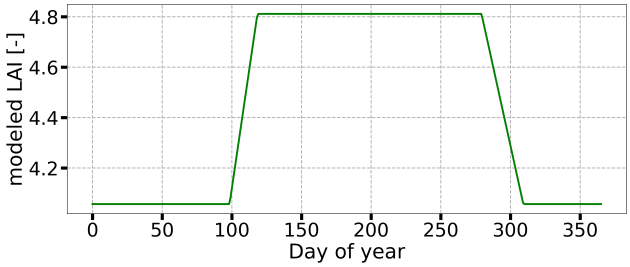

Figure 1. LAI following van Zanten et al. (2010) for measured fractions of coniferous forest (81.1%) and deciduous forest (18.9%) within the flux foot print for a year.

Considering only R_a and R_b, the maximum deposition velocity permitted by micrometeorological conditions is

$$v_{d,max}(z-d) = (R_a(z-d) + R_b)^{-1} \tag{5}$$

Subtracting $v_{d,max}(z-d)$ from measured $v_d(z-d)$, allows to determine an effective canopy resistance ($R_{c,eff}$) for ΣN_r

$$R_{c,eff} = \frac{1}{v_d(z-d)} - \frac{1}{v_{d,max}(z-d)} \tag{6}$$

Commonly, $R_{c,eff}$ consists of different resistances contributing to the uptake capacity of the surface, e.g., a stomatal resistance (R_{stom}), a cuticular resistance (R_w), and a soil resistance (R_{soil}). R_{stom} and R_w describe the exchange through the stomata of plants and with wet leaf surfaces, respectively. Interactions with the soil are merged in R_{soil}.

For N_r species exhibiting a bidirectional exchange pattern like NH_3 (e.g., Farquhar et al., 1980; Sutton et al., 1995, 1998; Wyers and Erisman, 1998; Flechard et al., 1999; Milford et al., 2001; Nemitz et al., 2001; van Zanten et al., 2010; Wichink Kruit et al., 2010, 2017) the existence of a compensation point is assumed. In case of NH_3, the stomatal compensation point is the concentration, at which the gaseous ammonia concentration is in equilibrium with dissolved ammonia in the apoplastic fluid at the reference height. In equilibrium state, the stomatal flux is zero (Farquhar et al., 1980; Sutton et al., 1994, 1998; Nemitz et al., 2000). Consequently, as long as the stomatal concentration is lower than the ambient concentration an uptake of N_r species happens. The cuticular exchange is also bidirectional for NH_3 (Wentworth et al., 2016). Observations by Neirynck

and Ceulemans (2008) indicated the existence of a cuticular compensation point (Nemitz et al., 2001; Massad et al., 2010; Wichink Kruit et al., 2010; Schrader et al., 2016; Wichink Kruit et al., 2017), at which the gaseous NH_3 concentration is in equilibrium with the solution on the external leaf surfaces.

Hints on NO_2 compensation points were found, for example by Thoene et al. (1996). Breuninger et al. (2013) detected compensation points for NO_2 but compensation point concentrations were not significant. However, the authors found a large uncertainty showing that the determination of compensation points for NO_2 is challenging (I.G. Chaparro-Suarez et al., 2011; Breuninger et al., 2013; Delaria et al., 2018; Delaria et al., 2020).

No clear evidence is found on compensation points for HNO_3. The assumption of an ideal uptake seems to be questionable (Tarnay et al., 2002). Farmer and Cohen (2008) detected significant emission fluxes of HNO_3 during summer above a spruce forest. HNO_3 emission during summer can be caused by evaporation of NH_4NO_3, which is favored at temperatures above 20°C (Wyers and Duyzer, 1997; Van Oss et al., 1998). The mechanism explaining the HNO_3 emission is still under investigation (Nemitz et al., 2004).

Nitrogen aerosols are likely deposited, and their flux pattern is driven by R_a (Wolff et al., 2010). Soil microbial activities imply a compensation point for soil NO fluxes, which depends on soil temperature, soil water content and N availability (David Fowler et al., 1998; Behrendt et al., 2014).

For the evaluation of v_d and corresponding resistances shown in Sec. 3.2, Eq. (2) to (6) were used.

2.5 ~~Modeling fluxes as gap-filling strategy~~

2.5.1 ~~Bidirectional resistance model DEPAC~~

~~DEPAC (Erisman et al., 1994) is a bidirectional resistance model, which models the canopy resistance R_c and determines the effective compensation point for NH_3. In addition to R_c, the aerodynamic resistance R_a and the quasi-laminar boundary resistance R_b are also needed for the calculation of the deposition velocity and therewith the flux. R_c is the sum of parallel connected resistances, which model the exchange behaviour of atmosphere with vegetation and soil: 1) stomatal resistance R_{stom}, 2) cuticular resistance R_w, and the soil resistance R_{soil}, which is connected in series to an in-canopy resistance R_{inc}. These resistances are treated differently for each N_r compound. Further details about the implementation of the resistances for each gas can be found in Sutton and Fowler (1993); Erisman et al. (1994); Van Pul, W. A. J. and Jacobs, A. F. G. (1994); Emberson, L. D. (van Zanten et al., 2010; Wichink Kruit et al., 2010; Massad et al., 2010; Wichink Kruit et al., 2017).~~

2.5.2 ~~Modeling of ΣN_r deposition (LOTOS-EUROS)~~

~~DEPAC is integrated in the 3D chemical transport model LOTOS-EUROS. The land-use specific and total dry deposition is calculated by LOTOS-EUROS on hourly basis for each N_r compound within a grid cell of $7\times7\,km^2$. For this reason, modeled concentrations, weather data from the European Centre for Medium-range Weather Forecast (ECMWF), and a~~

land-use classification for each grid cell are needed. The land-use classification of the grid cell, in which the tower is located, was divided into 46.0% semi-natural vegetation, 37.2% coniferous forest, 15.9% deciduous forest, 0.7% water bodies, and 0.2% grassland. The land-use class weighting is based on the Corine Land Cover 2012 classification. However, the actual structure of the forest stand shows 81.1% coniferous forest and 18.9% deciduous forest within the footprint of the tower. Due to the differences in the the distribution of vegetation types in the footprint of the tower, concentrations and depositions were recalculated with a corrected weighting of the land-use classes. The low contribution of coniferous forest and deciduous forest within the grid cell may be related to the evaluation of older aerial photographs showing larger areas of deadwood. Finally, the dry deposition of ΣN_r is calculated as the sum of NO, NO_2, HNO_3, NH_3, and particulate NH_4NO_3 fluxes. The version of DEPAC used in this study differs from the one documented in van Zanten et al. (2010) in two main aspects: Firstly, the implementation of a function considering codeposition of SO_2 and NH_3 (Wichink Kruit et al., 2017) in the non-stomatal pathway and secondly, the usage of a monthly moving average of NH_3 concentration for determining the stomatal compensation point (Wichink Kruit, R. J. and Schaap, M. and Sauter, F. J. and van Zanten, M. C. and van Pul, W. A. J., 2012).

2.5.3 Site-based modeling of ΣN_r deposition (DEPAC-1D)

As mentioned before, DEPAC-1D was used for filling the gaps in flux data. For running DEPAC as stand-alone, it was extended with a FORTRAN90 (Adams, Jeanne C. and Brainerd, Walter S. and Martin, Jeanne T. and Smith, Brian T. and Wagener, Jerrold program that allows the use of arbitrary input data sources. DEPAC-1D uses measured parameters of micrometeorology and concentration for the determination of R_c and the compensation point of NH_3. The atmospheric resistances R_a and R_b and the fluxes of NH_3, NO, NO_2, and HNO_3 were calculated with a Python script. Parameterizations were done for R_a after Garland (1977) and for R_b after Jensen and Hummelshøj (1995, 1997) followed by stability corrections after Webb (1970) and Paulson (1970). R_{stom} was calculated after Emberson, L. D. and Ashmore, M. R. and Cambridge, H. M. and Simpson, D. and Tuovinen, J Further details can be found in van Zanten et al. (2010). For estimating fluxes with DEPAC-1D, concentration measurements on monthly and half-hourly basis are used. NH_3 fluxes were based mostly on NH_3 half-hourly concentration measurements of the NH_3-QCL. Gaps in NH_3 concentration time series were filled with DELTA measurements or – if these were missing, too – with passive sampler data. HNO_3 was taken from DELTA measurements, and NO_x was provided by the NPBW with half-hourly time resolution. The difference in measurement height was considered in the calculation of R_a. Temperature and relative humidity data corresponded to the average of measurements from 20 m and 40 m. Since profile measurements of temperature and relative humidity started in April 2016, measurements by the NPBW were used until end of March 2016. Pressure and global radiation were provided by the NPBW. Indicators of stability and turbulence such as Obukhov-Length L and u_* were taken from momentum flux measurements of the sonic anemometer. All micrometeorological and turbulent flux data were aggregated half-hourly. For determining compensation points and additional deposition corrections, SO_2 and NH_3 concentrations collected by DELTA samplers were used. Passive sampler measurements were used to replace missing or low-quality NH_3 measurements in DELTA time series, and gaps in the SO_2 data were filled by the long-term average. Leaf area index (LAI) was modeled as described by van Zanten et al. (2010). For modeling R_a the solar zenith angle, which is calculated

by using celestial-mechanic equations, the roughness length z_0 and displacement height d are needed. By using the same height as proposed by LOTOS-EUROS for z_0 (2.0 m), fluxes were slightly underestimated. However, influence on the dry deposition budget was negligible. Thus, we set z_0 to 2.0 m and d to 12.933 m for coniferous forest and to 11.60 m for deciduous forest. Shifting z_0 or d by $\pm 50\%$ caused a change of +5.0%/-3.2% and +5.6%/-9.1%, respectively, in the dry deposition after 2.5 years. An incorrect assessment of the LAI by $\pm 50\%$ has significant influence on the dry deposition. It leads to a change of +18.9%/-27.7%. The calculation of the dry deposition was done for NH_3, NO, NO_2, and HNO_3 with the mentioned parameters on half-hourly basis. Fluxes of DEPAC-1D were weighted after the actual land-use classes (81.1% coniferous forest and 18.9% deciduous forest). The LAI, which is based on the LOTOS-EUROS land-use weighting, ranges between 1.9 and 2.8 while considering only deciduous and coniferous forest land-use classes in the flux footprint. The LAI based on the actual land-use weighting ranges between 4.1 and 4.8. Including grassland in the determination of LAI is less useful since characteristics, for example an increase in LAI from the beginning of year, is not representative for the vegetation within the flux footprint. Thus, modeled nitrogen budgets of LOTOS-EUROS should be seen as lower and upper estimates.

After post-processing of TRANC data, we applied two gap-filling strategies. In the first one, DEPAC-1D was used for replacing all missing values in flux data. The second one used MDV for filling gaps up to five days and DEPAC-1D for longer gaps. For comparing the methods with each other we developed a validation strategy: After filling the gaps in the TRANC time series with DEPAC-1D, we used LOTOS-EUROS with the corrected weighting of land-use classes for closing remaining gaps in DEPAC-1D results as well as in TRANC data ensuring a comparison for every time step. Gaps in DEPAC-1D are mostly related to power outages causing gaps micrometeorological data. Since DEPAC-1D did not include deposition of particles and the actual land-use class in the grid cell did not agree with the land-use class used in LOTOS-EUROS, recalculations of LOTOS-EUROS with a corrected land-use class and/or without considering particulate deposition were performed. Averaged flux time series of LOTOS-EUROS, DEPAC-1D, and TRANC were compared to look for seasonal deviations throughout the observation period. Finally, the annual dry deposition sums of LOTOS-EUROS, DEPAC-1D, TRANC, and CBT were evaluated.

3 Results

3.1 Concentrations, deposition velocities, and fluxes of ΣN_r during the measurement campaign

Figure 2 shows ambient concentrations of ΣN_r (black), NH_3 (red) and NO_x (blue) as half-hourly averages for the entire measurement campaign. Data gaps ~~are~~ were mostly related to instrumental performance problems. No ΣN_r measurements were possible until end of May 2016 due to heating problems of the TRANC.

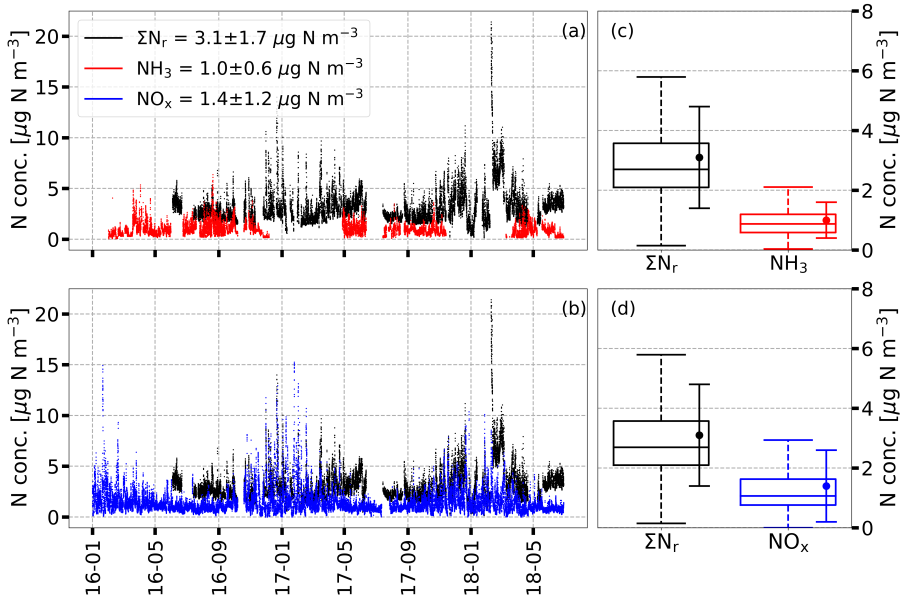

Figure 2. Half-hourly averaged concentrations of ΣN_r (black), NH_3 (red) and NO_x (blue) in ~~ppb~~ μg N m^{-3} from 1 January 2016 to 30 June 2018 displayed in (a) and (b). Box plots (box frame = 25 % to 75 % interquartile range (IQR), bold line = median, whisker = 1.5· IQR) with average values (dots) shown in (c) and (d). Error bars represent one standard deviation.

ΣN_r concentrations exhibited highest values during the winter months. For example, values were higher than ~~20 ppb~~ 10 μg N m^{-3} during January 2017 and February 2018. NO_x showsed a relatively high concentration level during winter, too. During spring and summer, NO_x values ~~are~~ were mostly lower than ~~5 ppb~~ 2 μg N m^{-3} and hence, their contribution to ΣN_r decreasesd. However, ΣN_r values remained around ~~5 ppb~~ 3 μg N m^{-3} and reached values up to ~~10 ppb~~ 6 μg N m^{-3}, which ~~is~~ was related to higher NH_3 concentrations during these periods. ΣN_r concentration ~~is~~ was ~~5.2 ppb~~ 3.1 μg N m^{-3} on average, NH_3 ~~is~~ ~~approximately~~ was ~~1.8 ppb~~ 1.0 μg N m^{-3}, and NO_x ~~is~~ was ~~2.5 ppb~~ 1.4 μg N m^{-3} on average~~. Values are~~ with the latter values being in agreement with concentrations reported by Beudert and Breit (2010). Averaged NH_3 concentrations of the QCL agreed well with NH_3 from passive samplers and DELTA measurements (Fig. S2). Overall, the agreement in the annual pattern was good, but a bias between the QCL and the diffusion samplers was found. From passive sampler measurements, an increase in the NH_3 concentration with measurement height could be observed. At 10 m (in the canopy), the lowest NH_3 concentrations were measured. No systematic difference was found between 20 m and 30 m. At 50 m, NH_3 was slightly higher (0.1 μg N m^{-3}) than 30 m. During winter, the difference in measurement heights diminished. Slightly higher NH_3 concentration were observed at 10 m in winter.

The observations made for the seasonal changes of the half-hourly ΣN_r concentrations are also visible for their monthly medians (Fig. S3). Figure S3 shows monthly box plots of the concentrations. In general, median concentrations were almost similar for the entire campaign with slight differences between the years. Medians were between 2 and 3.5 μg N m^{-3}. From July to September, concentrations were slightly higher in 2016 than in 2017. During this period, IQRs and whiskers were the

smallest for the entire year showing less variability in ΣN_r concentrations. In spring and winter, median concentrations were higher, and concentrations covered a wider range compared to the summer month. Figure S4 shows the corresponding diurnal patterns for each month. During the day, ΣN_r concentrations were almost stable. Averaged values showed variations of less than 1 μg N m^{-3}. If concentrations were averaged for each season (not shown), slightly higher concentrations were observed from 9:00 to 15:00 LT and lower values during the night.

~~The elevated NO_x concentration level also affects its contribution to ΣN_r measured by the TRANC. Figure B1 shows the contribution of N_r species, which are converted inside the TRANC, to ΣN_r as pie charts. Contributions from NO_3, NH_3, NH_4, and HNO_3 are determined from monthly DELTA measurements. NO_x concentrations are averaged to the exposition periods of the DELTA samplers. The ΣN_r concentration measurements are dominated by NO_x. On average, NO_x contributes with 51.6% to ΣN_r. At lowest and highest ΣN_r concentrations, its influence on ΣN_r differs only slightly. NH_3 exhibits a contribution of 21.6% on average, which is lower than the sum of HNO_3, NH_4, and NO_3 ($\sim 26.8\%$). Compared to NO_x, NH_3 varies significantly from lowest to highest ΣN_r concentrations. At the lowest average ΣN_r concentration, the contribution of NH_3 is significantly high whereas the contribution of NH_3 gets negligible compared to the contribution of particulate and acidic N_r compounds ($\sim 35.5\%$) at the highest average ΣN_r concentration.~~ Figure 3 shows absolute concentrations of individually measured N_r compounds as stacked bars and ΣN_r from the TRANC from January 2016 to June 2018. TRANC and NO_x measurements were averaged to exposition periods of DELTA measurements. DELTA measurements recorded at an insufficient pump flow were excluded from the analysis. Missing NH_3 values in the DELTA time series were filled by NH_3 data determined from the passive sampler mounted at 30 m. Remaining data gaps in the DELTA time series of NH_3, HNO_3, NH_4^+, and NO_3^- were replaced by monthly averages from other years. The procedure was not applied to the time period covering February 2018 due to the unusually high ΣN_r concentrations.

The comparison of the TRANC with DELTA+NO_x revealed slight overestimations by the latter from August 2016 to October 2016 and from January to March 2017. On average, an underestimation by DELTA+NO_x of approximately 0.3 μg N m^{-3} with a standard deviation of 0.7 μg N m^{-3} was observed. The median value was about 0.35 μg N m^{-3}.

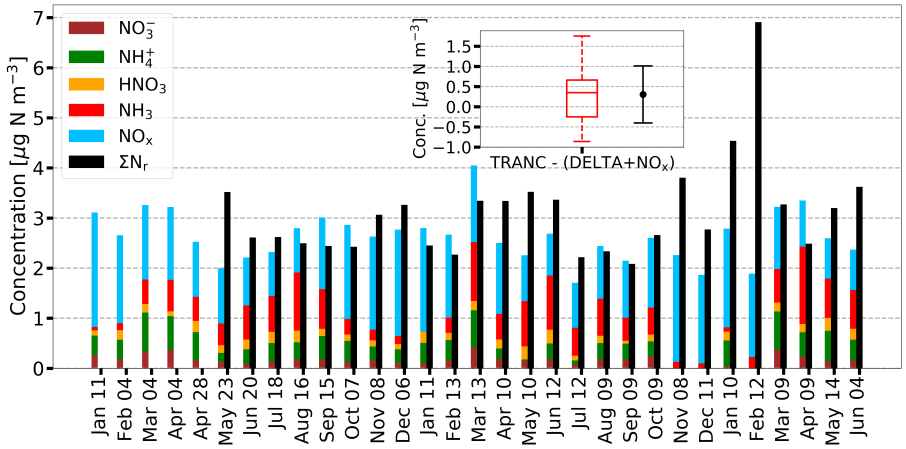

Figure 3. Monthly stacked concentration of TRANC, DELTA, and NO_x in μg N m^{-3} for the entire measurement campaign. Missing NH_3 measurements from the DELTA measurements caused by a low pump flow were filled with passive sampler values from 30 m. Replacing was done for December 2016 and 2017, January 2017, November 2017, and from February to April 2018. Gaps in the time series of the individual components were replaced by monthly averages estimated from other years if possible. NO_x and ΣN_r were averaged to the exposition periods of the DELTA samplers.

HNO_3, NH_4^+, and NO_3^- concentrations were nearly equal through the entire measurement campaign. Seasonal differences existed mainly for NH_3 and NO_x. We measured average concentrations of 0.56, 0.17, 0.40, 0.19, and 1.40 μg N m^{-3} for NH_3, HNO_3, NH_4^+, NO_3^-, and NO_x for the entire campaign, respectively. On average, the relative contribution of NH_3, HNO_3, NH_4^+, and NO_3^- to ΣN_r was less than 50% for the entire measurement campaign as visualized by Fig. 4. We further observed a low particle contribution to the ΣN_r concentrations ($\sim$ 22% on average) showing that the ΣN_r concentration pattern was mainly influenced by gaseous N_r compounds.

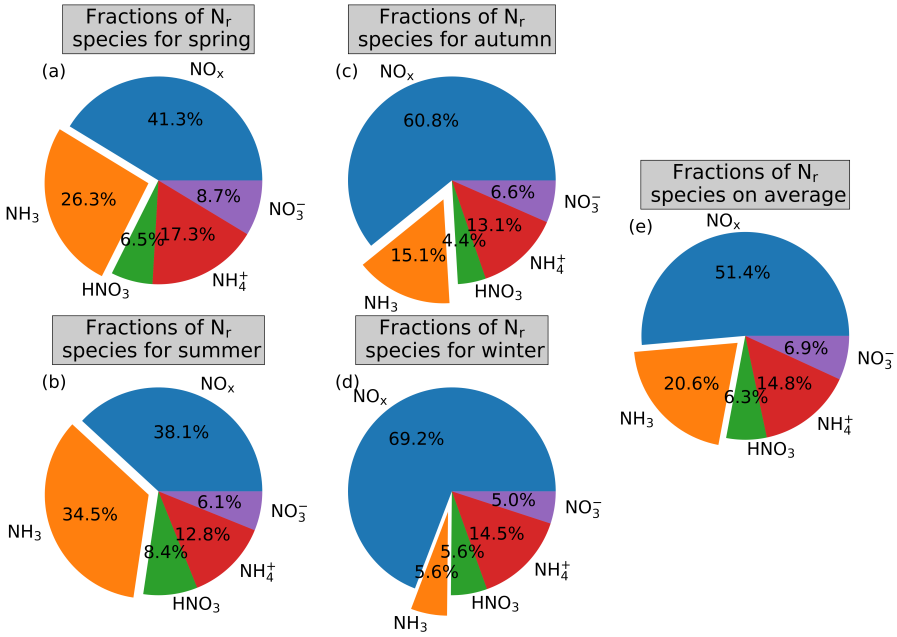

Figure 4. Pie charts showing the relative contribution of concentrations for NO_x, NH_3, NO_3^-, NH_4^+, and HNO_3 to ΣN_r based on DELTA samplers and NO_x measurements for different seasons of the year. NO_x measurements are averaged to exposition periods of the DELTA samplers. (a) to (d) refer to spring, summer, autumn, and winter, respectively. (e) shows the average relative contribution to ΣN_r for the entire measurement period.

In general, NO_x showed the highest contribution to ΣN_r and followed seasonal changes with highest values during winter and lowest values in summer. NH_3 showed also seasonal changes with concentrations lowest in winter and highest values in spring and summer. The contribution of HNO_3 was almost stable. A slight increase in the contribution was found for summer. As reported by Tang et al. (2020), HONO sticks to carbonate coated denuder surfaces, which are designed for collecting HNO_3. Thus, HNO_3 concentrations may be biased. NO_3^- and NH_4^+ exhibited slightly higher values for spring. Only small seasonal changes in the overall ΣN_r concentration were observed. As seen by Fig.3, ΣN_r concentrations were mostly between 2 and 4 μg N m^{-3}. We measured 3.3, 2.6, 2.5, and 3 μg N m^{-3} with the TRANC system for spring, summer, autumn, and winter, respectively.

Figure 5 shows the non-gapfilled ΣN_r fluxes depicted as box plots on monthly time scale. The convention is as follows: ~~N~~negative fluxes represent deposition, positive fluxes emission. ~~Quality screening and post-processing was done after the criteria mentioned in Sec 2.3.~~

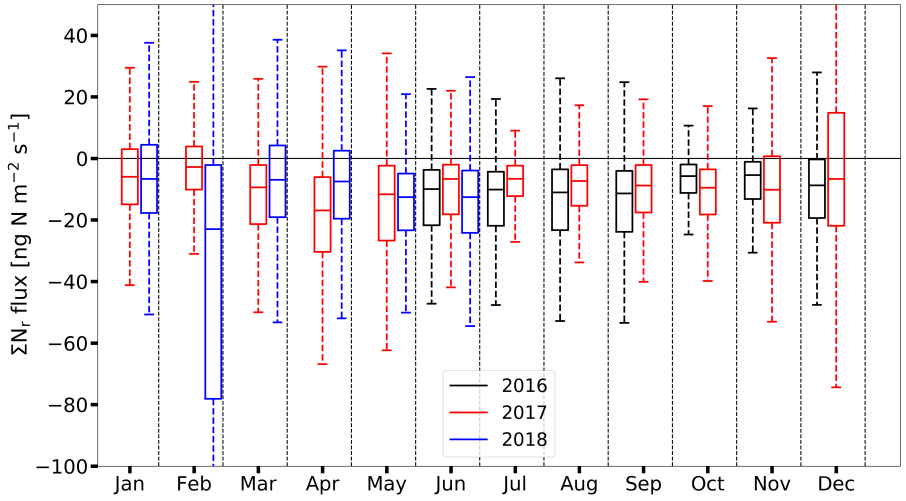

Figure 5. Time series of measured high-quality (flags "0" and "1") ΣN_r fluxes depicted as box plots on monthly basis (box frame = 25% to 75% interquartile ranges (IQR), bold line = median, whisker = 1.5· IQR) in ng N m^{-2} s^{-1}. Colors indicate different years. The displayed range was restricted from -100 to 50 ng N m^{-2} s^{-1}.

Almost all ΣN_r flux medians ~~are~~ were between -15 and -5 ng N m^{-2} s^{-1} indicating that mainly deposition of ΣN_r occurred at our measurement site. Quality assured half-hourly fluxes showed 8~~5~~0% deposition and ~~15~~20% emission fluxes. On half-hourly basis, fluxes ~~are~~ were in the range from ~~-409~~-516 to ~~216~~399 ng N m^{-2} s^{-1}. The mean random flux error of the non-gapfilled, half-hourly fluxes ~~is~~ was 5.~~7~~9 ng N m^{-2} s^{-1} after Finkelstein and Sims (2001). The flux detection limit ~~is~~ was calculated by multiplying 1.96 with the flux error (95% confidence limit) (see Langford et al., 2015). The latter ~~is~~ was 11.~~3~~5 ng N m^{-2} s^{-1}. Both values refer to the entire measurement campaign. Similar values were found by Zöll et al. (2019) at the same site covering a shorter period. In total, 51% of the non gap-filled fluxes were higher than the flux detection limit. It shows that for large parts nitrogen dry deposition was close to detection limit of the used measuring device and that nitrogen exchange happened at a comparatively low level.

In general, median deposition ~~is~~ was almost on the same level for the entire campaign with slight seasonal differences. For instance, median deposition ~~is~~ was slightly higher during spring and summer than during winter for 2016. However, median deposition during winter 2017 ~~is~~ was similar to median deposition in summer 2017. Median deposition was significantly stronger from June 2016 till September 2016 than for the same period in 2017. IQR and whisker covered a wider range, too. The pattern change~~s~~d for the time period from October to December. In December 2017, the IQR expand~~s~~ed in the positive range indicating emission events for a significant time period. The largest median deposition with 25 ng N m^{-2} s^{-1} and the widest range in IQR reaching approximately -~~7~~80 ng N m^{-2} s^{-1} were registered in February 2018 indicating strong deposition phases during that month with sporadic emission events. Such phenomenons were not observed in the years before. In the following month, the deposition ~~is~~ was slightly higher from March to April 2017 than for the same period in 2018. Fig. 6 shows averaged daily cycles for every month.

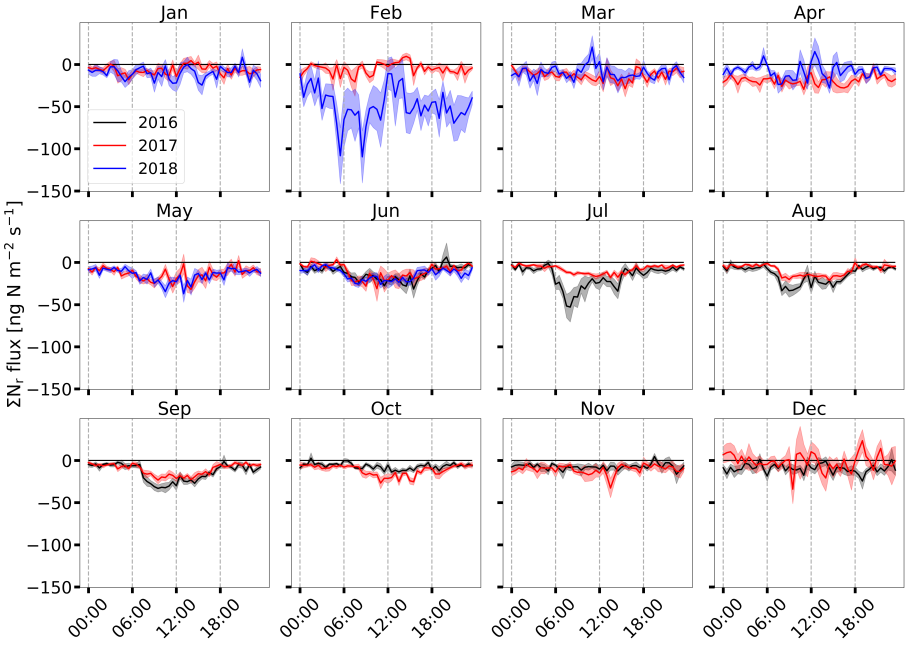

Figure 6. Mean daily cycle for every month of ΣN_r fluxes from June 2016 to June 2018 on half-hourly basis. The shaded area represents the standard error of the mean. Colors indicate different years.

In general, the ΣN_r daily cycle exhibit~~s~~ed low deposition or neutral exchange during nighttime/evening and increasing deposition during daytime. Deposition rates ~~are~~ were similar during the night for the entire campaign except for February 2018. Maximum deposition ~~is~~was reached between 9:00 and 15:00 ~~CET~~ LT. Deposition is enhanced from May until September showing fluxes between -40 and -20 ng N m^{-2} s^{-1}. ~~During autumn (~~ From October - to November~~)~~ and ~~winter (~~ from December - to February~~)~~, the daily cycle weaken~~s~~ed with almost neutral or slightly negative fluxes, mostly lower than -10 ng N m^{-2} s^{-1}. The daily cycles of the respective same months ~~are~~ were mainly similar. However, during certain months, which differ in their micrometeorology and/or in the composition of ΣN_r, differences can be significant. For example, the daily cycle of March and April 2017 ~~is~~ was clearly different to daily cycle of March and April 2018. During spring 2017, slight deposition fluxes ~~are~~ were found whereas the ΣN_r exchange ~~is~~ was close to neutral a year later. The median deposition ~~is~~ was also slightly larger in March and April 2017 than in the year after (Fig. 5). In December 2017, the daily cycle ~~is~~ was close to the zero line and positive fluxes were observed, although standard errors ~~are~~ were relatively large (± 1~~0~~1.5 ng N m^{-2} s^{-1} on average). In December 2016, slight deposition fluxes ~~are~~ were observed for the entire daily cycle. The daily cycle of February 2018 show~~s~~ed high deposition values during the entire day, the highest values during the measurement campaign. Again, average standard error ~~is~~ was relatively large (± 1~~7~~9.9 ng N m^{-2} s^{-1}) for February 2018 compared to February 2017.

Figure S5 shows the median v_d to the corresponding fluxes. Values ranged between 0.2 and 0.5 cm s^{-1} for the entire campaign. In general, median v_d followed closely the seasonality of their corresponding fluxes (Fig. 5). During autumn and winter, v_d remained mostly stable. From May to September, the curve was approximately bell-shaped. Similar to the diurnal

fluxes, maximum v_d values were reached between 9:00 and 15:00 LT. During that time, values of v_d were close to 1 cm s^{-1} or even higher (Fig. S6).

3.2 Controlling factors of measured ΣN_r ~~fluxes~~ deposition velocities and resistances

~~Fig. 6 reveals that the pattern of ΣN_r daily cycle~~ The analysis of v_d and corresponding fluxes show that their diurnal pattern was characterized by lower deposition during the night and highest values around noon~~The deposition is enhanced from May until September compared to the rest of the year.~~, in particular from May to September (Fig. 6 and Fig. S6). Micrometeorological parameters such as global radiation (Zöll et al., 2019), temperature (Wolff et al., 2010), humidity (Wyers and Erisman, 1998; Milford et al., 2001), ~~concentrations (Brümmer et al., 2013; Zöll et al., 2016)~~, and turbulence (Wolff et al., 2010), dry/wet leaf surfaces (Wyers and Erisman, 1998; Wentworth et al., 2016), and concentration of ΣN_r, especially changes in the concentration of the sub components, (Brümmer et al., 2013; Zöll et al., 2016) were reported to control the deposition of N_r compounds.

In order to investigate the effect of micrometeorology and vegetation on deposition, we further determined atmospheric and effective canopy resistances according to the equations given in Sec. 2.4. For visualizing the effect of turbulence on the fluxes, Fig. 7 shows the dependency of the measured fluxes on their concentrations for different u_* classes and global radiation (R_g) higher than 50 W m^{-2}.

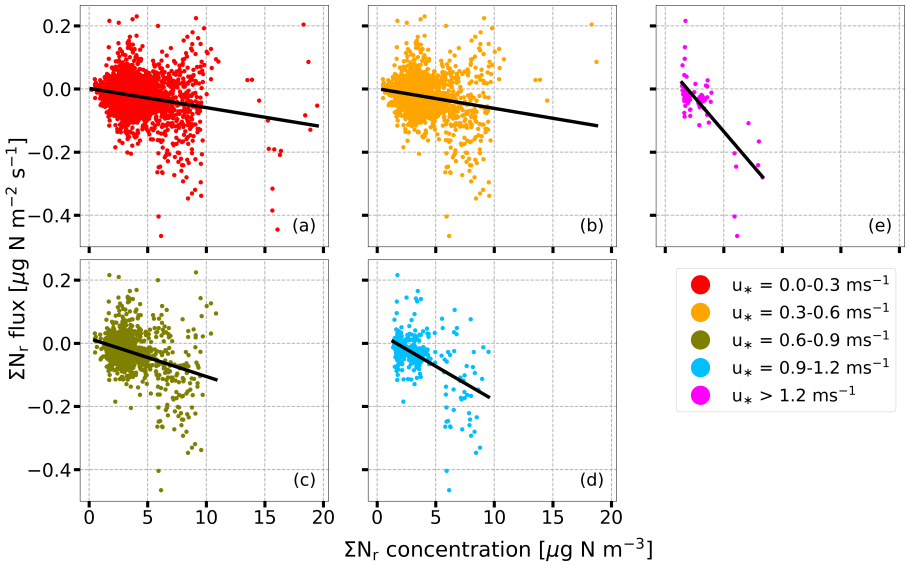

Figure 7. Dependency of measured concentrations on corresponding ΣN_r fluxes shown as scatter plots during daylight ($R_g > 50$ W m^{-2}). Colors indicate different u_* classes. Linear regressions between concentrations and fluxes are made for each u_* class indicated by black lines.

We found a decreasing slope with increasing u_*. The slope corresponds to v_d. Results of the linear regressions, v_d and squared correlations (R^2), are listed in Table 1. In addition, numbers of half-hours used for the regressions are given.

Table 1. Results of linear regressions from Fig. 7 for selected u_* ranges. The slope of the linear function corresponds to v_d, R^2 is the squared correlation of concentrations and fluxes, and n is the number of half-hours used for the regression.

u_* range [m s^{-1}]	v_d [cm s^{-1}]	R^2 [-]	n [-]
0.0–0.3	0.61	0.07	9085
0.3–0.6	0.63	0.05	6124
0.6–0.9	1.20	0.14	2296
0.9–1.2	2.16	0.28	485
> 1.2	4.34	0.51	79

For u_* values lower than 0.6 m s^{-1}, v_d was almost invariant. For u_* values higher than 0.6 m s^{-1} or even higher, an increase in v_d was found. Since R_a (Garland, 1977) and R_b (Jensen and Hummelshøj, 1995, 1997) decrease with increasing u_*, v_d increases. The highest R^2 was determined for u_* higher than 1.2 m s^{-1}. For other u_* ranges, correlations were negligible. However, only 79 half-hourly concentrations and fluxes were available for u_* values higher than 1.2 m s^{-1}. Considering the number of half-hours, atmospheric turbulence had an influence on the deposition of ΣN_r but u_* could not be solely responsible for the observed exchange of ΣN_r.

Recently, Zöll et al. (2019) identified R_g as an important controlling factor for the ΣN_r fluxes at the measurement site from July to September. u_* did not emerge as controlling factor as reported by the authors. Figure S7 shows the daily cycle of concentration, R_g, u_*, air temperature (T_{air}), and v_d for the period from May to September. During that period, a clear diurnal pattern in v_d was observed with largest values around noon and lowest values during the night. Figure S8 is made for the same variables but for December, January, and February. During winter, v_d was almost equal and even lower during the day, which resulted in lower deposition of ΣN_r during winter. The different shapes of v_d were related to plant activity mainly controlled by R_g.

~~Therefore,~~ Within the period of sufficient global radiation inducing ΣN_r exchange, we investigated the dependency of the ΣN_r ~~fluxes~~ deposition velocities and resistances on temperature, humidity, dry/wet leaf surface, and ΣN_r concentration. We separated half-hourly ~~fluxes~~ v_d and $R_{c,eff}$ into ~~classes~~ groups of low and high temperature, humidity, and concentration according to their median. ~~The threshold values, which are calculated from May to September, based on the median of the mentioned parameters.~~ v_d and $R_{c,eff}$ determined during rain were treated separately. In case of separating v_d and $R_{c,eff}$ into groups of dry and wet leaf surfaces, we used the proposed calculation scheme of a leaf wetness boolean (see Sec. 2.2) ~~Leaf wetness value is calculated after the scheme described in Sec. 2.2 for same time period.~~ No significant influence of the different installation heights on leaf surface wetness was found (see Fig. S9 and corresponding description in the supplement). Figures 9 and 10 show the results for v_d and $R_{c,eff}$, respectively.

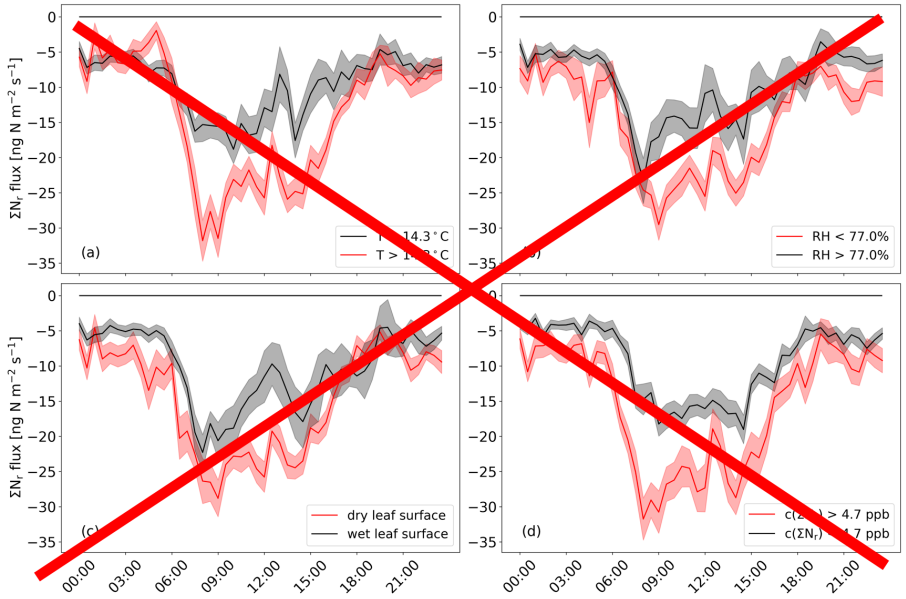

Figure 8. ~~Mean daily cycle from May to September of ΣN_r fluxes for low and high temperature, humidity, and concentration. Median values of temperature, humidity, and concentration, which are derived for the same time period, are used as threshold values for separating fluxes. For separating dry and wet leaf surfaces, the scheme proposed in Sec. 2.2 is applied. The shaded area represents the standard error of the mean.~~

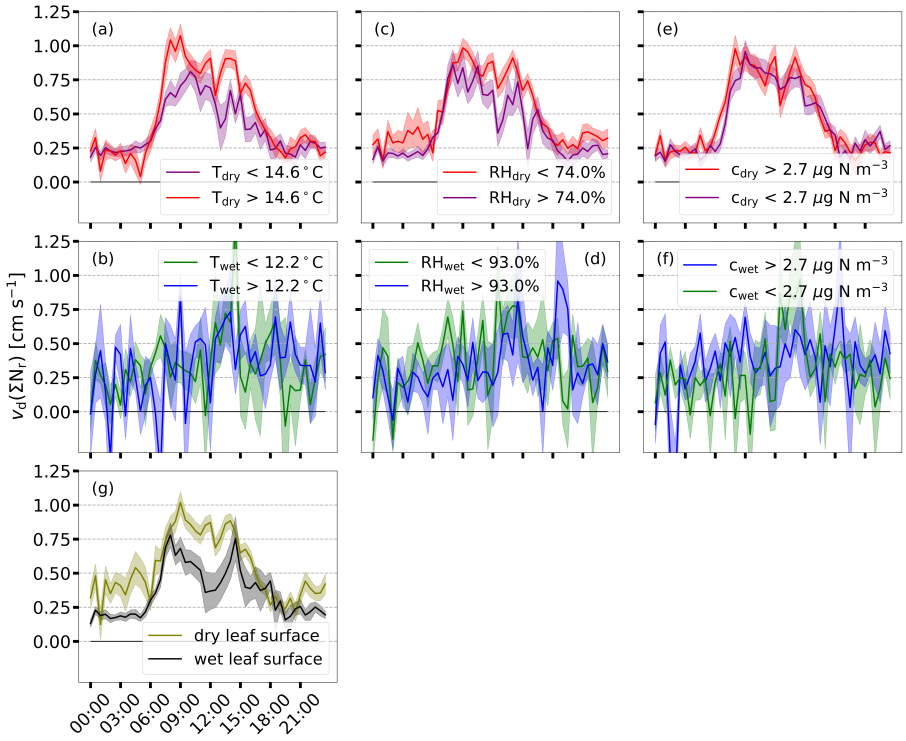

Figure 9. Mean daily cycle from May to September of v_d for low and high temperature, relative humidity, and concentration separated by precipitation in the conditions "dry" and "wet". Panel (a), (c), and (e) represent the case dry (no precipitation), (b), (d), and (f) the case wet. Median values of temperature, humidity, and concentration, which are derived for the same time period, are used as threshold values for separating v_d. In panel (g), the mean daily cycle of v_d for dry and wet leaf surfaces is shown. For classifying leaf surfaces as dry or wet, the scheme proposed in Sec. 2.2 is applied. The shaded areas represent the standard error of the mean.

In general, higher temperatures, less humidity~~, higher concentrations~~, ~~and~~ dry leaf surfaces ~~favour~~ , and dry conditions (no precipitation) enhanced deposition of ΣN_r, ~~. Temperature seem to affect ΣN_r fluxes from 6:00 to 18:00 CET stronger leading to differences of more than -10 ng N m^{-2}s^{-1}, for instance around 9:00 and 15:00 CET.~~ and a clear diurnal pattern was observed for v_d with high values around noon and low, non-zero values in the night during dry conditions. ~~During dawn/nighttime fluxes show no significant temperature dependence. Concentration has the strongest impact on the deposition. The effect is increased from 6:00 to 15:00 CET exhibiting a difference -5.5 ng N m^{-2}s^{-1} on average, but also nighttime deposition fluxes are enhanced at higher concentrations. The impact of less humidity and dry leaves is slightly lower than concentration and temperature, but they affect nighttime deposition stronger than temperature.~~ During dawn/nighttime, deposition velocities exhibited no significant difference between the applied thresholds. Overall, no difference was found for low and high concentration regimes. In case of precipitation, v_d was reduced during daytime and exhibited a high variability for the entire day. No difference and distinct pattern could be found for low and high temperature, humidity, and concentration regimes during precipitation. During other times of the year, no diurnal pattern was observed during dry conditions. In those periods, v_d was almost constant

and exhibited lower values during daylight compared to the May to September time frame. Occasionally, negative deposition velocities referring to emission of ΣN_r were recorded during times of lower radiation. Figure 10 is in accordance to Fig. 9 but for $R_{c,eff}$.

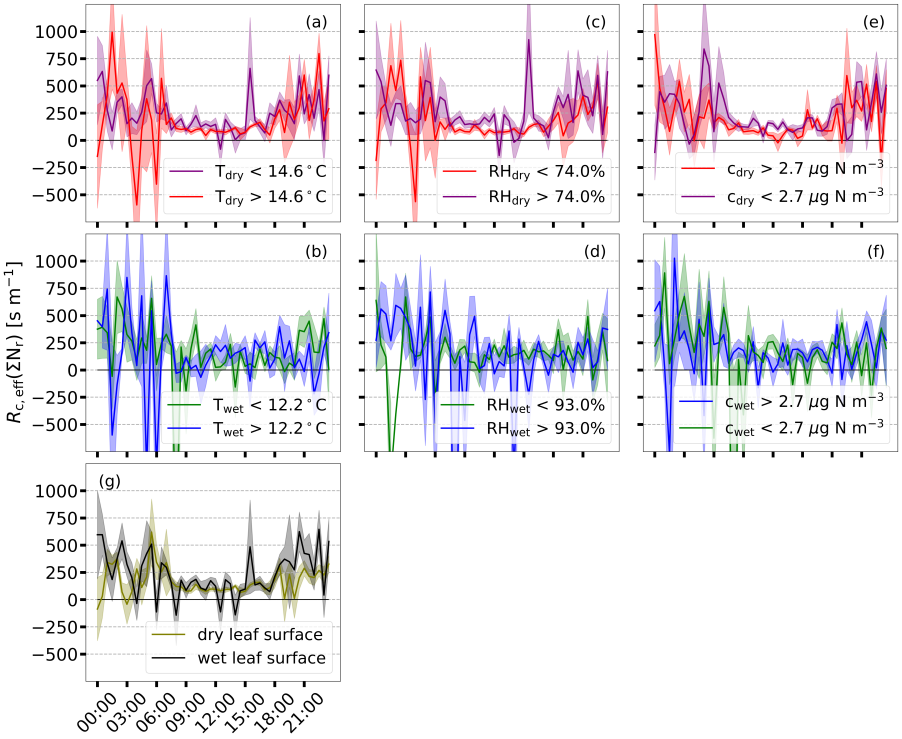

Figure 10. Mean daily cycle from May to September of $R_{c,eff}$ for low and high temperature, relative humidity, and concentration separated by precipitation in the conditions "dry" and "wet". Panel (a), (c), and (e) represent the case dry (no precipitation), (b), (d), and (f) the case wet. Median values of temperature, humidity, and concentration, which are derived for the same time period, are used as threshold values for separating $R_{c,eff}$. In panel (g), the mean daily cycle of $R_{c,eff}$ for dry and wet leaf surfaces is shown. For classifying leaf surfaces as dry or wet, the scheme proposed in Sec. 2.2 is applied. The shaded area represents the standard error of the mean.

$R_{c,eff}$ exhibited lowest values during the day and highest values at night. During nighttime, the variability in $R_{c,eff}$ was enhanced whereas $R_{c,eff}$ was almost stable during daylight. Only slight differences between the applied threshold were found. $R_{c,eff}$ was slightly lower at higher concentrations only for short periods during daylight, for example around noon. In case of relative humidity, $R_{c,eff}$ exhibited slightly lower values for less humid air. Temperature had nearly no effect on $R_{c,eff}$. During precipitation, no difference between the applied thresholds was found. Similar to v_d, $R_{c,eff}$ had a higher variability compared to dry conditions during the day resulting in higher uncertainties. Also phases with negative $R_{c,eff}$ values were observed during rain indicating emission of nitrogen from the canopy.

A similar analysis was made for R_a and R_b. During daylight, values of R_a and R_b were close to zero showing that v_d was mostly driven by the pattern of $R_{c,eff}$. Lower values of R_a and R_b were found for lower air humidity and higher temperature.

In case of wet leaf surfaces, R_a and R_b were higher in the morning and evening. If wet leaf surfaces were excluded from the analysis, the differences for v_d and resistances to micrometeorological parameters diminished. Wet leaf surfaces reduced the uptake of ΣN_r at the measurement site. During the night or at lower radiation, R_a and R_b were comparable in magnitude to $R_{c,eff}$. In autumn and winter, $R_{c,eff}$ showed partly negative values and no diurnal pattern. It should be noted that the shapes of the daily cycles of each parameter shown in Fig. 9 and 10 are almost similar for the chosen threshold values and differ only in amplitude.

~~Finally, it should be mentioned that the shapes of the daily cycles for each parameter shown in Fig. 8 are similar for both threshold values and differ only in amplitude. It indicates that other drivers may influence the pattern of ΣN_r fluxes stronger than the shown parameters here.~~

3.3 Sensitivity of ΣN_r dry deposition sums to micrometeoroglogical parameters

We found that higher temperatures, lower relative humidity, and no precipitation enhance deposition velocities and fluxes. The application of data-driven gap-filling methods like MDV (Falge et al., 2001) for estimating dry deposition could lead to biased results if micrometeorological conditions of the certain gap are different to fluxes used for filling the gap. We further applied a u_*-filter, which had removed preferentially smaller fluxes occurring at low turbulent conditions. Therefore, we determined dry deposition budgets with and without u_*-filter and conducted gap-filling with additional restrictions for temperature, humidity, and precipitation. Figure 11 shows the non gap-filled ΣN_r fluxes depicted as box plots and their cumulative sums with and without a u_*-filter if MDV is used as gap-filling approach. The threshold was set to 0.1 m s^{-1}, and the window for filling each gap was set to $\pm$5 days. Uncertainties of the gap-filled fluxes were estimated by the standard error of the mean. The total uncertainties were calculated as the sum of the standard errors.

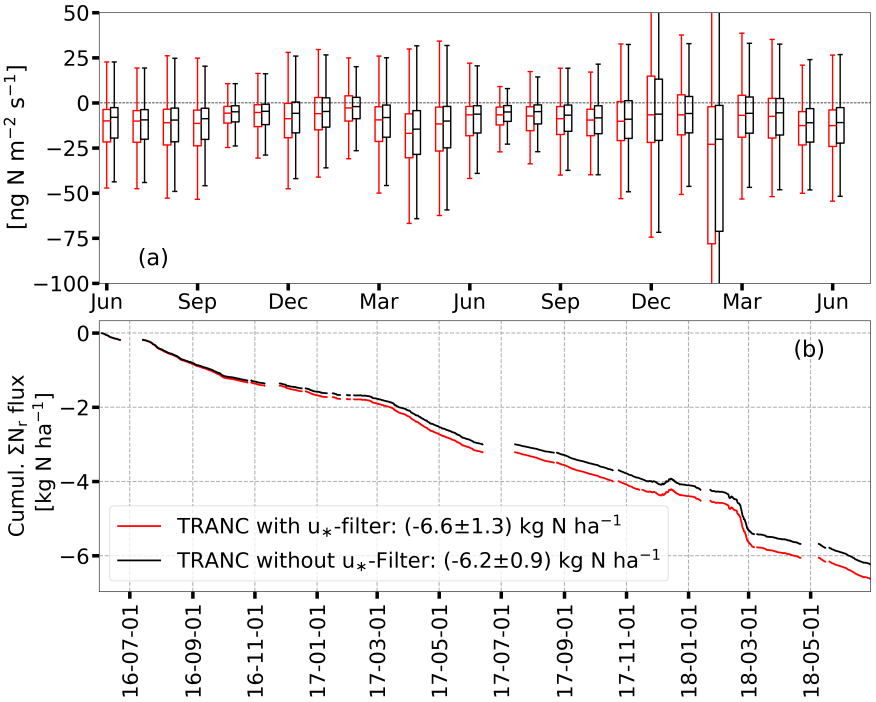

Figure 11. Panel (a) shows the non-gap filled ΣN_r fluxes depicted as box plots with (red) and without (black) u_*-filter in ng N m^{-2} s^{-1} (box frame = 25% to 75% interquartile ranges (IQR), bold line = median, whisker = 1.5· IQR). The threshold for u_* was set to 0.1 m s^{-1}. In panel (b), the cumulative dry deposition of ΣN_r is plotted for both cases in kg N ha^{-1}. For determining the cumulative curves, MDV was used as gap-filling method, and gaps were filled with fluxes being in a range of $\pm$5 days. Remaining gaps were not filled.

The difference in dry deposition was approximately 400 g N ha^{-1} after 2 years and is within the uncertainty range of the estimated dry depositions. Panel (a) of Fig. 11 shows that median depositions of the ΣN_r fluxes with u_*-filter were almost equal to or larger than the median depositions without u_*-filter. Figure 7 indicates that we measured large and small fluxes below 0.1 m s^{-1}. Thus, the applied u_* threshold removed not only small fluxes resulting in a consistent bias between the median depositions. The contribution of the water vapor correction (Eq. 1) to the estimated dry deposition was very low. ΣN_r interference fluxes were between -3 and -0.3 ng N m^{-2}s^{-1}. The uncertainty ranged between 0.0 and 0.5 ng N m^{-2}s^{-1}. Considering two years of TRANC flux measurements with MDV as gap-filling approach, the correction contributed with 132 g ha^{-1} to the estimated dry deposition of 6.6 kg ha^{-1}.

We further investigated the impact of temperature, humidity, and precipitation on the dry deposition sums of ΣN_r compared to the dry deposition without restrictions when using MDV as gap-filling approach since we found differences in the diurnal patterns of ΣN_r for micrometeorological parameters. Therefore, we considered only fluxes in the time frame of $\pm$5 days, at which temperature varied by $\pm$3°C, humidity by $\pm$5%, or precipitation was recorded. Remaining, long-term gaps (see panel (b) of Fig. 11) were filled by a monthly average of the respective half-hourly value estimated from non-gap-filled fluxes (Fig. 6). Those averages were also calculated for low and high humidity and temperature regimes separated by their monthly median.

The calculations were made with and without the application of a u_*-filter. Figure 12 shows the annual dry deposition of the measurement years from the beginning of June to end of May.

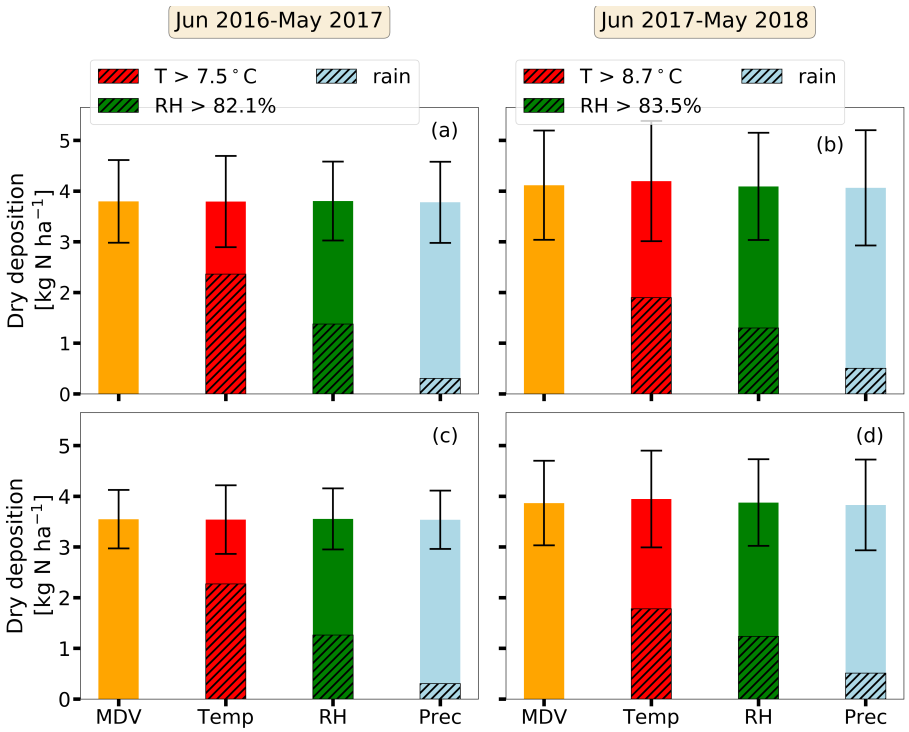

Figure 12. Annual ΣN_r dry deposition depicted as bar graphs from June to May in kg N ha^{-1}. For the orange bar, short-term gaps were filled with the MDV approach while using only fluxes in the time frame of ± 5 days. In case of the red, green, and blue bar, fluxes used for gap-filling have to additionally fulfilled criteria for temperature (± 3°C), humidity ($\pm 5\%$), or precipitation (wet or dry). Remaining gaps were replaced by monthly averages estimated for each half-hour calculated from the non-gap-filled fluxes. For the meteorological cases, monthly medians were used to determine those averages for low and high humidity and temperature regimes. (a) and (b) were made for fluxes with u_*-filter, (c) and (d) without it. The hatched area of the bars represent the dry deposition for temperatures and relative humidity values higher than the annual median shown in the legend and for wet conditions.

No significant difference could be found between the dry depositions sums for both measurement years. Consequently, the applied selection criteria did not lead to biased sums compared to the dry deposition determined without restrictions for meteorological parameters. Warm, drier conditions exhibited a higher contribution to the annual dry deposition, in particular for the first measurement year. During rain, dry deposition was less than 500 g N ha^{-1} per 12-month period. As shown before, a difference in the application of a u_*-filter exists but is within the uncertainty range. Dry deposition was higher in 2017/2018, which was related to the large deposition fluxes observed in February 2018. In total, we estimated 3.8 ± 0.8 kg N ha^{-1} and 4.1 ± 1.1 kg N ha^{-1} with the MDV approach (orange bar) and u_*-filter for 2016/2017 and 2017/2018, respectively.

Wet deposition was estimated from measurements of bulk and wet-only samplers. Table 2 shows the deposition estimates of NH_4^+-N, NO_3^--N, dissolved organic nitrogen (DON), and the resulting total nitrogen from wet deposition (TWD).

Table 2. Annual sums of NH_4^+-N, NO_3^--N, dissolved organic nitrogen (DON), and the resulting total wet depostion (TWD) from wet deposition samplers (bulk and wet-only). ∅ represents the average and s the standard deviation.

Sampler type	year	NH_4^+-N [kg ha^{-1}]	NO_3^- [kg ha^{-1}],	DON [kg ha^{-1}]	TWD [kg ha^{-1}]
Bulk	2016	3.8	3.4	1.5	8.7
	2017	3.4	3.4	0.7	7.5
	2018	2.8	2.7	0.7	6.2
	∅	3.3	3.2	1.0	7.5
	s	0.5	0.4	0.5	1.3
Wet-only	2016	4.0	3.6	0.9	8.5
	2017	3.4	3.6	0.5	7.5
	2018	2.9	2.6	0.6	6.1
	∅	3.4	3.3	0.7	7.4
	s	0.6	0.6	0.2	1.2

Differences between deposition estimates from bulk and wet-only samplers were not significant, and deposition estimates of NH_4^+-N and NO_3^--N were almost equal. Results from both sampling systems have in common that wet deposition of NH_4^+ and NO_3^- decreased from 2016 to 2018. In 2018, TWD was possibly lower due to the decreased amount of precipitation. Annual precipitation was approximately 200 mm lower in 2018 compared to 2017. In comparison to the results from dry deposition, wet deposition was about a factor two higher than dry deposition. Mean TWDs of wet-only samplers were 8.0 kg N ha^{-1} and 6.8 kg N ha^{-1} for the timeframe 2016/2017 and 2017/2018, respectively. In total, we got a total nitrogen deposition of 11.8 kg N ha^{-1} for 2016/2017 and 10.9 kg N ha^{-1} for 2017/2018.

3.4 ~~Cumulative N exchange and method comparison~~

~~For determining the ΣN_r dry deposition, gaps were filled in flux time series with DEPAC-1D and MDV (see Sec. 2.3). Fluxes estimated through the EC technique covered 47.8% of the measurement period after quality filtering. The low amount of valid flux measurements was expected, for example, related to insufficient turbulence during nighttime, performance issues of the instruments, etc. Applying MDV allows to increase the coverage to 65.0%. With DEPAC-1D alone nearly all gaps were closed. Remaining gaps in DEPAC-1D were about 4% due to power failures and were filled with LOTOS-EUROS results. Afterwards, fluxes were added up to get a cumulative sum. In the following, the results of the method comparison described in Sec. 2.3 are presented. Figure 13 shows the cumulative ΣN_r dry deposition of the different methods for the duration of the campaign.~~

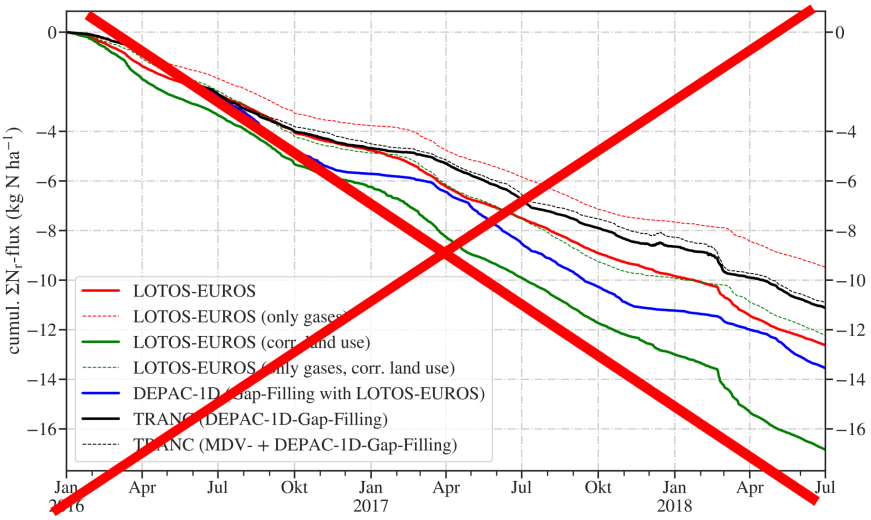

Figure 13. ~~Comparison of measured and modeled cumulative ΣN_r dry deposition after gap-filling for the entire measurement campaign. Colors indicate different methods: TRANC+DEPAC-1D (black, solid), TRANC+MDV+DEPAC-1D (black, dashed), DEPAC-1D+LOTOS-EUROS (blue), LOTOS-EUROS with corrected land use (green, solid), LOTOS-EUROS with corrected land use, but only gases (green, dashed), LOTOS-EUROS (red, thick), and LOTOS-EUROS with corrected land use, but only gases (red, dashed)~~

~~The ΣN_r dry deposition values estimated by each method for 2.5 years are listed in Table 3.~~

Table 3. ΣN_r dry deposition of TRANC, DEPAC-1D, LOTOS-EUROS, and CBT for the entire measurement campaign, i.e. January 2016 to June 2018. Annual dry deposition of 2018 is extrapolated for TRANC, DEPAC-1D, and LOTOS-EUROS. CBT lower and upper estimates were weighted according to the measured land use. For a visualisation of annual dry deposition see Fig. 14.

		ΣN_r dry deposition [kg N ha^{-1}]			
Data set	Gap-filling strategy	after 2.5 years	2016	2017	2018
TRANC	MDV+DEPAC-1D	10.9	4.68	3.97	5.0
TRANC	DEPAC-1D	11.1	4.50	3.78	5.34
DEPAC-1D	LOTOS-EUROS	13.6	5.71	5.51	4.69
LOTOS-EUROS	–	9.5	-	-	-
only gases					
LOTOS-EUROS	–	12.6	4.76	5.07	5.63
LOTOS-EUROS	-	12.2	-	-	-
with corrected land use and only gases					
LOTOS-EUROS	-	16.8	6.24	6.75	7.76
with corrected land use					
CBT lower estimate	–	13.7	3.30	4.35	6.09
CBT upper estimate	-	22.6	6.44	6.98	9.14

Overall, DEPAC-1D and and LOTOS-EUROS seem to overestimate ΣN_r dry deposition compared to our measurements, in particular LOTOS-EUROS with the corrected land use. The dry deposited ΣN_r modeled by DEPAC-1D consists of 76% NH_3, 13% HNO_3, 11% NO_2, and less than 1% NO. It shows that modeled deposition of DEPAC-1D is mostly driven by NH_3. HNO_3 and NH_3 deposition velocities are nearly equal (1.81 cms^{-1} and 1.86 cms^{-1}). Also, emission phases are modeled for NH_3 due to the low compensation point indicated by the negative whisker of the box plot (Fig.C1.). However, their influence on total deposition is negligible since only short emission phases of NH_3 were modeled. Deposition velocity for NO_2 and NO are relatively low. 0.08 cms^{-1} is determined for NO_2 and 0.0 cms^{-1} for NO.

ΣN_r exchange of DEPAC-1D is rather neutral during the entire winter, and thus the difference to measured deposition is close to zero. During summer a systematic overestimation of DEPAC-1D to measured fluxes is observed. Modeled deposition by LOTOS-EUROS is slightly lower than DEPAC-1D during summer and consequentially closer to measured fluxes. However, during autumn and spring predicted deposition by LOTOS-EUROS is significantly higher than deposition determined by DEPAC-1D and TRANC. The agreement of the measured, non gap-filled ΣN_r fluxes (results not shown) with LOTOS-EUROS for the same half-hours without particulate input is conspicuous after 2.5 years. TRANC measurements show a cumulative, non gap-filled dry deposition of 4.7 kg N ha^{-1}, LOTOS-EUROS exhibits 4.5 kg N ha^{-1}. This agreement has to be regarded with caution since the TRANC also converts particulate ΣN_r compounds and the land-use class weighting of LOTOS-EUROS is not valid for the measurement site. Correcting the land-use class based on actual vegetation of the flux footprint, exhibit

a significant overestimation of the dry deposition. We determined 8.2 kg N ha^{-1} with LOTOS-EUROS for measured, non gap-filled half-hours including particulate deposition and the actual land-use class weighting, and 16.8 kg N ha^{-1} is calculated for the entire measurement campaign. The applied gap-filling strategies result in similar dry deposition after 2.5 years (Table 3). The difference between both curves is enhanced from July 2017 to mid February 2018. Due to the strong deposition occurring in late February 2018, the difference between the curves is significantly reduced. Obviously, DEPAC-1D could not model the deposition event accurately.

Since all cumulative curves exhibit generally the same shape, we conclude that the variability in fluxes is reproduced by DEPAC-1D and LOTOS-EUROS well, although the amplitude and duration of certain deposition events is different. This observation is valid for the strong deposition event in late February 2018 observed by the TRANC, but it is treated differently by DEPAC-1D and LOTOS-EUROS. As stated before, it is not accurately modeled by DEPAC-1D and also not by LOTOS-EUROS without considering particle deposition. Including particle deposition in LOTOS-EUROS leads to better agreement with TRANC measurements for a few weeks. It seems that the deposition during late February 2018 is most likely driven by particulate N_r compounds. Such compounds are not implemented in DEPAC-1D. After the deposition event, measured ΣN_r exchange is almost neutral whereas modeled deposition of LOTOS-EUROS increases resulting in significant disagreement in ΣN_r deposition. However, the emission event, which is calculated from TRANC measurements for December 2017, is not captured by LOTOS-EUROS and DEPAC-1D.

In the following, a comparison of the ΣN_r dry deposition separated by method and measurement years is given in Fig. 14. The dry deposition values for 2018 are extrapolated. The extrapolation is kept simple. We extrapolated the deposition of the first half of 2018 until the end of the year.

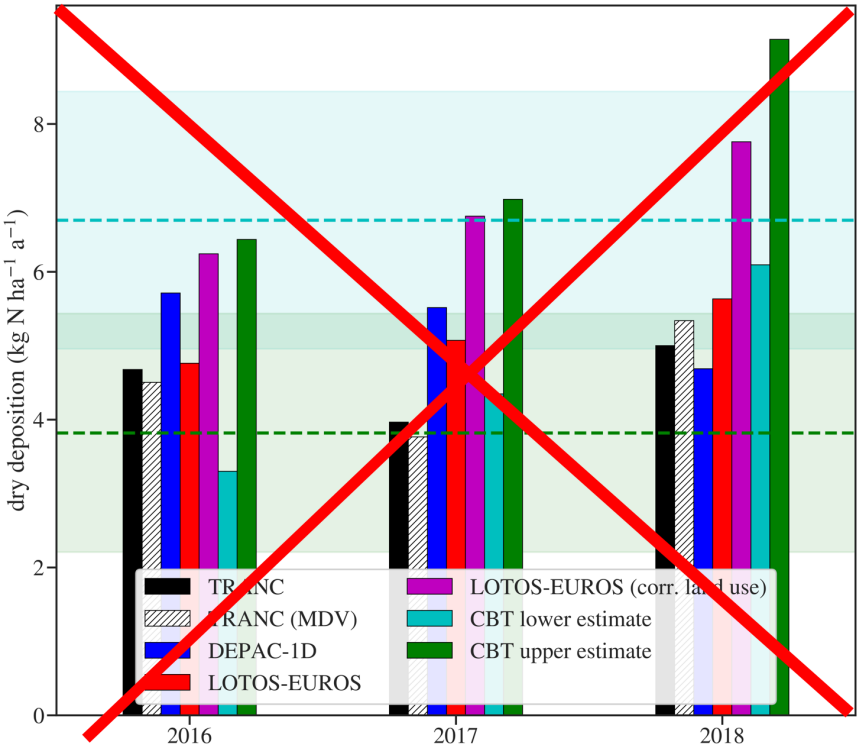

Figure 14. ~~ΣN_r dry deposition for the years 2016, 2017, and 2018 displayed as bar chart. Colors indicate different methods: TRANC+DEPAC-1D (black), TRANC+MDV (shaded),DEPAC-1D (blue), LOTOS-EUROS (red), LOTOS-EUROS with corrected land use (purple), and canopy budget technique (turquoise and green). Data from TRANC, DEPAC-1D, and LOTOS-EUROS are extrapolated for 2018. CBT lower and upper estimates were weighted according to the measured land use. The colored dashed lines indicate the averaged dry deposition of the lower and upper estimates from 2010 to 2018, the shaded areas represent their standard deviation.~~

~~Annual dry deposition of the TRANC ranges from 3.8 kg N ha^{-1} a^{-1} to 5.3 kg N ha^{-1} a^{-1}. 4.7 kg N ha^{-1} a^{-1} to 5.7 kg N ha^{-1} a^{-1} is modeled by DEPAC-1D, 4.8 kg N ha^{-1} a^{-1} to 5.6 kg N ha^{-1} a^{-1} is predicted by LOTOS-EUROS with uncorrected land use, and 6.2 to 7.8 kg N ha^{-1} a^{-1} by LOTOS-EUROS with corrected land use. Annual dry deposition estimated by CBT are similar for 2016 and 2017. Values are close to the long-term average estimated by CBT for 2010 until 2018 (~ 3.8 kg N ha^{-1} a^{-1} as lower estimate and ~ 6.7 kg N ha^{-1} a^{-1} as upper estimate). For 2018 the application of CBT results in a significantly higher lower and upper estimates (6.1 and 9.1 kg N ha^{-1} a^{-1}). Therewith, CBT estimates for 2018 are outside the range of one standard deviation of the long-term average.~~

~~Averaged annual ΣN_r dry deposition is 4.5 kg N ha^{-1} a^{-1} for both gap-filling approaches, DEPAC-1D shows 5.3 kg N ha^{-1} a^{-1}, and LOTOS-EUROS predicts 5.2 kg N ha^{-1} a^{-1} to 6.9 kg N ha^{-1} a^{-1} depending on the weighting of land-use classes. 7.5 kg N ha^{-1} a^{-1} is estimated with CBT for the period from 2016 to 2018 as upper estimate. 4.6 kg N ha^{-1} a^{-1} are determined as lower estimate. It shows that dry depostion estimated by TRANC, DEPAC-1D, and LOTOS-EUROS is within~~

the frame of minimum and maximum deposition estimated by CBT but generally closer to the lower estimate of CBT except for LOTOS-EUROS with the corrected land use weighting.

Annual dry deposition of LOTOS-EUROS and CBT is higher in 2017 than in 2016, whereas TRANC and DEPAC-1D exhibit less deposition in 2017. Values of TRANC with and without MDV are almost similar for 2016 and 2017. Using only DEPAC-1D as gap-filling strategy results in slightly higher dry deposition for 2016 and 2017. For 2018 using MDV leads to higher deposition since DEPAC-1D predicts the lowest deposition compared to years before. The difference for 2018 is caused by the deposition event in February 2018, which has an influence on the MDV method leading to significantly larger deposition fluxes. The high deposition values of 2018 modeled by LOTOS-EUROS are probably related to the generally higher modeled concentrations in the first half of 2018.

3.5 Sensitivity of measured vs. modeled input parameters to deposition estimates

As stated before, LOTOS-EUROS exhibits relatively high deposition values. Running LOTOS-EUROS with the corrected land-use class, leads to the highest dry deposition values for all years, without considering canopy budgets technique. For a closer investigation of this issue we conduct a comparison of model input parameters such as temperature, relative humidity, NH_3 concentration, global radiation, and friction velocity to measured data and evaluate their impact on NH_3 fluxes modeled by DEPAC within LOTOS-EUROS. These parameters hold an important role in the modeling of the NH_3 exchange (e.g., Nemitz et al., 2001). Air temperature controls the influence of the emission potential, the apoplastic concentration ratio, at surfaces on the NH_3 compensation point (Sutton et al., 1994; Nemitz et al., 2000). Relative humidity is used as approximation for the canopy humidity and controls the cuticular deposition (Sutton et al., 1994). NH_3 concentration is proportional to the NH_3 flux (van Zanten et al., 2010), global radiation enhances the opening width of the stomata (Wesely, 1989), and friction velocity is a measure of the turbulence and has an influence on the aerodynamic and quasi-laminar resistance (Webb, 1970; Paulson, 1970; Garland, 1977; Jensen and Hummelshøj, 1995, 1997). NH_3 was chosen since it is the most abundant compound in modeled ΣN_r (see Fig. E1), and resistance models are most developed for NH_3. Fig. 15 illustrates the results of the sensitivity study.

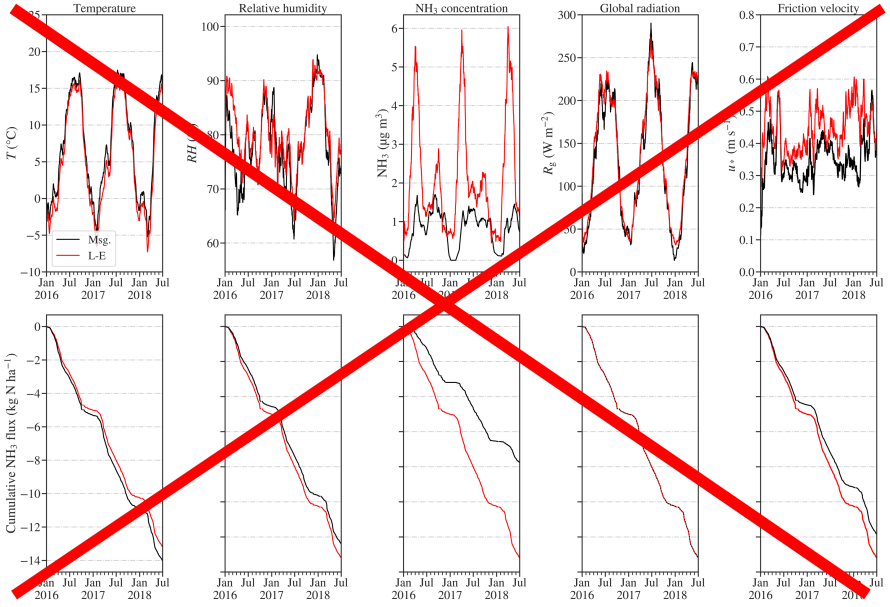

Figure 15. ~~Comparison of modeled (red) and measured (black) input data and their impact on cumulative NH_3 deposition predicted by DEPAC-1D for land-use class spruce forest. The comparison is carried out for air temperature (T), relative humidity (RH), NH_3 concentration, global radiation (R_g), and friction velocity (u_*). A 30 day running average is applied to the input data for better visibility. Modeled input data are the same as used for the LOTOS-EUROS calculations.~~

~~Overall, the agreement of measured and modeled input data is excellent for temperature and global radiation. Values of r^2 are 0.78 for global radiation and 0.97 for temperature. A slight difference is visible for relative humidity in the first half of 2016 with r^2 being 0.67. In case of relative humidity, using locally measured values leads to a reduction in deposition by 6%. The deposition increases by approximately 6% if measured temperature values are used. The impact on deposition using measured global radiation is negligible. u_* of LOTOS-EUROS is systemically higher, and the seasonal pattern is different to values determined from the sonic anemometer. Thus, r^2 is only 0.43 but using measured values for u_* leads only to 10% less deposition. The difference between measured and modeled NH_3 is most pronounced. Modeled concentrations are approximately 2 to 3 times larger in spring and autumn. Furthermore, the seasonal pattern of the measured NH_3 disagrees with the modeled values. Using measured NH_3 concentration reduces the deposition by approximately 42% compared to the modeled deposition. Consequentially, NH_3 concentration is most responsible for the discrepancy of modeled and measured ΣN_r fluxes. The generally high NH_3 concentration also influences its contribution to ΣN_r concentration modeled by LOTOS-EUROS. Figure E1 shows the contribution of the N_r species to modeled ΣN_r as pie charts. LOTOS-EUROS states out NH_3 as the main contributor. NO_x, which is identified as main contributor to ΣN_r from measurements, takes only 22.2% of the modeled ΣN_r. At highest ΣN_r concentration, NH_3 corresponds to almost half of the ΣN_r. Particulate and acidic N_r compounds have a higher contribution than NO_x on average ($\sim$ 41.7%). Their contribution is also higher than values extracted from DELTA measurements, but decreases from lowest to highest ΣN_r concentration. HNO_3 gets even negligible for the highest ΣN_r~~

~~concentration. On average, NH_3 and NO_x account for 58.2% of ΣN_r concentrations whereas DELTA measurements show 73.2% for both gases on average.~~

4 Discussion

4.1 Interpretation of measured concentrations, deposition velocities, and fluxes

Measured half-hourly ΣN_r concentrations are ~~very low in comparison to other sites~~ low relative to sites exposed to agricultural activities or urban environments. On average, we measured 5.~~2~~5 ppb ΣN_r, 1.8 ppb NH_3, and 2.5 NO_x. Wintjen et al. (2020) determined an average ΣN_r concentration level of 21 ppb for a seminatural peatland, Brümmer et al. (2013) measured between 7 and 23 ppb as monthly averages above a cropland site, and Ammann et al. (2012) measured half-hourly ΣN_r concentrations ranging from less than 1 ppb to 350 ppb for a grassland site. Only for certain time periods, ΣN_r concentrations reached significantly higher values. During winter, NO_x increased due to emission from heating with fossil fuels and from combustion processes, for example through traffic and power plants. A generally lower mixing height, which is often observed during winter, also leads to ~~a~~ higher ground-level concentrations of air pollutants. In spring and autumn, higher ΣN_r concentrations can be attributed to NH_3 emission from the application of fertilizer and livestock farming in the surrounding environment (Beudert and Breit, 2010). NH_3 emissions from livestock farming in rural districts around the NPBW are approximately half of the emissions compared to rural districts located in the Donau-Inn valley (Beudert and Breit, 2010), who measured concentrations of NO_2 (~~1.9-4.4~~2.1-4.8 ppb), NO (0.4-1.~~5~~6 ppb) and NH_3 (1.~~3~~4 ppb) at the same site. Those values for NO_2 and NO refer to 1992 until the end of 2008, NH_3 was measured from mid of 2003 to 2005. The low concentration level and seasonal variability of the ΣN_r compounds, in particular NH_3 and NO_2, are in agreement with Beudert and Breit (2010). ~~Values~~ Concentration values of NH_3 and NO_x are expectable for a site, which is some kilometers away from anthropogenic emission sources. ~~Studies like Wyers and Erisman (1998); Horii et al. (2006); Wolff et al. (2010); Geddes and Murphy (2014) dealing with different ΣN_r compounds, which were conducted for different time periods of the year, confirm the seasonal pattern of ΣN_r. Obviously, measured concentration levels were significantly higher since the observed ecosystems were subject of agricultural management or in close proximity to industrial or agricultural emissions.~~ Studies like Wyers and Erisman (1998); Horii et al. (2004); Wolff et al. (2010) conducted measurements of NH_3 and NO_2 above remote (mixed) forests and reported similar concentrations for those gases. In general, a comparison of ΣN_r concentrations and fluxes to other studies is difficult due to the measurement of the total nitrogen. Most studies, which have been published so far, focused only on a single or a few compounds of ΣN_r and are limited to selected sites and time periods of a few days or months. Only a few studies had been focusing on ΣN_r flux measurements using the EC method (see Ammann et al., 2012; Brümmer et al., 2013; Zöll et al., 2019; Wintjen et al., 2020).

Brümmer et al. (2013) measured ΣN_r exchange above an agricultural land. During unmanaged phases, fluxes were between -20 ng N m^{-2} s^{-1} and 20 ng N m^{-2} s^{-1}. Apart from ~~managing~~ management events, fluxes ~~of~~ above the arable field site were closer to neutral conditions compared to our unmanaged forest site, which is mainly characterized by deposition fluxes and is therefore a larger sink for reactive nitrogen. Ammann et al. (2012) measured ΣN_r fluxes above a managed grassland. In the growing season, mostly deposition fluxes ~~up~~ of -40 ng N m^{-2} s^{-1} were measured. The authors reported slightly increased

deposition due to weak NO emission during that phase. Similar to Brümmer et al. (2013), ~~their flux pattern~~ the flux pattern observed by Ammann et al. (2012) is influenced by fertilizer application and thus, varying contributions of N_r compounds, for instance by bidirectionally exchanged NH_3 leading to both net emission and deposition phases of ΣN_r. Flux detection limit is almost equal to Zöll et al. (2019) but slightly higher than upper flux detection limits determined by Ammann et al. (2012) and Brümmer et al. (2013) for the same model. Despite the low signal-to-noise ratio at the measurement site, we were able to investigate the exchange pattern of ΣN_r and could estimate reliable dry deposition sums. To our knowledge, flux measurements of ΣN_r above mixed forests have not been carried out so far. We found that flux magnitude and diurnal flux pattern were similar to observations reported for individual N_r species above forests, e.g. NH_3 (Wyers and Erisman, 1998; Hansen et al., 2013; Hansen et al., 2015), NO_2 (Horii et al., 2004; Geddes and Murphy, 2014), HNO_3 (Munger et al., 1996; Horii et al., 2006), and total ammonium (tot-NH_4^+) and total nitrate (tot-NO_3^-) (Wolff et al., 2010). As seen by the flux values and measurements of individual compounds, deposition prevails in the reported flux pattern, which corresponds to our measurements.

However, under certain circumstances regarding micrometeorology or the availability of ΣN_r compounds large deposition or emission fluxes can be observed. In February 2018, remarkably high ΣN_r concentrations and depositions were measured. Unfortunately, we had no DELTA measurements for February 2018, which could provide insights in the ambient concentrations of individual N_r species, but we found that SO_2 concentrations were unusually high (daily means up to 5.5 μg m^{-3}). During the entire campaign, we measured 1.0 μg m^{-3} SO_2 on average. SO_2 concentrations were slightly correlated with ΣN_r concentrations during the deposition period in February 2018. For the period of enhanced ΣN_r concentrations, a correlation of 0.29 was determined. Since reactions involving SO_2 and N_r species happen at different timescales, and ΣN_r consists of several, chemically different compounds, low correlations are reasonable. SO_2 is rapidly converted to H_2SO_4. The latter is neutralized by NH_3 resulting in the formation of ammonium sulfate $(NH_4)_2SO_4$, a secondary inorganic aerosol. In the presence of HNO_3, NH_4NO_3 is formed by the reaction with NH_3. However, the formation of $(NH_4)_2SO_4$ is favored over the neutralization of HNO_3 at low NH_3 concentrations (Seinfeld and Pandis, 2006; Squizzato et al., 2013). Passive sampler measurements showed a low NH_3 concentration level in February 2018.

If the [NH_4^+]/[SO_2^{-4}] molar ratio is lower than two (Squizzato et al., 2013), the aqueous or solid phase of $(NH_4)_2SO_4$ is prevailed aerosol form. At higher ratios, most of the sulfate is expended, and NH_3 is available for the neutralization of HNO_3. The existence of the solid phases depends highly on humidity, temperature, and the concentration of the constituents (Bok Haeng Baek et al., 2004; Seinfeld and Pandis, 2006; Squizzato et al., 2013). The concentration of NH_3 needed for the formation of solid $(NH_4)_2SO_4$ is higher than values measured at our site, but the threshold depends on micrometeorology, for example, it reduces towards lower humidity levels (Seinfeld and Pandis, 2006). Presumably, not only $(NH_4)_2SO_4$ contributes to ΣN_r during February 2018 but compounds formed at lower ratios, e.g., ammonium bisulfate.

In December 2017, large emission fluxes were measured. Compared to 2016, significant difference in temperature and snowdepth were observed. Figure 16 shows recorded temperature, snow fall, concentrations, and estimated fluxes of ΣN_r from 6 December to 15 December for 2016 and 2017. Here, $\pm$3 days were chosen for filling the gaps in order to keep the short-term variability of the fluxes.

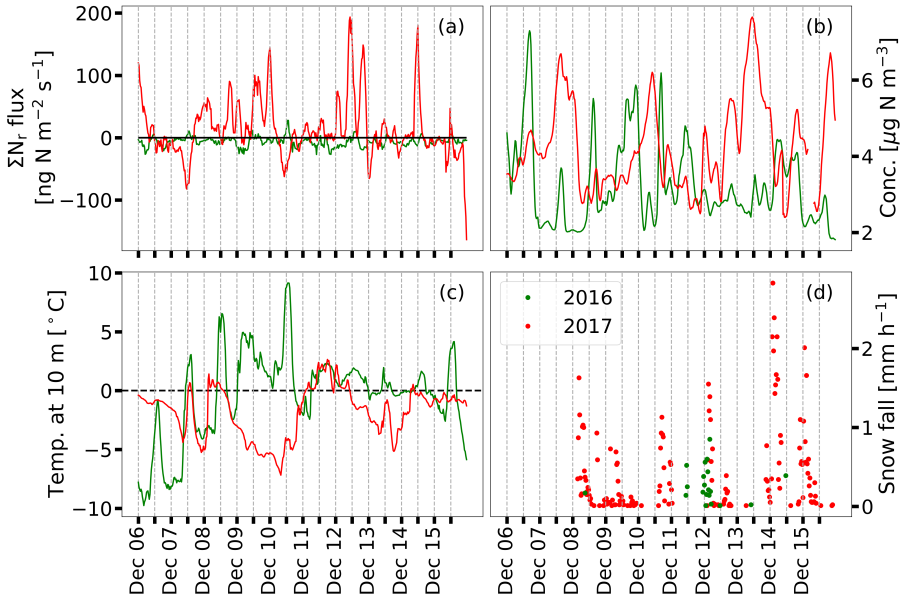

Figure 16. ΣN_r gap-filled fluxes (a), ΣN_r concentrations (b), air temperature at 10 m height above ground (c), and snow fall (d) from 6 December to 15 December for 2016 (green) and 2017 (red). Gaps are filled with the MDV approach with fluxes being in a range of ± 3 days. Fluxes and concentrations of ΣN_r were smoothed with a 3-h-running mean for better visualization.

In 2017, we observed substantial snow fall and a slower varying temperature compared to 2016 leading to significant snow depths compared to 2016. On the 1st of December, 1 cm and 20 cm snow depth were measured in the fetch of the tower for 2016 and 2017, respectively. Two weeks later, snow depth increased to 5 cm and 60 cm, respectively. In addition, temperatures were mostly higher than 0°C in December 2016. In 2017, temperatures were mostly below 0°C and only for one day above 0°C, and global radiation was mostly below 100 W m^{-2}.

Hansen et al. (2013) reported a change in the NH_3 flux pattern from deposition to emission due to the senescing of fallen leaves. The decomposition of litter leading to NH_3 emissions from the forest ground could be responsible for the observed emission fluxes of ΣN_r although the decomposition rate of litter is reduced at lower temperatures. However, the snow pack could act as an insulator and inhibited soil frost penetration. Therefore, decomposition of litter could have been happened under the snow pack. Kreyling et al. (2013) compared different snow treatments and their effect on decomposition. The authors observed nearly no soil frost penetration under snow insulation. The annual cellulose decomposition was greatly reduced for the snow removal treatment ($\sim 46\%$). An increasing mass loss rate was found under a deeper snow pack (Saccone et al., 2013) depending on the type and age of litter (Stef Bokhorst et al., 2013). Due to a small snow depth in 2016, soil frost penetration had a higher potential to reduce the decomposition rate. In addition, temperatures were mostly above the freezing point leading to partial melting of the snow layer, which probably inhibited the release of hygroscopic N_r species such as NH_3. Thus, emission of nitrogen from the soil or the decomposition of leaves was probably reduced compared to 2017. The deeper snow layer promoted microbial activity, and the generally lower temperatures and radiation inhibited a melting of the upper snow

layers. Thus, leakage of N_r species like NH_3 could have happened in December 2017. NO seems to be less responsible for the observed emission pattern following the findings of Medinets et al. (2016). They measured soil NO, N_2O, and CO_2 fluxes at a spruce forest during the 'cold' season (daily average temperature $< 3°C$). They found that NO fluxes were positively correlated to air and soil temperature. Snow cover was not identified as a determining factor for the NO fluxes by the authors, since NO efflux during snow cover and snow free periods were similar. However, the reported snow depth was only 4.6 cm on average. Soil frost penetration could have happened in the topsoil and lowered the NO emissions leading to lower correlation between NO and snow cover. As stated by the authors, different results had been published about the origin of NO emissions from snow covered soils (see Medinets et al., 2016, and references therein). An influence of NO either emitted from the snow pack or the soil cannot be fully excluded. A correlation of the measured fluxes with temperature was not found. This could be related to a time-shift between emission and dropping temperature. It has also to be considered that we measure approximately 30 m above the forest soil, and not only NO contributes ΣN_r. In addition, NO emitted from the forest floor can be converted to NO_2. Thus, low correlations were expected.

Our measurements further indicated that NO_x had the highest contribution to the measured ΣN_r concentrations. At the measurement height, the contribution of NO to NO_x was probably negligible. Median contribution of NO to NO_x is approximately 10% at 50 m. NO exhibits higher concentrations and fluxes close to the forest floor as shown by Rummel et al. (2002). Even if soil NO was converted to NO_2 it could still contribute to the measured ΣN_r flux except for the fraction that is removed by the canopy. NH_3 had strong presence in the ΣN_r concentration within the growing period of the plants, in particular during spring and summer. DELTA results revealed that gaseous N_r species have a high potential to influence the exchange pattern of ΣN_r. The slight increase in HNO_3 and decrease of NH_4^+ can be related to the evaporation of NH_4NO_3 (Wyers and Duyzer, 1997; Van Oss et al., 1998). However, the findings of Tang et al. (2020) revealed that HNO_3 concentrations measured by the DELTA system using carbonate coated denuders may be significantly overestimated (45% on average) since HONO sticks also at those prepared surfaces. Thus, the HNO_3 contributions should be seen as an upper estimate. The comparison of the total N concentrations shows that the TRANC can adequately measure ΣN_r concentration. Obviously, not all components of ΣN_r were included in this comparison, for example, higher oxidized components like N_2O_5 could not be considered. As mentioned in Sec. 2.2, NO_2 had been measured at 50 m. However, Seok et al. (2013) found only slight differences in NO_2 concentrations above the canopy at a remote site. Thus, height differences in NO_2 are likely insignificant. Issues in the temperature stability or CO supply resulting in instabilities in the conversion efficiency of the TRANC, or a reduced sensitivity of the CLD could lead to differences to DELTA+NO_x. DELTA measurements report concentrations integrated over long time periods. Concentration peaks could not be collected sufficiently by the coated surfaces. The latter are exposed to environmental influences like temperature and moisture, and their sensitivity may reduce over time.

~~A few studies measured N_r compounds above (mixed) forests. Hansen et al. (2015) measured NH_3 fluxes between -60 and 120 ng N m^{-2} s^{-1} above a deciduous forest. Due to the selected measuring time of the year, emission of NH_3 through fallen leaves had an influence on measured fluxes leading to probably less deposition during late summer and autumn. High emission fluxes were also measured at our measurement site in December, which could be induced by the decomposition of fallen leaves. Pictures from the 50 m platform showed a substantial snow cover for the whole footprint. The snow layer~~

acts as an insulator for the soil, prevents soil from frost penetration effectively, and thus protects plants and microorganisms (Alvin T. Bleak, 1970; Vogt, Kristiina A. and Grier, Charles C. and Meier, Calvin E. and Keyes, Michael R., 1983; T. R. Moore, 1983; Ine

900 Thus, processes, which lead a decomposition of leaves, needles or lichens by microorganisms, can happen under the snow layers with substantial losses, especially for lichens (Taylor, Barry and Jones, H., 1990). The authors further discovered an increase in nitrogen concentration in the investigated samples. Since we observed a slower varying air temperature with temperatures below zero for 2 to 3 days followed short periods of less than one day with temperatures close to zero degrees and even higher, the accumulation of nitrogen under the snow layer and a immediate release due to freeze-thaw cycles probably happened. The

905 determined order of magnitude by Hansen et al. (2015) is comparable to our flux measurements.

Since we also measured other N_r compounds such as HNO_3 and NO_2, which exhibit mostly deposition (Horii et al., 2004, 2006), deposition fluxes predominated at our measurement site compared to Hansen et al. (2015). NO is mainly observed as emission from soil if it is produced through (de)nitrification processes (Butterbach-Bahl, K. and Gasche, R. and Breuer, L. and Papen, H., 1997; Ros The contribution of NO to ΣN_r is probably negligible because NO is rapidly converted to NO_2 in the presence of O_3 within

910 the forest canopy, especially close to the ground (Rummel et al., 2002; Geddes and Murphy, 2014). Therefore, a comparison with chamber measurements, which could had been conducted at the ground for measuring N_r compounds was considered as less useful due to the large footprint of the flux measurements, fast conversion processes within the forest canopy, and uptake possibilities like leaf surfaces for N_r compounds (e.g., Wyers and Erisman, 1998; Rummel et al., 2002; Sparks et al., 2001; Geddes and Mu

The findings of DELTA measurements revealed that NO_x, in particular NO_2, is the most abundant compound in ΣN_r

915 followed by NH_3. Both gases account for 73.2% of ΣN_r. The values of NO_x and NH_3 differ significantly from values proposed by Zöll et al. (2019), in particular NO_x. This is related to the different periods, which were considered for averaging. Zöll et al. (2019) reported values for summertime. In this study, values are influenced by seasonal impacts. It has to be considered that the contribution of NH_3 differs with increasing ΣN_r concentration whereas the contribution NO_x remain almost similar. At the highest average ΣN_r concentration, we determined a substantial contribution of particulate and acidic N_r

920 species, which is higher than the influence of NH_3 on ΣN_r at that concentration level. Findings of Tang et al. (2020) had shown that HNO_3 concentrations measured by DELTA system using carbonate coated denuders may be significantly overestimated (45% on average) since HONO sticks also at those prepared surfaces. Thus, the HNO_3 contributions should be seen as an upper estimate.

Consequentially, other compounds such as NO_2 and HNO_3 are also important for the interpretation of the ΣN_r flux

925 pattern. NO_2 deposition and emission fluxes, which depend on the concentration level, were observed during the day by Horii et al. (2004) above a mixed forest, and mostly deposition of NO_2 during the night. NO_2 exhibits also a bidirectional exchange pattern in natural ecosystems (Horii et al., 2004; Geddes and Murphy, 2014; Min et al., 2014). The diurnal cycle of NO is reversed to NO_2 during the day and is almost neutral with a tendency of slight emission during the night (Horii et al., 2004; Geddes an It has to be taken into account that NO_2 is removed from the atmosphere by the reaction with O_3. During the day and night NO_3

930 reacts with NO_2 to N_2O_5. The latter can react with H_2O to HNO_3. HNO_3 is an effective removal for NO_2 and has a significant impact on the measured deposition flux (Munger et al., 1996). However, Min et al. (2014) stated that peroxy nitrates and akyl nitrates are also responsible for the removal of NO_x, apparently more important than HNO_3. Horii et al. (2006) measured all

~~oxidized nitrogen species (NO_y), which is the sum of NO, NO_2, NO_3, dinitrogen pentoxide (N_2O_5), HNO_3 + peroxyacetyl nitrate (PAN), other organic nitrates, and aerosol nitrate such as NH_4NO_3, at the same site as Horii et al. (2004). They measured only deposition fluxes for NO_y. Fluxes were mostly below -40 ng N m^{-2} s^{-1}, but could achieve up to -80 ng N m^{-2} s^{-1}. HNO_3 fluxes were almost as high as the NO_y fluxes. Munger et al. (1996) did also NO_y flux measurements above the same forest some years earlier and took measurements at less polluted spruce forest. At the latter location, only slight deposition of NO_y occurred. At the former location, results are similar to Horii et al. (2006). It shows that HNO_3 seems to have a significant influence on the deposition of ΣN_r even at sites exhibiting a low concentration level of ΣN_r compounds like NO_2.~~

~~The observed daily cycle, which exhibits low negative or neutral fluxes during the night, increasing deposition in the morning, and decreasing deposition in the evening, is in agreement with other studies dealing with ΣN_r compounds above different forest ecosystems. For example, Wyers and Erisman (1998) measured similar daily cycles of NH_3 above a coniferous forest, Munger et al. (1996), Horii et al. (2006), and Geddes and Murphy (2014) reported daily patterns of NO_y above mixed forests, Horii et al. (2006) did similar observations for HNO_3, and Wolff et al. (2010) observed higher deposition of total ammonium (NH_4^+) and total nitrate NO_3^- fluxes, the aqueous phase of NH_4NO_3, above a spruce forest during the day.~~

~~Apparently, fluxes measured at our location have high NO_x, or, more precisely, a high NO_2 fraction, a generally low NH_3 fraction, which is higher for low ΣN_r fluxes, and considerable fraction of particulate and acidic N_r species, especially for high ΣN_r fluxes. In principle, the order of magnitude of the ΣN_r flux is similar to values reported in the above-mentioned publications. Even if other NO_y compounds are not the main flux contributors, they change the composition of the ΣN_r flux. NO_y compounds have an influence on the NO-NO_2-O_3 cycle and on the reaction pathways of NH_3 and HNO_3. These are not limited to gas phase reactions (Meixner, F. X., 1994), but also gas-particle interactions (Wolff et al., 2010) can occur. Thus, individual measurement devices are needed to measure single N_r species for a precise quantification of the ΣN_r flux. Implementing such a setup will be challenging due to high technical requirements of the instruments in case of technical complexity, dimensions, and power consumption. Running such a setup for at least a year should also be considered for a representative data set.~~

As shown in Fig. S5, median v_d of ΣN_r were low compared to deposition velocities determined for NH_3 or HNO_3 above other forests. Values range between 1.1 and 2.2 cm s^{-1} for NH_3 (see Schrader and Brümmer, 2014, and references therein) and between 2 and 8 cm s^{-1} for HNO_3 (S.C. Pryor and Klemm, 2004; Horii et al., 2006; Farmer and Cohen, 2008). v_d values reported for NO_2 are closer to v_d of ΣN_r. In the literature, v_d is between 0.015 and 0.51 cm s^{-1} for NO_2 (e.g., Rondon et al., 1993; Horii et al., 2004; Breuninger et al., 2013; Delaria et al., 2018; Delaria et al., 2020). For tot-NH_4^+ and tot-NO_3^-, mean v_d of 3.4 cm s^{-1} and 4.2 cm s^{-1} were determined by Wolff et al. (2010), respectively. Since the analysis of the different N_r species contributing to the ΣN_r concentrations states NO_2 as the dominant compound, a similarity of v_d for ΣN_r to deposition velocities of NO_2 can be excepted. It further implicates a lower contribution of NH_3 than NO_2 to the measured flux.

4.2 Influence of micrometeorology and nitrogen concentrations on deposition and emission

4.2.1 Influence of R_g on ΣN_r exchange

Figure S7 and S8 showed that the shape of v_d and other micrometeorological variables is strongly correlated to R_g. ~~Overall, the shape and maximum deposition of the daily cycles shown in Fig. 6 is mostly driven by~~. ~~g~~Global radiation had been identified ~~, which acts~~ as ~~primary~~ an important 'driver' for the ΣN_r exchange, recently verified by an artificial neural network approach conducted by Zöll et al. (2019). The word 'driver' is a paraphrase of the expression 'controlling input variable' (Moffat et al., 2010). Drivers are identified by their correlation with the flux. As a remark, correlations could also be influenced by other parameters, which have not or could not considered by Zöll et al. (2019), for example chemical interactions of components contributing to ΣN_r.

As shown by Zöll et al. (2019), ΣN_r and CO_2 fluxes exhibited a similar daily cycle and showed a strong dependence on R_g during summer. The latter controls the opening of the stomata (Jarvis, 1976), i.e. lowers the stomatal resistance. Thus, photosynthesis controlling the CO_2 exchange through stomatal pathway appears to be the mechanism for controlling the ΣN_r exchange as compounds like NO_2 (Thoene et al., 1996) or NH_3 (Wyers and Erisman, 1998) are taken up by the stomatal pathway, too. However, ΣN_r compounds are not willingly absorbed by the plants as seen by the light response curves of Zöll et al. (2019, Fig. 5). The light response curve of ΣN_r has a reversal instead of a saturation point as observed for CO_2 (Zöll et al., 2019). Consequently, a second mechanism, the stomatal compensation point firstly proposed by Farquhar et al. (1980) likely controls the uptake of the ΣN_r compounds. Basically, if the stomatal concentration is lower than the ambient concentration, deposition is observed. Thus, both parameters, the stomatal resistance and the stomatal compensation point, which are regulated by R_g and concentration, respectively, affect the uptake of ΣN_r. As further shown by Zöll et al. (2019), other parameters like u_* were not identified as important drivers for ΣN_r. Photochemistry and stomatal control appear to be more important than turbulent mixing. Radiation changes the composition of ΣN_r due to the formation of O_3. In addition, R_g had an influence on u_* as seen by their similar shapes in daily cycle (Fig. S7 and S8). The low correlations of ΣN_r fluxes to concentration for most of the selected u_* ranges show that atmospheric turbulence had a generally low influence on nitrogen deposition at the measurement site. Thus, u_* adds almost no additional information to the ΣN_r exchange and was not identified as important controlling factor for the ΣN_r exchange from July to September by Zöll et al. (2019). Similar conclusions can be drawn for temperature and relative humidity. They are also affected by light/energy input into the ecosystem and follow a similar diurnal pattern. It shows that R_g contains most of the information for the explanation of the ΣN_r fluxes.

It has to be noted that the study was conducted for ΣN_r at the same natural, unmanaged site from July to September. Micrometeorological parameters were controlled by natural processes. The low response to micrometeorological parameters may also related to other processes influencing the composition of ΣN_r, to opposing effects on N_r species, or effects happened on a shorter time scale such as molecular interactions between the ΣN_r compounds. R_g was not identified as primary controlling factor for NH_3 by Milford et al. (2001). Milford et al. (2001) measured NH_3 fluxes above moorland, which has a generally higher humidity level than our measurement site. They concluded that NH_3 exchange is mostly driven by canopy temperature, wetness, and ambient concentrations. Radiation was not identified as primary controlling factor by the authors. They found higher deposition of NH_3 through the cuticular than through the stomatal pathway. However, Zöll et al. (2019) found only

minor improvements in their driver analysis if water vapor pressure deficit was considered as secondary driver. Additionally, we found that v_d was reduced for high ambient humidity and wet leaf surfaces. Since we measured NH_3 indirectly by the TRANC and above an ecosystem characterized by lower humidity than a peatland, R_g favoring the exchange through the stomatal pathway appears to be more important for ΣN_r at the measurement site.

4.2.2 Influence of N_r species on measured v_d

~~The authors~~ Zöll et al. (2019) further identified ΣN_r concentration as secondary driver for the ΣN_r deposition. ~~The influence of concentration on ΣN_r fluxes and its compounds had been reported in several studies (e.g., Brümmer et al., 2013; Zöll et al., 2016).~~ The impact of increasing concentration on nitrogen (deposition) fluxes is well documented, for example, by Ammann et al. (2012) and Brümmer et al. (2013) for ΣN_r, by Horii et al. (2006) for NO_y, Horii et al. (2004) for NO_x, and by Zöll et al. (2016) for NH_3. We measured almost the same ΣN_r concentration for each season. Consequently, it was not only the change in the overall ΣN_r concentration that influences v_d. The changes in the contribution of the components of ΣN_r had a higher influence on v_d of ΣN_r than the overall concentration. ~~Also, micrometeorological parameters such as relative humidity and temperature favor the exchange of ΣN_r compounds (Wyers and Erisman, 1998; Milford et al., 2001; Wolff et al., 2010; Wentworth et al., 2016). Global radiation was not identified as primary controlling factor for NH_3 by Milford et al. (2001). They found that NH_3 exchange was mostly driven by canopy temperature, canopy wetness, and ambient concentrations. Thus, global radiation favoring the exchange through the stomatal pathway appears to be an important controlling factor under low NH_3 concentrations.~~

The higher nitrogen deposition in ~~March and~~ April 2017 (Fig. 5) compared to ~~spring~~ April 2018 ~~could be related to an enhanced photosynthetic activity in spring 2017. Average temperature was approximately 5°C in March 2017, and during March 2018 average temperature was only 0.3°C. Mid of April 2018, an immediate increase of temperature was observed leading to temperatures comparable to April 2017. Consequentially, the wider opening of the stomata was most likely shifted to mid or end of April 2018 which is confirmed by the similar shape of the daily cycle for May 2017 and 2018.~~ was mainly related to gaps in flux time series. In 2018, we had no flux measurements from mid of April to the beginning of May. During that time, foliage began in 2018 providing uptake of ΣN_r compounds. Increased plant activity was caused by continously, high radiation values during daylight ($> 400\,W\,m^{-2}$) leading to higher temperatures in April 2018 ($\sim 11.0°C$) than in April 2017 ($\sim 6.0°C$). We further observed high NH_3 concentrations measured by passive samplers and the DELTA system for the same time. Elevated NH_3 concentrations were likely caused by emissions from agricultural management in the surrounding region. In 2017, leaf emergence began in early May. Thus, measured N deposition would have been higher in April 2018 than a year before presumably related to a lower stomatal resistance in 2018. Almost equal patterns of v_d and $R_{c,eff}$ were determined for May 2017 and 2018. The conditions for uptake of ΣN_r by the canopy were comparable. Consequently, the different contributions in NH_3 and conditions in radiation and temperature strongly affected v_d and $R_{c,eff}$ and therewith the deposition of ΣN_r. ~~Also, ΣN_r concentration was approximately 3.3 ppb on average for April 2018 and approximately 6.3 ppb a year before. Higher concentration level probably induced by agricultural management in the surrounding region likely favoured N deposition, too.~~

In the summer of 2016 and 2017, differences in the ΣN_r median concentration were lower than 1 ppb. No remarkable differences in micrometeorology were found between summer 2016 and 2017. Figure 3 revealed that the contribution of components to ΣN_r differed between the investigated time periods. From July to September 2017, the mean NH_3 concentration was about 0.3 μg N m^{-3} lower than a year before. HNO_3, NH_4^+, and NO_3^- were remarkably low in July 2017 compared to July 2016. ~~Deviations in deposition during summer 2016 and 2017, especially from July to September, were probably related to different ΣN_r concentration levels. ΣN_r concentration was 4.7 ppb for summer 2016 and only 2.8 ppb on average for summer 2017. Standard deviations were almost similar demonstrating comparable variability in concentrations. Almost the same average and pattern were investigated for humidity and temperature in July and August. It seems that an enhanced concentration level of ΣN_r compounds were most responsible for discrepancies in the observed fluxes confirming results of Zöll et al. (2019), who identified ΣN_r concentration as an important driver for ΣN_r exchange at the same site.~~. In conclusion, the deviations in the median deposition were not related to differences in the ΣN_r concentration. The differences in the composition of ΣN_r affected v_d, in particular the canopy compensation point, more and therewith the uptake of ΣN_r.

However, we found that higher ΣN_r concentrations led to lower $R_{c,eff}$ during no precipitation around noon, which could be related to an increased energy input or/and to an increased contribution of nitrogen compounds like NH_3 to ΣN_r. Since the impact of concentration on $R_{c,eff}$ was comparatively low, it was superimposed by slight differences induced by R_a and R_b. Thus, ΣN_r concentration had almost no measurable net effect on v_d. Since we had measured the ΣN_r exchange in a low nitrogen environment, the influence of the stomatal compensation point on the uptake of N_r species may be reduced. Zöll et al. (2019) calculated a light response curve of ΣN_r for the same site. The increase in deposition got lower for R_g between 300 and 500 W m^{-2} and reached a reversal point around 600 W m^{-2}. We found slight differences in $R_{c,eff}$ for the concentration threshold around noon, at times with the highest radiation. It shows that a stomatal compensation point exists but its influence is limited by the low, ambient nitrogen concentrations and radiation.

4.2.3 Seasonal changes in ΣN_r uptake capacity

Within the period of high incident radiation, in particular from May to September, a distinct diurnal pattern for v_d was observed, and no precipitation, high temperatures (> 14.6°C), low relative humidity ($< 74.0\%$), and dry leaf surfaces, were found to enhance the surface uptake, presumably through the stomatal pathway, of nitrogen during daylight. The observed differences in v_d for relative humidity and temperature were mostly related to R_a and R_b. $R_{c,eff}$ showed only a slight response to lower air humidity. Responses to the chosen temperature threshold and to dry leaf surfaces were not found.

During the rest of the year, no diurnal pattern was found under dry conditions (no precipitation) since stomata were likely closed, or requirements for stomatal deposition were not fulfilled (stomatal compensation point). Since we still observed a low, non-zero v_d but also short phases of ΣN_r emission during seasons with lower radiation, cuticular, soil, and turbulent driven processes were likely to be responsible for the ΣN_r exchange. In periods of reduced plant activity, for instance in winter and autumn, the uptake through the stomatal pathway was greatly reduced or even inhibited due to reduced radiation or leaf area

surfaces. Besides stomatal deposition, cuticular deposition is also an important pathway for ΣN_r compounds, which likely deposit on wet surfaces such as NH_3, HNO_3 or NH_4^+.

However, v_d was lower under wet conditions. Presumably, requirements for cuticular deposition were not fully met. Measurements of ΣN_r were conducted several kilometers away from nearby sources, and thus hydrophilic ΣN_r components could be washed out before air masses reached the site. We showed that the contribution and concentrations of N_r species, which can deposit on wet leaf surfaces, was comparatively low at the measurement site. Furthermore, those species were only indirectly measured, and wet leaf surfaces could be already saturated with water soluble N_r species leading to a high cuticular compensation point. These issues may reduce the cuticular contribution to exchange processes with the canopy. Presumably, cuticular deposition was probably not as important as stomatal deposition during the timeframe of high incident radiation, in particular from May to September. Stomatal deposition seems to be more important than other in-canopy uptake processes for the ecosystem in close proximity to the measurement site for those month.

~~Therefore, an in-depth investigation of relative humidity, temperature, leaf surface wetness, and concentration was conducted. The analysis of Fig.8 has shown that dry conditions, induced by higher temperatures and low relative humidity, favour ΣN_r deposition. Higher concentrations values lead to higher deposition values through the entire daily cycle. The impact of increasing concentration on nitrogen (deposition) fluxes is well documented, for example, by Ammann et al. (2012) and Brümmer et al. (2013) for ΣN_r, by Horii et al. (2006) for NO_y, Horii et al. (2004) for NO_x, and by Zöll et al. (2016) for NH_3. The effect of temperature on the ΣN_r fluxes is most pronounced during daytime. Higher temperatures increase the opening size of the stomata leading to increased photosynthetic activity.~~

The statement holds for the estimated fractions of N_r species found for this ecosystem. Ecosystems which are exposed to enhanced concentrations of NH_3 or nitrogen aerosols may differ in their uptake capacities. Wyers and Erisman (1998) measured highest NH_3 deposition if the canopy has a high water storage level (CWS) (> 2 mm). The deposition efficiency was reduced if CWS was higher than 0.25 mm but lower than 2 mm. By comparing different measurement years, they found differences in the deposition efficiency even if the canopy was saturated with water. They attributed the effect to the solubility of NH_3 in the water film. If canopy gets drier, evaporation of water occurs and the concentration of NH_3 increases in the water film. The cuticular resistance increases and deposition of NH_3 is reduced. Even emission of NH_3 was observed by Wyers and Erisman (1998), especially during the day when the canopy was dry, and NH_3 exchange was bidirectional. They showed that stomatal resistance was higher than canopy resistance. The authors identified cuticular deposition as more important for NH_3 as stomatal deposition.They measured an average NH_3 concentration of 5.2 μg m^{-3}. We measured 0.65 μg m^{-3} on average and found that the contribution of NH_3 to ΣN_r was comparatively low at the measurement site. If contribution of NH_3 or other soluble N_r species to ΣN_r is comparatively low, cuticular deposition is most likely reduced under wet conditions. The authors proposed that even under low ambient humidity leaf surfaces can exhibit high humidity due to the accumulation of particles. In case of conifer needles, Burkhardt et al. (1995) showed that particles deposit close to their stomata. Most of them are hygroscopic. Therewith, cuticular deposition seems to be possible even under low ambient humidity. However, our measurement site was several kilometers away from potential (anthropogenic) emission sources. Concentrations of NO_3^-, NH_4^+, sulphur dioxide (SO_2), and NO_x were comparatively low at the site, in particular during summer. Thus, stomatal deposition appears to be more

important for ΣN_r under high temperatures, low relative humidity, and no precipitation. This conclusion is valid for months with sufficient light/energy input leading to an increased plant activity, i.e. from May to September. Within the other seasons, aerosol concentrations originating from natural or anthropogenic emission sources are probably higher resulting in a higher particle density on leaf surfaces promoting cuticular deposition.

Wolff et al. (2010) observed high deposition of tot-NH_4^+ and tot-NO_3^- during sunny days. During rain or fog, tot-NO_3^- exchange was almost neutral and emission was observed for tot-NH_4^+. They measured median concentration of 0.57, 0.12, 0.76, and 0.45 μg m^{-3} for NH_3, HNO_3, NH_4^+, and NO_3^-, respectively. For the September months, we measured average concentrations of 0.76, 0.46, 0.50, and 0.78 μg m^{-3} for NH_3, HNO_3, NH_4^+, and NO_3^-, respectively. Measured tot-NO_3^- and tot-NH_4^+ of Wolff et al. (2010) exhibited a higher particle than gaseous contribution. At our measurement site, the gaseous contribution was higher than the values reported by Wolff et al. (2010). Median deposition velocities of tot-NO_3^- and tot-NH_4^+ were higher than values measured for ΣN_r at our site, and they found that deposition was mainly driven by aerodynamic resistance rather than by surface resistance, in particular during periods of high radiation. It shows that changes in the contribution of N_r species to ΣN_r lead to different deposition pathways.

~~Wolff et al. (2010) observed higher deposition for total ammonium and total nitrate under dry conditions, which correspond to temperatures higher than 15°C and relative humidity below 70%. During foggy or rainy conditions, deposition was close to neutral or even emission occurred. Their ranges and corresponding limits for temperature and humidity are comparable to the values examined at our site.However, Wyers and Erisman (1998) reveal that NH_3 deposition is maximized if canopy exhibits a high canopy water storage level ($>$ 2 mm). They found that leaf surfaces could act as a sink and as a source of NH_3. An elevated relative humidity level increase the thickness of the water layer covering the leaf surface, and thus wet leaves act as an effective removal of atmospheric NH_3 until a certain equilibrium in concentration is reached. Thus, we examined the influence of precipitation on measured fluxes. A separation of fluxes into different precipitation classes is shown in Fig. F1. In general, median deposition gets lower with increasing precipitation, and emission fluxes can be found in classes with significant rainfall (>0.5 mm h^{-1}). Strongest dry deposition occurs mainly during dry conditions, which is in contrast to the observations of Wyers and Erisman (1998). It has to be considered that the catchment, in which the flux tower is located, has a size of approximately 0.69 km^2 (Beudert and Breit, 2010) and is larger than the catchment of Wyers and Erisman (1998). Also, the surrounding forested area is much larger and the entire area is mountainous. The forest stand is relatively young since it is recovering from a bark beetle outbreak in the 1990s and 2000s (Beudert and Breit, 2014). Wyers and Erisman (1998) determined an average NH_3 concentration of 5.2 μgm^{-3} and median concentration of 3.5 μgm^{-3}. Their values are at least two times higher than measured NH_3 concentrations at our site. Presumably, if NH_3 concentrations are low, ΣN_r dry deposition seems to be favored by dry conditions. Also, Wolff et al. (2010) measured low NH_3 concentrations at their forest site. Figure F1 also demonstrates that concentrations of ΣN_r are elevated if leave surfaces are dry. It shows that wet deposition is important for the uptake of ΣN_r compounds at our measurement site. As mentioned in Sec. 2.1, we measured substantial rainfall during 2.5 years at our measurement site. Due to the remoteness of the measurement site, air mass transport starting at potential nitrogen~~

~~emission sources has to overcome long distances before reaching the site. Thus, a significant amount of ΣN_r is probably deposited outside the footprint of the flux tower during rainy periods.~~

4.3 Uncertainties ~~in applied gap-filling approaches~~ in dry deposition estimates

Fluxes determined with the eddy-covariance method are exposed to systematic and random errors. Systematic errors are related to the design of the measurement setup and the instruments, data processing steps including calibration, tilt correction, detrending, and corrections due to low and high-frequency attenuation (Wintjen et al., 2020), and advection fluxes originating preferentially from non-homogeneous surfaces. Uncertainties from the measurement setup were likely caused by an insufficient pump performance, issues in temperature stability of the TRANC and CLD, sensitivity loss of the CLD, and problems in the O_2 and CO supply. Therefore, regular maintenance and continuous observation of instrument performance parameters such as TRANC temperature and flow rate were made. With manual screening of measured half-hours and the recording of these parameters, low-quality half-hours could be effectively excluded from analysis. A basic assumption for the EC method is that the terrain needs to be flat, and the canopy height and density should be uniform (Burba, 2013). These site criteria are not perfectly fulfilled at our measurement site. The site is located in a low mountain range and tree density is rather sparse south of the flux tower. Such diverse terrain characteristics could lead to unwanted turbulent fluctuations (non-stationarity of time series), which introduce noise in the cross-covariance function.

Random errors are mostly related to turbulence sampling errors (Finkelstein and Sims, 2001; Hollinger and Richardson, 2005; Loescher et al., 2006). An inadequate sample size results in an incomplete sampling of large-scale eddies, which compromises the cross-covariance of the vertical wind and the scalar of interest. The method of Finkelstein and Sims (2001) allows to quantify the random error of the measured fluxes ($F_{\mathrm{unc,meas}}$). In order to determine the effect of the random flux error on the estimated dry deposition sums, we used the method proposed by Pastorello et al. (2020):

$$F_{\mathrm{unc,cum_i}} = \sqrt{\Sigma_i^n (F_{\mathrm{unc,meas_i}})^2} \tag{7}$$

Using Eq. (7), we determined an uncertainty of 11 g N ha^{-1} for 2016/2017 and 21 g N ha^{-1} for 2017/2018 due to insufficient sampling of turbulent motion. The uncertainty related to u_* filtering is difficult to quantify since common approaches for estimating u_* thresholds, i.e. Moving Point Threshold (Reichstein et al., 2005) or Change Point Dectection (A.G. Barr et al., 2013), are designed for CO_2. Applying these threshold detection algorithms to N_r species is not suggested since their exchange patterns are characterized by a higher variability for different time scales. The chosen u_* threshold of 0.1 cm s^{-1} should be interpreted as minimal filter to exclude periods of insufficient turbulence (for details see Zöll et al., 2019, Sec. 2.4). In combination with the MDV approach as gap-filling method, the applied threshold may lead to biased dry deposition sums. As seen in Fig. 11, the difference between dry deposition sums was within the error range of the dry deposition sum. Presumably, not only small fluxes were removed from the analysis by the u_*-filter. Figure 7 shows that large fluxes were observed at low turbulent conditions. We further showed that the contribution of the water vapor correction was negligible. Brümmer et al. (2013) and Ammann et al. (2012) reported a low contribution of the correction to their observed TRANC fluxes.

We calculated the uncertainties for the annual sums as standard error of the averaged flux, which is appropriate in case of the MDV method. We showed that the results when applying the MDV method were independent of the applied temperature,

humidity, and precipitation criteria. The differences in v_d to micrometeorology were observed for a limited time period of the year. During other months, we found no influence of temperature, humidity, and precipitation on diurnal pattern of the ΣN_r fluxes. Thus, the dry deposition sums were almost equal for the applied micrometeorological criteria. The difference between the estimated dry depositions for the measurements was likely related to the large deposition occurring in February 2018. Presumably, the difference would have been even higher if flux measurements during the foliage period were available. It highlights the important role of radiation and the contribution of nitrogen compounds to the ΣN_r exchange at measurement site.

Using the MDV approach is recommended for gaps spanning over not more than a few days. Using statistical gap-filling approaches such as LUT, NLR, or MDV (Falge et al., 2001) for longer gaps, is not suggested. Statistical methods like MDV assume a periodic variability with high auto-correlation of fluxes. This assumption is mostly valid for CO_2, which have a distinctive daily cycle. Reactive gases mostly do not exhibit a clearly predictable flux pattern. Their flux variability depends on micrometeorological conditions and their chemical and physical properties sometimes leading to instationarities in data time series. Gap-filling methods based on inferential modeling or artificial neural networks may be a further valuable option, especially for long-term gaps - if models would be available. Monthly averages estimated for each half-hour do not account for short-term deposition or emission events. Since we measured mostly ΣN_r deposition at the measurement site, the applied gap-filling method for long-term gaps is somewhat justified. Also, biases due to the usage of statistical methods can be eliminated, for example, the shown effect of the u_*-filter on MDV. However, exchange patterns of every N_r species, at least the most important ones such as NO, NO_2, HNO_3, NH_3, NH_4^+, and NO_3^- have to be accurately modeled. In case of NH_3, stomatal and cuticular exchange is well documented (see references in Sec. 2.4). Investigations on other nitrogen compounds are still needed. As mentioned in Sec. 2.4, there are significant uncertainties in compensation points of NO_2 and HNO_3.

The results of wet deposition have shown that dry deposition contributes approximately one third to the total deposition, which is comparable to results of canopy outflow measurements conducted at the same site. The comparison of TRANC measurements with canopy outflow measurements will be shown the second part of this study. Wet deposition results from both sampler types were almost similar. It shows that deposition of sedimenting organic and inorganic particles is not relevant at the site.

4.4 ~~Comparison of different methods for calculating N budgets~~

4.4.1 ~~Uncertainties of flux measurements and gap-filling approaches~~

~~The different gap-filling approaches led to almost the same deposition after 2.5 years. The advantage of inferential modeling is that long gaps in flux time series can be filled. This is not possible with MDV or other recently published gap-filling methods (e.g., Falge et al., 2001; Reichstein et al., 2005; Moffat et al., 2007; Wutzler, T. and Lucas-Moffat, A. and Migliavacca, M. and Knauer, J. because the latter are optimized for inert gases. Statistical methods like MDV assume a periodic variability of fluxes. This~~

assumption is mostly valid for inert gases, which have a distinctive daily cycle. Reactive gases mostly do not exhibit a predictable flux variability. Their flux variability depends on micrometeorological conditions and their chemical and physical properties sometimes leading to instationarities in the data time series. Therefore, the application of statistical methods is rather questionable. However, also DEPAC-1D has some issues, which are not solved or implemented yet. For example, particle deposition is not considered, the implementation of N_r species like HNO_3 is relatively straightforward compared to NH_3, an exchange path with soil is not implemented yet, and the cuticular compensation point of NH_3 is underestimated under high concentrations and temperatures (Schrader et al., 2016). DEPAC-1D fluxes during winter were close to neutral whereas TRANC measurements show slight deposition and even emission under special circumstances. Further comparison to flux measurements at different sites can help to solve these issues. Gap-filling techniques based on artificial neural networks may be a further valuable option - if available.

Uncertainties of the ΣN_r fluxes were estimated with the method by Finkelstein and Sims (2001). The uncertainties of gap-filled fluxes through MDV were calculated by the error of the average. Gap-filled fluxes through DEPAC-1D were not assigned with an uncertainty by the model. As an approximation, we assigned DEPAC-1D fluxes with a relative error of 20%. This relative error is a guess based on uncertainties in the implementation of DEPAC-1D and of the input data. In the following, possible uncertainties sources are mentioned. Considering the input data needed for site based modeling, uncertainties in concentration of N_r compounds and turbulence measurements seem to have the largest impact on the modeled fluxes. Besides some power outages of a few days, instruments for recording meteorological data were operating continuously. The agreement with modeled data from the ECMWF for the investigated grid cell was excellent (Fig. 15). Thus, uncertainties in meteorological data have a negligible impact on the modeled fluxes. Due to the low time resolution of DELTA and passive samplers, short-term variability is missing in NH_3 and HNO_3 concentration time series, especially for HNO_3. NH_3 measurements were conducted by the NH_3 QCL, which allows to measure NH_3 with a high time resolution. The low deposition fluxes modeled by DEPAC-1D during winter are caused by measurement outages of QCL, which led to a missing variability in concentrations of NH_3. Thus, missing values had to be replaced by monthly averages measured by passive and DELTA samplers. Lower temperatures, which are (at mid-latitude sites) directly related to high stomatal resistances, also lead to low deposition values during winter. Since NH_3 concentration level is generally low during winter and assigned with a low variability as found by measurements, this procedure is reasonable for a limited time period. Differences in half-hourly fluxes during these times are difficult to interpret due to the low time resolution of the input data.

No fast recording of HNO_3 was available at the measurement site. Since HNO_3 has also a significant contribution to the ΣN_r flux, using fast-response measurements of HNO_3 (Farmer et al., 2006; Farmer and Cohen, 2008) in DEPAC-1D or other site-based inferential deposition models would be a much needed approach for further campaigns. At the moment, the implementation of HNO_3 in DEPAC is relatively simple (see Sec. 4.3). At agricultural sites, such an instrumentation for HNO_3 is not needed since exchange processes of ΣN_r are most likely driven by a high NH_3 background concentration.

Uncertainties also arise from the measurement setup: Insufficient pump performance, issues in temperature stability of the TRANC and CLD, sensitivity loss of the CLD, and problems in the O_2 and CO supply. Therefore, regular maintenance and continuous observation of instrument performance parameters such as TRANC temperature and flow rate were done.

With manual screening of measured half-hours and the recording of these parameters, compromised half-hours could be effectively excluded from analysis. Since certain sonic anemometers give an incorrect sonic temperature signal, which can be biased or exhibit a non-linear relationship (Aubinet et al., 2012), sonic temperature was adjusted with the averaged temperature determined from measurements at 20 m and 40 m. Incorrect high-frequency temperature measurements affect the high-frequency damping, and therefore the determination of damping factors for ΣN_r. Periods of insufficient turbulence were ruled out with a threshold for u_* lower than 0.1 ms^{-1} (for details see Zöll et al., 2019, Sec. 2.4) and with the criteria of Mauder and Foken (2006). A basic assumption for the eddy covariance method is that the terrain needs to be flat, and the canopy height and density should be uniform (Burba, 2013). These site criteria are not perfectly fulfilled at our measurement site. The site is located in a low mountain range and tree density is rather sparse south of the flux tower. Such diverse terrain characteristics could lead to unwanted turbulent fluctuations (non-stationarity of time series), which introduce noise in flux cross-covariance function. Consequentially, time lag estimation is compromised, and in particular fluxes close to the detection limit may not be determined correctly. However, situations of insufficient turbulence are mostly likely identified by the applied quality selection criteria.

Adding the random flux errors determined with Finkelstein and Sims (2001) to the assumed relative errors that correspond to 20% of DEPAC-1D fluxes results in approximately ± 3.4 kg N ha^{-1} for TRANC+DEPAC-1D and ± 3.8 kg N ha^{-1} if MDV is used before applying DEPAC-1D. An uncertainty of ± 2.6 kg N ha^{-1} is determined for DEPAC-1D. The dry deposition budget errors of the different approaches are similar. It shows that the discrepancy to DEPAC-1D lies in the upper range of the estimated flux uncertainties. Yearly uncertainties of ΣN_r fluxes were between ± 1.0 kg N ha^{-1} a^{-1} and ± 1.3 kg N ha^{-1} a^{-1} for 2016 and between ± 1.2 kg N ha^{-1} a^{-1} and ± 1.7 kg N ha^{-1} a^{-1} for 2017 resulting in an agreement with annual dry deposition modeled by DEPAC-1D within the flux error range. Higher flux errors correspond to the gap-filling approach that applies MDV to short gaps.

4.4.2 Uncertainties of site-based modeling of fluxes

Generally, dry deposition of ΣN_r was overestimated by DEPAC-1D. The high contribution of NH_3 to ΣN_r, followed by HNO_3, NO_2, and NO predicted by DEPAC-1D seems reasonable since NH_3 is the most abundant ΣN_r compound in certain ecosystems. However, most of the studies were conducted above ecosystems, which are close to N_r sources and agriculturally managed sites. Sites with low variability in pollutants show a different contribution of N_r compounds as shown by our DELTA measurements, especially in NH_3. Particulate and acidic N_r compounds hold also an important fraction of the ΣN_r flux. On average, their contribution was higher than NH_3 showing that the current implementation of N_r compounds such as HNO_3 or NO_2 should be reevaluated, and the inclusion of exchange mechanisms for NO_3 and NH_4 should be considered in-situ modeling approaches.

Since a direct comparison to NH_3 flux measurements, the main compound in the deposition models, was not possible, only assumptions about the difference to measured fluxes can be given. The parameterization of the NH_3 exchange inside DEPAC could be responsible for the discrepancy to TRANC fluxes. Schrader et al. (2016) discovered problems in the calculation of the cuticular NH_3 compensation point, especially under high ambient NH_3 concentrations and high temperatures, for

instance during summer. Thus, cuticular deposition is overestimated. This issue is not solved yet and could not be verified for our measurement site due to generally low NH_3 concentrations and to the implementation of monthly averaged NH_3 concentration instead of half-hourly values. Since flux measurements on ΣN_r were conducted, we cannot extract the reason for the overestimation from measurements. Due to the low NH_3 concentrations cuticular compensation point exhibits no bell-shaped trend, which pronounced at high temperatures and high NH_3 concentrations (see Fig. 2(b) of Schrader et al., 2016). Thus, this issue is not the main reason for the difference to flux measurements at our site. It should be kept in mind that the determination of the compensation point may be critical, and a precise determination may not be possible under low concentrations of ΣN_r compounds. The measurement site is located in a low polluted mountain range. As stated in Sec. 4.2, mechanisms for favoring the dry deposition of ΣN_r are different to sites located in high polluted surroundings. Currently, a compensation point for the exchange path with soil is not implemented in DEPAC. Including such an exchange path in DEPAC, can lead to a reduction in deposition at sites with generally low ΣN_r deposition.

As mentioned in Sec. 4.1, HNO_3 has a significant influence on the ΣN_r fluxes. The median deposition velocity of HNO_3 modeled by DEPAC-1D is almost similar to NH_3. Thus, HNO_3 holds an important role in the ΣN_r exchange at our site. The implementation of HNO_3 inside DEPAC by a constant, low canopy resistance is rather simple. Compensation points are only calculated for NH_3. Thus, other N_r compounds can only be deposited in the model. It is expressed in the positive deposition velocities. Overall, median, modeled deposition velocities are close to the values propagated by VDI (2006) (Fig.C1.). NH_3 deposition velocity is in agreement with Schrader and Brümmer (2014) for different forest types. The negative whisker indicates few phases of emission, but they had hardly any influence on the nitrogen budget. In the case of HNO_3, the assumption of an ideal uptake seems to be questionable (Tarnay et al., 2002). Flux measurements of HNO_3 were conducted by Farmer and Cohen (2008) above spruce forest. They detected significant emission of HNO_3 during summer. HNO_3 emission during summer can be caused by evaporation of NH_4NO_3, which favored at temperatures above 20°C (Wyers and Duyzer, 1997; Van Oss et al., 1998). The mechanism explaining the HNO_3 emission is still under investigation (Nemitz et al., 2004).

DEPAC-1D models a low, positive deposition velocity for NO_2 since no bidirectional pathway is implemented for NO_2 in DEPAC. Low deposition velocities of NO_2 for different tree types are also reported by Wang, W. and Ganzeveld, L. and Rossabi, S. and Hu but the investigated tree types are not representative for our site. However, the order of magnitude is comparable to the modeled deposition velocity of 0.08 cms^{-1} for NO_2. Since they detected no NO uptake for all tree types, a modeled deposition velocity of 0.0 cms^{-1} with a negligible extension of the box for NO seems to be reasonable. Delaria et al. (2018) also observed low deposition velocities for NO_x. They found a stomatal deposition velocity of 0.007 cms^{-1} and a cuticular deposition velocity of 0.005 cms^{-1} for NO. This indicates a marginal NO uptake, which was about one magnitude smaller than the NO_2 uptake (Delaria et al., 2018). In general, canopy resistance mostly driven by water solubility. Thus, gases with a low water solubility like NO and NO_2 exhibit similar deposition velocities for different tree types. A compensation point for NO_2 was not found by Delaria et al. (2018) showing forest as an effective removal of NO_2 (Rosenkranz, P. and Brüggemann, N. and Papen, H. and Xu, Z. and Seu Taking no compensation point for NO_2 by DEPAC seems to be reasonable. For verifying these assumptions further comparisons of flux measurements with exchange models are recommended because they can lead to significant improvements of the

implemented parameterizations for various ΣN_r compounds. Focusing on NH_3, the most abundant species in rural areas, is also recommendable.

4.4.3 Uncertainties in the implementation of LOTOS-EUROS

The high nitrogen deposition values modeled by LOTOS-EUROS at the measurement site is mostly related to a general overestimation of ammonia concentrations especially occurring above Baden-Württemberg and Bavaria (Schaap, M. and Wichink Kruit, R. The disagreement to CBT deposition estimates was observed for elevated locations, which are exposed to a high amount of occult deposition (Schaap, M. and Wichink Kruit, R. and Hendriks, C. and Kranenburg, R. and Segers, A. and Builtjes, P. and Banzhaf, S. Ge, X. and Schaap, M. and Kranenburg, R. and Segers, A. and Reinds, G. J. and Kros, H. and de Vries, W. (2020) compared LOTOS-EUR NH_3 emission for two emission scenarios to satellite and surface observations for Germany and Benelux. The first emission scenario is the emission inventory from MACC-III (Modeling Atmospheric Compostion and Climate), which is originally used by LOTOS-EUROS, the second one is an updated version with increased detail level in nitrogen emission sources. Calculated annual total columns from the first scenario underestimated NH_3 from the satellite IASI (Infrared Atmospheric Sounding Interferometer), annual total columns from the second scenario under and overestimated NH_3 satellite-derived total columns. In the latter case, the overestimation was located to Southern Germany. A comparison to surface observations showed that LOTOS-EUROS overestimates NH_3 concentrations from January to March for both scenarios. At the measurement site, we also found a disagreement to NH_3 measurements conducted with QCL, DELTA, and passive samplers during winter (Fig. 15). Until mid of February, measured values were lower than 0.5 ppb whereas modeled concentrations ranged from 0.5 to 1.5 ppb. The difference to LOTOS-EUROS NH_3 concentrations was highest during periods with significant amount of NH_3 in the atmosphere like in spring and autumn, which is caused by emissions from fertilizer leading to a high load of modeled concentrations. Hence, modeled dry deposition is clearly overestimated.

The influence of emissions caused by management processes at adjacent sites on measured ΣN_r fluxes could not be verified. The largest amount of N_r released from those processes into the atmosphere will be deposited close to their sources. A small amount will be transported up to distances of 100 km (Asman, Willem A. H. and Sutton, Mark A. and Schjørring, J. K., 1998; Ferm, Martin The released NH_3 going into long-range transport is highly variable (Loubet, Benjamin and Asman, Willem A.H. and Theobald, Mark and and the distance depends on several parameter like atmospheric stability, atmospheric chemistry, topology, etc. In case of stable stratification, inversion layers often occurring in mountain ranges can prohibit air mass exchange. Probably, the measurement site is mostly outside the transport range. Thus, nitrogen enriched air-masses are deposited before reaching the height of the flux tower. A reduction in grid cell size could lead to a more precise localisation of potential nitrogen emission sources. Since all exchange processes contribute to single concentration within a grid cell, an improvement in horizontal resolution will lead to a refinement in predicted concentrations.

The aerodynamical reference height, which is used by LOTOS-EUROS for flux calculation, is also lower than the measurement height of the flux tower. Thus, slight differences in micrometeorological data can be expected, for example the difference in relative humidity in the first half of 2016. Differences for that time period are related to the usage of meteorological data

provided by the NPBW, with their instrumentation being installed at the 50 m platform. The deviations in u_* are most likely related to the complex terrain within the foot print of the flux tower. The surface roughness length and the tree composition is not uniform for the entire footprint. It is not possible to model such a diverse canopy structure within $7\times7\,km^2$ grid cell accurately. As stated earlier, the weighting of the land-use classes within the grid cell was not representative for the foot print. The class "semi-natural grassland" has the highest contribution. However, Norway spruce and European Beech were found to be the most dominated tree type within the flux foot print. This issue could be partly solved by increasing the spatial resolution. The reduction in grid cell size could affect the fractions of N_r compounds to modeled ΣN_r concentrations (Fig. E1). The influence of NH_3 on ΣN_r could change, and thus the predicted ΣN_r dry deposition can be lowered since reduction in NH_3 has the strongest influence on the deposition (Fig. 15).

As stated in Sec. 2.3, an incorrect setting of the LAI and z_0 can have a significant influence on ΣN_r deposition. The results of our sensitivity analysis for LAI and z_0 are comparable to values presented recently by van der Graaf, S. C. and Kranenburg, R. and Segers, A who used satellite-derived LAI and z_0 data from Moderate Resolution Imaging Spectroradiometer (MODIS) to calculate ΣN_r deposition with LOTOS-EUROS for a grid cell size of $7\times7\,km^2$. Overall, they observed changes in ΣN_r dry deposition of up to 30%. However, there is almost no change in ΣN_r dry deposition and in NH_3 concentration observable for the Bavarian Forest measurement site if LAI and z_0 from MODIS are used. However, the attempts of van der Graaf, S. C. and Kranenburg, R. and Segers, A. J. and Ge, X. and Schaap, M. and Kranenburg, R. and Segers, A. and Reinds, G. J. and Kros, H. and de Vries, W. (2020) did not provide a solution for the general overestimation of NH_3 deposition above southern Germany. It seems that the larger scale and temporal discrepancies in input NH_3 concentrations in LOTOS-EUROS are mainly responsible for the disagreement to flux measurements, and overestimation is only partly related to other issues, for example, the grid cell size of $7\times7\,km^2$.

Finally, two special ΣN_r exchange events need to be discussed, the ΣN_r emission fluxes in December 2017 and the deposition fluxes in February 2018. The emission phase in December 2017 may be related to the decomposition of fallen leaves (Hansen et al., 2015). Since the compensation point of the soil is set to zero for all land-use classes, the decomposition of fallen leaves is not considered in the models, and thus emissions from the soil could not be modeled. The deposition event in February 2018 seen by the TRANC seems to be driven by particulate N_r. Comparing the different runs of LOTOS-EUROS shows that the contribution of particulate deposition to total deposition is much larger than gaseous deposition during that time. However, the amount of deposited ΣN_r of this event is underestimated by DEPAC-1D and LOTOS-EUROS. A second deposition event, which occurred directly after the mentioned one, was predicted by the models, but not confirmed by the measured fluxes.

Considering the yearly uncertainties of TRANC measurements, upper CBT estimates of nitrogen deposition values are outside the error range of flux measurements. TRANC values are closer to the lower estimate of CBT. CBT values for 2016 and 2017 are almost similar whereas high dry deposition was determined for 2018. The difference to the previous years may be related to the higher particle input in February 2018 as shown by LOTOS-EUROS and TRANC measurements. However, the order of magnitude is the same and measured dry deposition is within one standard deviation of the averaged lower CBT estimates from 2010 to 2018 under consideration of the flux error range. LOTOS-EUROS and DEPAC-1D yearly estimates are within the error range of the CBT estimates, in particular close to the overlap area of the error ranges. By applying the correct

land-use class weighting, LOTOS-EUROS values are close to the upper estimate of CBT. It shows that dry deposition of the different methods are in the range of statistical uncertainty. Deviations from TRANC measurements are most likely related to differences in the vegetation of the footprint and the selected tree types. Inside the footprint, the forest stand consists of dead wood in south direction and young and matured trees in easterly direction. The investigated trees for CBT were selected from a matured tree stand. Thus, the leaf area surfaces can be significantly different. Their susceptibility to precipitation may differ, too. Different leaf sizes and different tree ages are probably the main reasons for the disagreement to TRANC fluxes.

5 Conclusions

Our study is the first one presenting 2.5 years flux measurements of total reactive atmospheric nitrogen (ΣN_r) measured with a custom-built converter called Total Reative Atmospheric nitrogen converter (TRANC) coupled to fast-response chemiluminescence detector (CLD) above a protected mixed forest. We investigated temporal dynamics of ΣN_r exchange, discussed conditions favouring natural exchange characteristics of ΣN_r under low atmospheric concentrations, and compare annual budgets of flux measurements to an in-situ deposition model, DEPAC-1D, and a long-range chemical transport model, LOTOS-EUROS.

A comparison of monthly averaged ΣN_r concentrations from the TRANC and DELTA (DEnuder for Long-Term Atmospheric sampling) and chemiluminescence measurements of nitrogen monoxide (NO) and nitrogen dioxide (NO_2) measurements showed a reasonable agreement in their seasonal patterns. On average, concentrations by the TRANC-CLD system were slightly higher ($\sim 0.3\,\mu$g N m^{-3}) showing that the TRANC-CLD system can adequately measure ΣN_r concentrations. Differences could be related to higher oxidized nitrogen compounds, which are not detected by the DELTA system, to a degrading of the denuder surfaces due to enviromental influences, issues in the conversion efficiency of the TRANC, etc. . Only nitrogen oxides (NO_x) and ammonia (NH_3) showed distinct seasonal changes in their concentrations whereas ΣN_r concentration remained stable through the year. NO_x exhibited highest concentrations during winter, NH_3 during spring and summer. In total, both gases had a mean contribution of 72.0% to the ΣN_r concentrations highlighting their importance for the observed ΣN_r exchange pattern.

Measured concentrations of ΣN_r were 5.2 ppb on average. Reactive compounds such as NH_3 and NO_2 had a concentration level of 1.8 ppb and 2.5 ppb, respectively. The latter exhibits highest concentrations during winter, the former during spring. Elevated concentration level is possibly related to anthropogenic emission during those periods. DELTA measurements showed that NH_3 and NO_2 are the main contributors to ΣN_r. On average, these gases contribute with 73.2% to ΣN_r. These reactive gases are most responsible for observed exchange pattern of ΣN_r at the measurement site. However, also particulate and acidic N_r compounds are important for the dynamics of ΣN_r exchange, especially at high ΣN_r concentrations.

We observed mostly deposition during 2.5 years of flux measurements. Median deposition rangesd from -15 to -5 ng N m^{-2} s^{-1}. Deposition velocities followed the diurnal pattern of the fluxes, and median values ranged between 0.2 and 0.5 cm s^{-1}. Highest deposition was observed during the timeframe of high incident radiation, in particular from May to September.mid spring and summer, lowest deposition occurred during late autumn and winter.Our findings suggest that seasonal changes in the concentrations of the ΣN_r compounds and radiation were most likely responsible for the observed pattern of v_d. Within periods of high incident radiation, e.g. from May to September, deposition velocity (v_d) was elevated in presence of dry leaf

surfaces, at a low humidity level, at higher temperatures, and during no precipitation. Calculated effective canopy resistance ($R_{c,eff}$) was slightly lower at lower humidity and higher concentrations of ΣN_r. Aerodynamic and boundary-layer resistances showed no significant contribution to v_d implicating a low influence of turbulent processes on the ΣN_r exchange during those times. During rain, v_d was greatly reduced or even negative resulting in emission of ΣN_r. During the year, uptake pathways for ΣN_r changed depending on the presence of individual ΣN_r compounds and micrometeorological conditions. Stomatal deposition seemed to be prevailing mostly from May to September. During the rest of the year, cuticular, soil, or turbulent processes appeared to be most responsible for the ΣN_r exchange.

~~From May to September, deposition was favored under high ambient concentration (> 4.7 ppb), low humidity level ($< 77\,\%$), and high temperatures ($> 14.3\,^{\circ}C$). Additionally, dry leaf surfaces seem to enhance deposition. We conclude that dry conditions seem to favour ΣN_r dry deposition at natural ecosystems supposedly related to a low contribution of NH_3 to the ΣN_r fluxes. We found that concentrations of ΣN_r were elevated in presence of dry leaf surfaces. Thus, wet deposition seems to be important for ΣN_r deposition at our measurement site during rainy periods.~~

From June 2016 to May 2017 and June 2017 to May 2018, we estimated dry deposition sums of $3.8 \pm 0.8\,kg\ N\ ha^{-1}$ and $4.1 \pm 1.1\,kg\ N\ ha^{-1}$, respectively. Influences of temperature, humidity, friction velocity, or precipitation were in the uncertainty ranges of the estimated dry depositions sums. Using other gap-filling approaches based on inferential modeling or artificial neural networks for long-term gaps, is a valuable option. Also, biases related to the usage friction velocity thresholds, which potentially removes lower fluxes from the analysis and therefore affects data-driven gap-filling methods, will be avoided. Mean total wet deposition were $8.0\,kg\ N\ ha^{-1}$ and $6.8\,kg\ N\ ha^{-1}$ for the timeframes 2016/2017 and 2017/2018, respectively. The reduction in wet deposition was most likely related to the reduced precipitation in 2018. In the first and second measurement year, we determined $11.8\,kg\ N\ ha^{-1}$ and $10.9\,kg\ N\ ha^{-1}$ as total nitrogen deposition, respectively.

~~After 2.5 years, nitrogen dry deposition of TRANC measurements resulted in $(11.1 \pm 3.4)\,kg\ N\ ha^{-1}$ with DEPAC-1D as gap-filling method, and $(10.9 \pm 3.8)\,kg\ N\ ha^{-1}$ was determined with MDV and DEPAC-1D as gap-filling methods. Both values are rather close to modeled fluxes of DEPAC-1D ($13.6\,kg\ N\ ha^{-1}$) considering the uncertainties of measured fluxes and possible uncertainty sources of DEPAC-1D. Difference of DEPAC-1D to TRANC could be related to the parameterizations of reactive gases or the missing exchange path with soil. Further comparisons of in-situ models to flux measurements are needed to address these issues. Both gap-filling approaches result in similar nitrogen dry deposition values. The advantage of DEPAC-1D is based on the gap-filling of long time series of missing data. However, there are still issues in the bidirectional resistance model DEPAC, which need to be solved. Up to now, there is no further option in replacing long-term gaps because most gap-filling methods are designed for inert gases. Gap-filling methods, which based on artificial neural networks, could also be useful for reactive gases.~~

~~LOTOS-EUROS exhibited the highest discrepancy to flux measurements, in particular for the actual land use of the grid cell ($16.8\,kg\ N\ ha^{-1}$). We showed that modeled NH_3 concentrations used as input parameter by LOTOS-EUROS were significantly higher than measured concentrations, and they disagreed in their seasonal pattern. Thus, modeled NH_3 concentrations were the main reason for the discrepancy in annual budgets. Also, the vegetation of the grid cell does not correspond to the vegetation~~

of the flux footprint. Increasing the horizontal resolution could be a solution to that issue. Supposedly, a large-scale issue is related to the overestimation of NH_3 concentration by LOTOS-EUROS.

Averaged annual ΣN_r dry deposition was 4.5 kg N ha^{-1} a^{-1} for both gap-filling approaches applied to TRANC measurements, DEPAC-1D showed 5.3 kg N ha^{-1} a^{-1}, and LOTOS-EUROS modeled 5.2 kg N ha^{-1} a^{-1} to 6.9 kg N ha^{-1} a^{-1} depending on the weighting of land-use classes. The application of CBT resulted in 7.5 kg N ha^{-1} a^{-1} as upper estimate and 4.6 kg N ha^{-1} a^{-1} as lower estimate. Dry deposition estimated by TRANC, DEPAC-1D, and LOTOS-EUROS is within the frame of minimum and maximum deposition estimated by CBT. The difference of flux measurements to CBT could be induced by the discrepancy in tree age of the selected trees for CBT compared to the forest stand within the footprint, and leaf area surfaces may also be different.

For a further improvement of deposition models and the investigation exchange characteristics of ΣN_r, long-term flux measurements are needed for different ecosystems differing in their nitrogen stress. However, installing a setup presented in this study at several locations is quite challenging due to power consumption, costs of the instruments, and their high technical requirements. A continuous monitoring of N_r species by low-cost samplers complemented by high-frequency measurements of ΣN_r and selected compounds like NH_3 for a limited time, for example during fertilization periods, can result in a better understanding of exchange processes and thus in a improvement of deposition models (Schrader, F. and Schaap, M. and Zöll, U. and Kranen Recently, Schrader, Frederik and Erisman, Jan Willem and Brümmer, Christian (2020) showed that stomatal conductances, essential for controlling the NH_3 exchange between vegetation and atmosphere, can be determined from CO_2 flux measurements. Using CO_2-derived stomatal conductances will lead to a significant improvement of biosphere–atmosphere exchange models making them sensitive to climate change effects.

The data set presented in this study provides an unique opportunity for a comparison to deposition models. In the second part of this paper, a comparison of the acquired dataset to the performance of deposition models will be made. Modeled exchange dynamics will be discussed in regard to their biophysical controlling factors. Annual N budgets from measurements, modeling approaches using in-situ and modeled input parameters, and canopy outflow measurements will be shown.

Code and data availability. All data are available upon request from the first author of this study (pascal.wintjen@thuenen.de). Also, Python 3.7 code for flux data analysis can be requested from the first author. LOTOS-EUROS v2.0 is available as open-source version and can be downloaded from the website https://lotos-euros.tno.nl/ (last access: 02 October 2020, (Manders, Astrid M. M. and Builtjes, Peter J. H. and Curier, Lyana

Appendix A: Time lag determination of the TRANC-CLD system

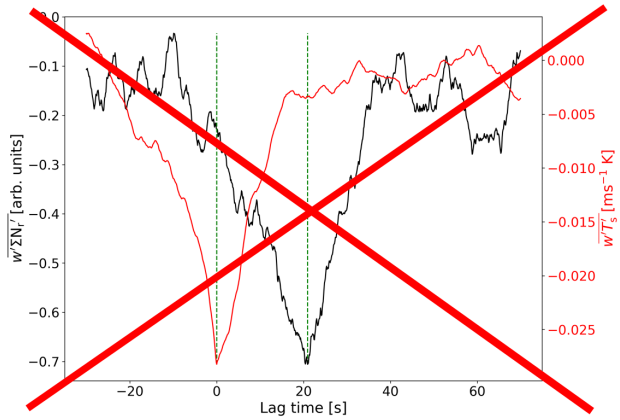

Figure A1. ~~Covariance function of vertical wind and temperature (red) and covariance function of vertical wind and ΣN_r concentration (black). Green, dashed lines indicate the maximum covariance, which is around 20 s for the TRANC-CLD. Data were recorded at the 22 April 2017 from 05:00 to 05:30 CET~~

1470

Appendix B: ~~Contribution of different of N_r gases and particles to ΣN_r based on DELTA measurements~~

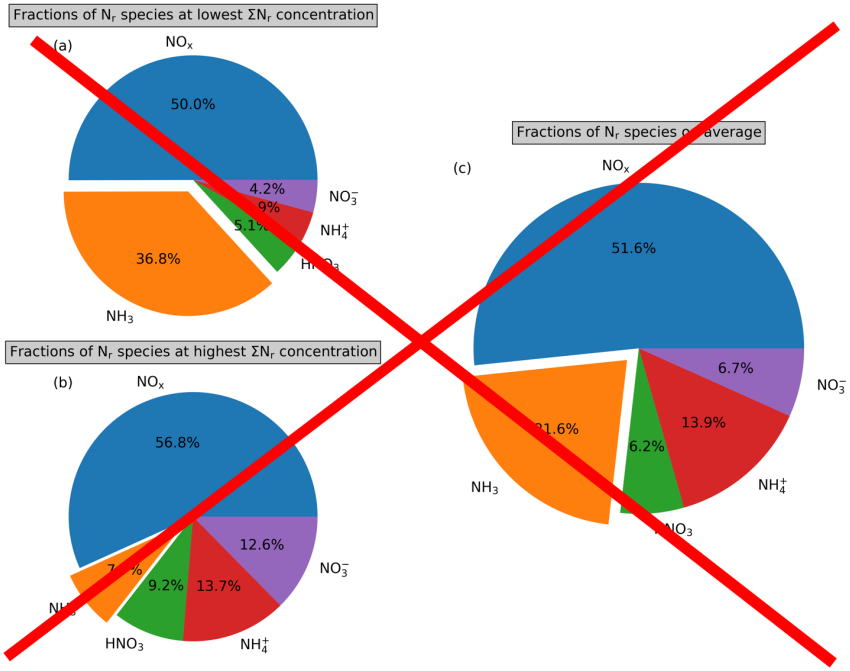

Figure B1. ~~Pie charts showing the contribution of NO_x, NH_3, NO_3, NH_4, and HNO_3 to ΣN_r based on measurements of DELTA samplers and NO_x measurements. NO_x measurements are averaged to exposition periods of the DELTA samplers. (a) and (b) show the contributions to the highest and lowest average ΣN_r concentration found for the measurement campaign. (c) shows the average contribution to ΣN_r for the entire measurement period.~~

Appendix C: ~~Deposition velocities determined by DEPAC-1D~~

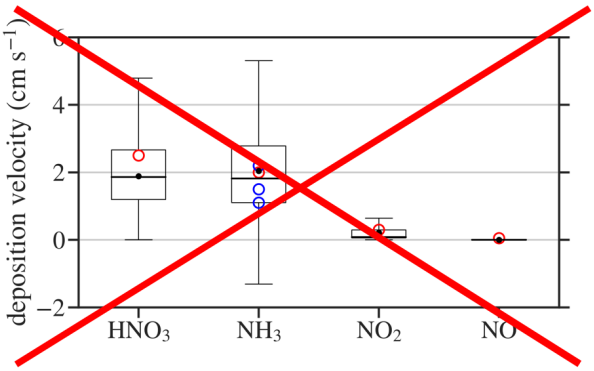

Figure C1. ~~Box plots of deposition velocities for NH_3, HNO_3, NO_2, and NO modeled by DEPAC-1D without outliers (the box frame is the 25% to 75% interquartile range (IQR); the length of whiskers is 1.5 times the IQR; the bold line is the median). Blue circles are NH_3 deposition velocities by Schrader and Brümmer (2014) for deciduous forest, mixed forest, and spruce forest (from low to high), red circles show deposition velocities after VDI (2006). Negative deposition velocities of NH_3 are related to modeled emission phases.~~

Appendix D: ~~Difference between measured and modeled ΣN_r fluxes for the entire campaign~~

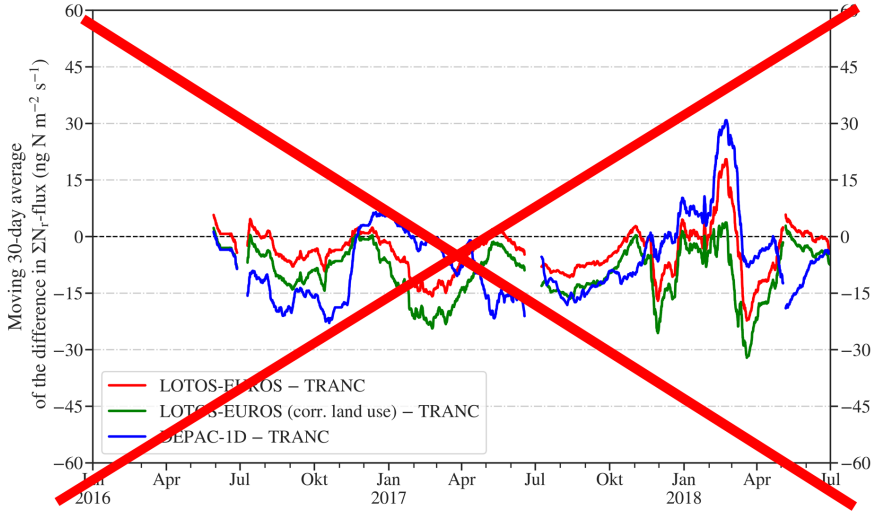

Figure D1. ~~Moving 30-days average of the difference between half-hourly measured and modeled ΣN_r fluxes. Negative values indicate an overestimation of the deposition by the DEPAC-1D and LOTOS-EUROS, positive values refer to an underestimation.~~

Appendix E: ~~Contribution of different of N_r gases and particles to ΣN_r based on LOTOS-EUROS~~

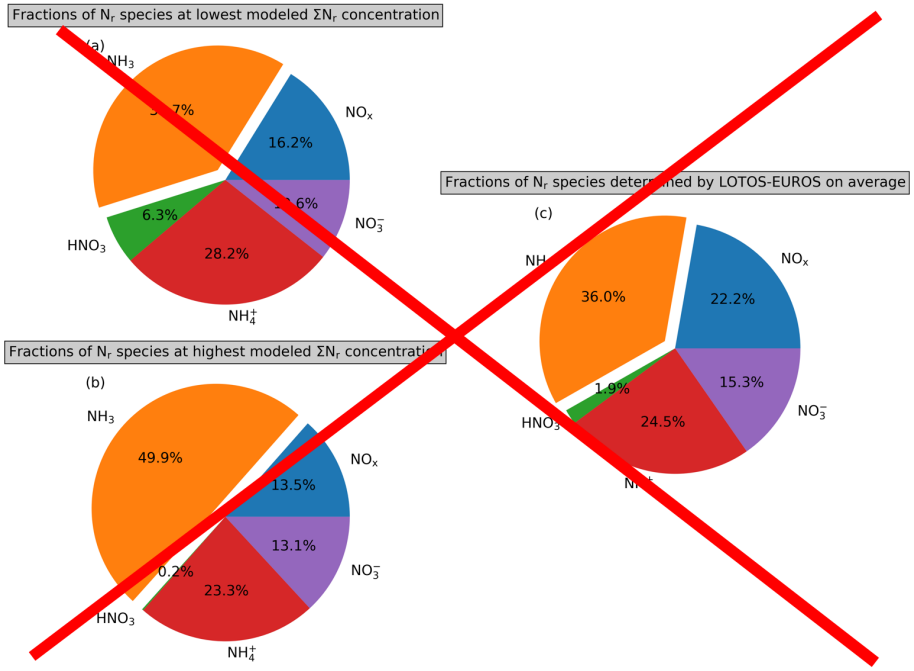

Figure E1. ~~Pie charts showing the contribution of NO_x, NH_3, NO_3, NH_4, and HNO_3 to ΣN_r based on modeled concentrations of LOTOS-EUROS. Modeled concentrations are averaged to exposition periods of the DELTA samplers. (a) and (b) show the contributions to the highest and lowest average ΣN_r concentration found for the measurement campaign. (c) shows the average contribution to ΣN_r for the entire measurement period.~~

Appendix F: ~~Box plots of ΣN_r concentrations for wet and dry leaves and fluxes separated into precipitation classes.~~

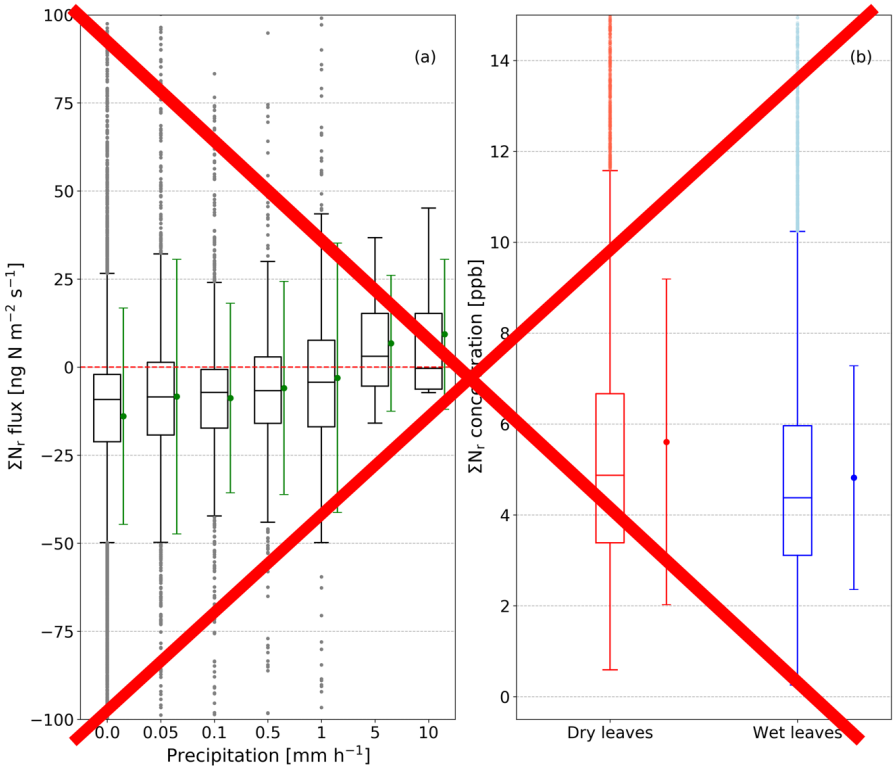

Figure F1. ~~Box plots of ΣN_r concentrations for wet (blue) and dry (red) leaves (b) and fluxes separated into precipitation classes (a) (the box frame is the 25% to 75% interquartile range (IQR); the length of whiskers is 1.5 times the IQR; the bold line is the median). Averaged values of the corresponding classes (green) are plotted to the right of the box. Uncertainty of the averaged values are indicated by error bars, whose lengths correspond to one standard deviation.~~

Author contributions. PW, FS, and CB conceived the study. PW wrote the manuscript, carried out the measurements at the forest site, and conducted flux data analysis and interpretation. FS ~~implemented the stand-alone version of DEPAC, analyzed the model output, and~~ evaluated meteorological measurements. FS and MS ~~provide the LOTOS-EUROS data~~ provided insights in interpreting deposition velocities and resistances.~~, and~~ BB performed the ~~canopy budgets~~ wet deposition analysis. CB installed the flux tower equipment and gave scientific advise to the overall data analysis and interpretation. All authors discussed the results and FS, MS, BB, and CB contributed to the manuscript.

Competing interests. The authors declare that they have no conflict of interest.

Acknowledgements. Funding by the German Environment Agency (UBA) (project FORESTFLUX, support code FKZ 3715512110) and by the German Federal Ministry of Education and Research (BMBF) within the framework of the Junior Research Group NITROSPHERE (support code FKZ 01LN1308A) is greatly acknowledged. We thank Undine Zöll for scientific and logistical help, Jeremy Rüffer and Jean-Pierre Delorme for excellent technical support, Ute Tambor, Andrea Niemeyer, and Dr. Daniel Ziehe for conducting laboratory analyses of denuder and filter samples, and the Bavarian Forest Nationalpark (NPBW) Administration, namely Wilhelm Breit and Ludwig Höcker for technical and logistical support at the measurement site.

References

Ammann, C., Wolff, V., Marx, O., Brümmer, C., and Neftel, A.: Measuring the biosphere-atmosphere exchange of total reactive nitrogen by eddy covariance, Biogeosciences, 9, 4247–4261, https://doi.org/10.5194/bg-9-4247-2012, http://www.biogeosciences.net/9/4247/2012/, 2012.

Aubinet, M., Vesala, T., and Papale, D., eds.: Eddy Covariance: A Practical Guide to Measurement and Data Analysis, Springer Science+Business Media B.V. 2012, Dordrecht, The Netherlands, 2012.

Beudert, B. and Breit, W.: Integrated Monitoring Programm an der Meßstelle Forellenbach im Nationalpark Bayerischer Wald, Untersuchungen zu Prozessen und Räumen der Hochwasserbildung im Forellenbachgebiets, Förderkennzeichen 351 01 012. Nationalparkverwaltung Bayerischer Wald, Sachgebiet IV, techreport, Umweltbundesamt, http://docplayer.org/80741933-Integrated-monitoring-programm-an-der-messstelle-forellenbach-im-nationalpark-bayerischer-wald.html, 2008.

Beudert, B. and Breit, W.: Integrated Monitoring Programm an der Meßstelle Forellenbach im Nationalpark Bayerischer Wald, Untersuchungen zum Stickstoffeintrag und zum wassergebundenen Stickstoffhaushalt des Forellenbachgebiets, Förderkennzeichen 351 01 012. Nationalparkverwaltung Bayerischer Wald, Sachgebiet IV, techinal report, Umweltbundesamt, Dessau-Roßlau, Germany, http://www.umweltbundesamt.de/sites/default/files/medien/370/dokumente/ece_im_forellenbach_berichtsjahr_2009.pdf, 2010.

Beudert, B. and Breit, W.: Kronenraumbilanzen zur Abschätzung der Stickstoffgesamtdeposition in Waldökosysteme des Nationalparks Bayerischer Wald, techninal report, Umweltbundesamt, Dessau-Roßlau, Germany, https://www.umweltbundesamt.de/sites/default/files/medien/370/dokumente/kronenraumbilanzen_stickstoffgesamtdeposition_nationalpark_bayerisches_wald_-_berichtsjahr_2013_im_forellenbach.pdf, 2014.

Beudert, B., Bernsteinová, J., Premier, J., and Bässler, C.: Natural disturbance by bark beetle offsets climate change effects on streamflow in headwater catchments of the Bohemian Forest, Silva Gabreta, 24, 21–45, https://www.npsumava.cz/wp-content/uploads/2019/06/2_sg_24_beudertetal.pdf, 2018.

Brümmer, C., Marx, O., Kutsch, W., Ammann, C., Wolff, V., Flechard, C. R., and Freibauer, A.: Fluxes of total reactive atmospheric nitrogen (ΣN_r) using eddy covariance above arable land, Tellus B: Chemical and Physical Meteorology, 65, 19 770, https://doi.org/10.3402/tellusb.v65i0.19770, https://doi.org/10.3402/tellusb.v65i0.19770, 2013.

Burba, G.: Eddy Covariance Method for Scientific, Industrial, Agricultural and Regulatory Applications: A Field Book on Measuring Ecosystem Gas Exchange and Areal Emission Rates, LI-COR Biosciences, Lincoln, Nebraska, USA, 2013.

Civerolo, K. L. and Dickerson, R. R.: Nitric oxide soil emissions from tilled and untilled cornfields, Agricultural and Forest Meteorology, 90, 307–311, https://doi.org/10.1016/S0168-1923(98)00056-2, http://www.sciencedirect.com/science/article/pii/S0168192398000562, 1998.

A. Remde, Slemr, F., and Conrad, R.: Microbial production and uptake of nitric oxide in soil, FEMS Microbiology Letters, 62, 221–230, https://doi.org/https://doi.org/10.1016/0378-1097(89)90246-2, https://www.sciencedirect.com/science/article/pii/0378109789902462, 1989.

A.G. Barr, Richardson, A., Hollinger, D., Papale, D., Arain, M., Black, T., Bohrer, G., Dragoni, D., Fischer, M., Gu, L., Law, B., Margolis, H., McCaughey, J., Munger, J., Oechel, W., and Schaeffer, K.: Use of change-point detection for friction–velocity threshold evaluation in eddy-covariance studies, Agricultural and Forest Meteorology, 171-172, 31–45, https://doi.org/https://doi.org/10.1016/j.agrformet.2012.11.023, https://www.sciencedirect.com/science/article/pii/S0168192312003607, 2013.

Alberto Rondón and Granat, L.: Studies on the dry deposition of NO2 to coniferous species at low NO2 concentrations, Tellus B: Chemical and Physical Meteorology, 46, 339–352, https://doi.org/10.3402/tellusb.v46i5.15809, https://doi.org/10.3402/tellusb.v46i5.15809, 1994.

Behrendt, T., Veres, P. R., Ashuri, F., Song, G., Flanz, M., Mamtimin, B., Bruse, M., Williams, J., and Meixner, F. X.: Characterisation of NO production and consumption: new insights by an improved laboratory dynamic chamber technique, Biogeosciences, 11, 5463–5492, https://doi.org/10.5194/bg-11-5463-2014, https://bg.copernicus.org/articles/11/5463/2014/, 2014.

Bok Haeng Baek, Aneja, V. P., and Tong, Q.: Chemical coupling between ammonia, acid gases, and fine particles, Environmental Pollution, 129, 89–98, https://doi.org/https://doi.org/10.1016/j.envpol.2003.09.022, https://www.sciencedirect.com/science/article/pii/S0269749103003816, 2004.

Breuninger, C., Meixner, F. X., and Kesselmeier, J.: Field investigations of nitrogen dioxide (NO_2) exchange between plants and the atmosphere, Atmospheric Chemistry and Physics, 13, 773–790, https://doi.org/10.5194/acp-13-773-2013, https://acp.copernicus.org/articles/13/773/2013/, 2013.

Burkhardt, J., Peters, K., and Crossley, A.: The presence of structural surface waxes on coniferous needles affects the pattern of dry deposition of fine particles, Journal of Experimental Botany, 46, 823–831, 1995.

Dämmgen, U., Thöni, L., Lumpp, R., Gilke, K., Seitler, E., and Bullinger, M.: Feldexperiment zum Methodenvergleich von Ammoniak- und Ammonium-Konzentrationsmessungen in der Umgebungsluft, 2005 bis 2008 in Braunschweig, vol. 337 of *Landbauforschung : Sonderheft*, Johann Heinrich von Thünen-Institut, Braunschweig, https://www.openagrar.de/receive/timport_mods_00006160, jahresberichtskategorie: 10-M4;10-3, 2010.

David Fowler, Flechard, C., Skiba, U., Coyle, M., and Cape, J. N.: The Atmospheric Budget of Oxidized Nitrogen and Its Role in Ozone Formation and Deposition, The New Phytologist, 139, 11–23, http://www.jstor.org/stable/2588244, 1998.

Delaria, E. R., Place, B. K., Liu, A. X., and Cohen, R. C.: Laboratory measurements of stomatal NO_2 deposition to native California trees and the role of forests in the NO_x cycle, Atmospheric Chemistry and Physics, 20, 14 023–14 041, https://doi.org/10.5194/acp-20-14023-2020, https://acp.copernicus.org/articles/20/14023/2020/, 2020.

Erisman, J. W. and Wyers, G. P.: Continuous measurements of surface exchange of SO_2 and NH_3; Implications for their possible interaction in the deposition process, Atmospheric Environment. Part A. General Topics, 27, 1937–1949, https://doi.org/10.1016/0960-1686(93)90266-2, http://linkinghub.elsevier.com/retrieve/pii/0960168693902662, 1993.

Farquhar, G. D., Firth, P. M., Wetselaar, R., and Weir, B.: On the Gaseous Exchange of Ammonia between Leaves and the Environment: Determination of the Ammonia Compensation Point, Plant Physiology, 66, 710–714, https://doi.org/10.1104/pp.66.4.710, http://www.plantphysiol.org/content/66/4/710, 1980.

Ferm, M.: A Sensitive Diffusional Sampler, Report L91-172, Swedish Environmental Research Institute, Gothenburg, 1991.

Ferrara, R. M., Di Tommasi, P., Famulari, D., and Rana, G.: Limitations of an Eddy-Covariance System in Measuring Low Ammonia Fluxes, Boundary-Layer Meteorology, https://doi.org/10.1007/s10546-021-00612-6, https://doi.org/10.1007/s10546-021-00612-6, 2021.

Flechard, C. R., Fowler, D., Sutton, M. A., and Cape, J. N.: A dynamic chemical model of bi-directional ammonia exchange between semi-natural vegetation and the atmosphere, Quarterly Journal of the Royal Meteorological Society, 125, 2611–2641, https://doi.org/10.1002/qj.49712555914, https://rmets.onlinelibrary.wiley.com/doi/abs/10.1002/qj.49712555914, 1999.

Gessler, A., Rienks, M., and Rennenberg, H.: NH3 and NO2 fluxes between beech trees and the atmosphere - correlation with climatic and physiological parameters, New Phytologist, 147, 539–560, https://doi.org/10.1046/j.1469-8137.2000.00712.x, http://doi.wiley.com/10.1046/j.1469-8137.2000.00712.x, 2000.

Gessler, A., Rienks, M., and Rennenberg, H.: Stomatal uptake and cuticular adsorption contribute to dry deposition of NH_3 and NO_2 to needles of adult spruce (Picea abies) trees, New Phytologist, 156, 179–194, https://doi.org/https://doi.org/10.1046/j.1469-8137.2002.00509.x, https://nph.onlinelibrary.wiley.com/doi/abs/10.1046/j.1469-8137.2002.00509.x, 2002.

Hansen, K., Sorensen, L. L., Hertel, O., Geels, C., Skjoth, C. A., Jensen, B., and Boegh, E.: Ammonia emissions from deciduous forest after leaf fall, Biogeosciences, 10, 4577–4589, https://doi.org/10.5194/bg-10-4577-2013, https://bg.copernicus.org/articles/10/4577/2013/, 2013.

Hollinger, D. Y. and Richardson, A. D.: Uncertainty in eddy covariance measurements and its application to physiological models, Tree Physiology, 25, 873–85, https://www.ncbi.nlm.nih.gov/pubmed/15870055, 2005.

Hurkuck, M., Brümmer, C., Mohr, K., Grünhage, L., Flessa, H., and Kutsch, W. L.: Determination of atmospheric nitrogen deposition to a semi-natural peat bog site in an intensively managed agricultural landscape, Atmospheric Environment, 97, 296–309, https://doi.org/10.1016/j.atmosenv.2014.08.034, http://www.sciencedirect.com/science/article/pii/S1352231014006281, 2014.

I.G. Chaparro-Suarez, Meixner, F., and Kesselmeier, J.: Nitrogen dioxide (NO2) uptake by vegetation controlled by atmospheric concentrations and plant stomatal aperture, Atmospheric Environment, 45, 5742–5750, https://doi.org/https://doi.org/10.1016/j.atmosenv.2011.07.021, https://www.sciencedirect.com/science/article/pii/S1352231011007461, 2011.

Jarvis, P. G.: The Interpretation of the Variations in Leaf Water Potential and Stomatal Conductance Found in Canopies in the Field, Philosophical Transactions of the Royal Society B: Biological Sciences, 273, 593–610, https://doi.org/10.1098/rstb.1976.0035, http://rstb.royalsocietypublishing.org/content/273/927/593http://rstb.royalsocietypublishing.org/cgi/doi/10.1098/rstb.1976.0035, 1976.

J.L. Durham and Stockburger, L.: Nitric acid-air diffusion coefficient: Experimental determination, Atmospheric Environment (1967), 20, 559–563, https://doi.org/0004-6981(86)90098-3, https://www.sciencedirect.com/science/article/pii/0004698186900983, 1986.

Kreyling, J., Haei, M., and Laudon, H.: Snow removal reduces annual cellulose decomposition in a riparian boreal forest, Canadian Journal of Soil Science, 93, 427 – 433, https://doi.org/10.1139/CJSS2012-025, https://doi.org/10.1139/CJSS2012-025, 2013.

Loescher, H. W., Law, B. E., Mahrt, L., Hollinger, D. Y., Campbell, J., and Wofsy, S. C.: Uncertainties in, and interpretation of, carbon flux estimates using the eddy covariance technique, Journal of Geophysical Research: Atmospheres, 111, https://doi.org/https://doi.org/10.1029/2005JD006932, https://agupubs.onlinelibrary.wiley.com/doi/abs/10.1029/2005JD006932, 2006.

Ludwig, J., Meixner, F., Vogel, B., and Förstner, J.: Soil-air exchange of nitric oxide: An overview of processes, environmental factors, and modeling studies, Biogeochemistry, 52, 225–257, https://doi.org/10.1023/A:1006424330555, 2001.

Massman, W. J.: A review of the molecular diffusivities of H2O, CO2, CH4, CO, O3, SO2, NH3, N2O, NO, and NO2 in air, O2 and N2 near STP, Atmospheric Environment, 32, 1111–1127, https://doi.org/10.1016/s1352-2310(97)00391-9, 1998.

Medinets, S., Gasche, R., Skiba, U., Schindlbacher, A., Kiese, R., and Butterbach-Bahl, K.: Cold season soil NO fluxes from a temperate forest: drivers and contribution to annual budgets, Environmental Research Letters, 11, 114 012, https://doi.org/10.1088/1748-9326/11/11/114012, https://doi.org/10.1088/1748-9326/11/11/114012, 2016.

Moffat, A. M., Beckstein, C., Churkina, G., Mund, M., and Heimann, M.: Characterization of ecosystem responses to climatic controls using artificial neural networks, Global Change Biology, 16, 2737–2749, https://doi.org/j.1365-2486.2010.02171.x, https://onlinelibrary.wiley.com/doi/abs/10.1111/j.1365-2486.2010.02171.x, 2010.

Neirynck, J. and Ceulemans, R.: Bidirectional ammonia exchange above a mixed coniferous forest, Environmental Pollution, 154, 424–38, https://doi.org/10.1016/j.envpol.2007.11.030, https://www.ncbi.nlm.nih.gov/pubmed/18258346, 2008.

Pastorello, G., Trotta, C., and Canfora, E. e. a.: The FLUXNET2015 dataset and the ONEFlux processing pipeline for eddy covariance data, Scientific Data, 7, 225, https://doi.org/10.1038/s41597-020-0534-3, https://doi.org/10.1038/s41597-020-0534-3, 2020.

Peake, E. and Legge, A. H.: Evaluation of methods used to collect air quality data at remote and rural sites in Alberta, Canada, in: Proc. 1987 EPA/APCA Symposium on Measurements of Toxic and Related Air Pollutants, APCA, 1987.

Peake, M.: A Preliminary Report on the Design and Testing of the KAPS (Kananaskis Atmospheric Pollutant Sampler) for the Collection of Acidic and Basic Gases and Fine Particles, Document 0012e/July 8/85. Typskript University Calgary, 1985.

Remde, A. and Conrad, R.: Role of nitrification and denitrification for NO metabolism in soil, Biogeochemistry, 12, 189–205, https://doi.org/110.1007/BF00002607, https://doi.org/10.1007/BF00002607, 1993.

Saccone, P., Morin, S., Baptist, F., Bonneville, J.-M., Colace, M.-P., Domine, F., Faure, M., Geremia, R., Lochet, J., Poly, F., Lavorel, S., and Clèment, J.-C.: The effects of snowpack properties and plant strategies on litter decomposition during winter in subalpine meadows, Plant and Soil, 363, 215–229, https://doi.org/10.1007/s11104-012-1307-3, https://doi.org/10.1007/s11104-012-1307-3, 2013.

S.C. Pryor and Klemm, O.: Experimentally derived estimates of nitric acid dry deposition velocity and viscous sub-layer resistance at a conifer forest, Atmospheric Environment, 38, 2769–2777, https://doi.org/https://doi.org/10.1016/j.atmosenv.2004.02.038, https://www.sciencedirect.com/science/article/pii/S1352231004002158, 2004.

Schindlbacher, A., Zechmeister-Boltenstern, S., and Butterbach-Bahl, K.: Effects of soil moisture and temperature on NO, NO2, and N2O emissions from European forest soils, Journal of Geophysical Research-Atmospheres, 109, 1–12, https://doi.org/10.1029/2004jd004590, https://agupubs.onlinelibrary.wiley.com/doi/abs/10.1029/2004JD004590, 2004.

Seinfeld, J. H. and Pandis, S. N.: Atmospheric Chemistry and Physics – From Air Pollution to Climate Change, John Wiley & Sons, New York, USA, 2 edn., 2006.

Seok, B., Helmig, D., Ganzeveld, L., Williams, M. W., and Vogel, C. S.: Dynamics of nitrogen oxides and ozone above and within a mixed hardwood forest in northern Michigan, Atmospheric Chemistry and Physics, 13, 7301–7320, https://doi.org/10.5194/acp-13-7301-2013, https://acp.copernicus.org/articles/13/7301/2013/, 2013.

Squizzato, S., Masiol, M., Brunelli, A., Pistollato, S., Tarabotti, E., Rampazzo, G., and Pavoni, B.: Factors determining the formation of secondary inorganic aerosol: a case study in the Po Valley (Italy), Atmospheric Chemistry and Physics, 13, 1927–1939, https://doi.org/10.5194/acp-13-1927-2013, https://acp.copernicus.org/articles/13/1927/2013/, 2013.

Stef Bokhorst, Metcalfe, D. B., and Wardle, D. A.: Reduction in snow depth negatively affects decomposers but impact on decomposition rates is substrate dependent, Soil Biology and Biochemistry, 62, 157–164, https://doi.org/j.soilbio.2013.03.016, https://www.sciencedirect.com/science/article/pii/S0038071713001041, 2013.

Sutton, M. A., Asman, W. A. H., and Schjorring, J. K.: Dry Deposition of Reduced Nitrogen, Tellus Series B-Chemical and Physical Meteorology, 46, 255–273, https://doi.org/10.1034/j.1600-0889.1994.t01-2-00002.x, https://onlinelibrary.wiley.com/doi/abs/10.1034/j.1600-0889.1994.t01-2-00002.x, 1994.

Sutton, M. A., Schjorring, J. K., Wyers, G. P., Duyzer, J. H., Ineson, P., and Powlson, D. S.: Plant—atmosphere exchange of ammonia, Philosophical Transactions of the Royal Society of London. Series A: Physical and Engineering Sciences, 351, 261–278, https://doi.org/10.1098/rsta.1995.0033, http://rsta.royalsocietypublishing.org/cgi/doi/10.1098/rsta.1995.0033, 1995.

Sutton, M. A., Burkhardt, J. K., Guerin, D., Nemitz, E., and Fowler, D.: Development of resistance models to describe measurements of bi-directional ammonia surface–atmosphere exchange, Atmospheric Environment, 32, 473–480, https://doi.org/10.1016/s1352-2310(97)00164-7, http://www.sciencedirect.com/science/article/pii/S1352231097001647http://linkinghub.elsevier.com/retrieve/pii/S1352231097001647, 1998.

Teklemmariam, T. and Sparks, J.: Leaf fluxes of NO and NO2 in four herbaceous plant species: The role of ascorbic acid, Atmospheric Environment, 40, 2235–2244, https://doi.org/10.1016/j.atmosenv.2005.12.010, 2006.

Thoene, B., Schröder, P., Papen, H., Egger, A., and Rennenberg, H.: Absorption of atmospheric NO2 by spruce (Picea abies L. Karst.) trees, New Phytologist, 117, 575–585, https://doi.org/https://doi.org/10.1111/j.1469-8137.1991.tb00962.x, https://nph.onlinelibrary.wiley.com/doi/abs/10.1111/j.1469-8137.1991.tb00962.x, 1991.

Thoene, B., Rennenberg, H., and Weber, P.: Absorption of atmospheric NO_2 by spruce (Picea abies) trees, New Phytologist, 134, 257–266, https://doi.org/j.1469-8137.1996.tb04630.x, https://nph.onlinelibrary.wiley.com/doi/abs/10.1111/j.1469-8137.1996.tb04630.x, 1996.

Adams, Jeanne C. and Brainerd, Walter S. and Martin, Jeanne T. and Smith, Brian T. and Wagener, Jerrold L.: Fortran 90 Handbook: Complete ANSI / ISO Reference, Intertext Publications, Mc Graw-Hill Book Company, New York, USA, 1992.

Alvin T. Bleak: Disappearance of Plant Material Under a Winter Snow Cover, Ecology, 51, 915–917, http://www.jstor.org/stable/1933989, 1970.

Asman, Willem A. H. and Sutton, Mark A. and Schjørring, J. K.: Ammonia: emission, atmospheric transport and deposition, New Phytologist, 139, 27–48, https://doi.org/10.1046/j.1469-8137.1998.00180.x, https://nph.onlinelibrary.wiley.com/doi/abs/10.1046/j.1469-8137.1998.00180.x, 1998.

Butterbach-Bahl, K. and Gasche, R. and Breuer, L. and Papen, H.: Fluxes of NO and N2O from temperate forest soils: impact of forest type, N deposition and of liming on the NO and N2O emissions, Nutrient Cycling in Agroecosystems, 48, 79–90, https://doi.org/10.1023/a:1009785521107, https://doi.org/10.1023/A:1009785521107, 1997.

Clarke, N. and Zlindra, D. and Ulrich, E. and Mosello, R. and Derome, J. and Derome, K. and König, N. and Lövblad, G. and Draaijers, G. P. J. and Hansen, K. and Thimonier, A. and Waldner, P.: Manual on methods and criteria for harmonized sampling, assessment, monitoring and analysis of the effects of air pollution on forests, chap. XIV: Sampling and Analysis of Deposition, pp. 1–65, UNECE, ICP Forests, Hamburg, http://www.icp-forests.org/Manual.htm, 2010.

de Vries, W. and Reinds, G. J. and Vel, E.: Intensive monitoring of forest ecosystems in Europe: 2: Atmospheric deposition and its impacts on soil solution chemistry, Forest Ecology and Management, 174, 97–115, https://doi.org/10.1016/S0378-1127(02)00030-0, http://www.sciencedirect.com/science/article/pii/S0378112702000300, 2003.

Draaijers, G. P. J. and Erisman, J. W.: A canopy budget model to assess atmospheric deposition from throughfall measurements, Water, Air, and Soil Pollution, 85, 2253–2258, https://doi.org/10.1007/BF01186169, https://doi.org/10.1007/BF01186169, 1995.

Emberson, L. D. and Ashmore, M. R. and Cambridge, H. M. and Simpson, D. and Tuovinen, J. P.: Modelling stomatal ozone flux across Europe, Environmental Pollution, 109, 403–13, https://doi.org/10.1016/S0269-7491(00)00043-9, http://www.sciencedirect.com/science/article/pii/S0269749100000439, 2000.

Ferm, Martin: Atmospheric ammonia and ammonium transport in Europe and critical loads: a review, Nutrient Cycling in Agroecosystems, 51, 5–17, https://doi.org/10.1023/A:1009780030477, https://link.springer.com/article/10.1023/A:1009780030477, 1998.

Foltýnová, Lenka and Fischer, Milan and McGloin, Ryan Patrick: Recommendations for gap-filling eddy covariance latent heat flux measurements using marginal distribution sampling, Theoretical and Applied Climatology, 139, 677–688, https://doi.org/10.1007/s00704-019-02975-w, https://doi.org/10.1007/s00704-019-02975-w, 2020.

Ge, X. and Schaap, M. and Kranenburg, R. and Segers, A. and Reinds, G. J. and Kros, H. and de Vries, W.: Modeling Atmospheric Ammonia using Agricultural Emissions with Improved Spatial Variability and Temporal Dynamics, Atmospheric Chemistry and Physics Discussions, 2020, 1–51, https://doi.org/10.5194/acp-2019-979, https://acp.copernicus.org/preprints/acp-2019-979/, 2020.

Hendriks, C. and Kranenburg, R. and Kuenen, J. J. P. and Van den Bril, B. and Verguts, V. and Schaap, M.: Ammonia emission time profiles based on manure transport data improve ammonia modelling across north western Europe, Atmospheric Environment, 131, 83–96, https://doi.org/10.1016/j.atmosenv.2016.01.043, http://www.sciencedirect.com/science/article/pii/S1352231016300668, 2016.

Inouye, D.W.: The ecological and evolutionary significance of frost in the context of climate change, Ecology Letters, 3, 457–463, https://doi.org/10.1046/j.1461-0248.2000.00165.x, https://onlinelibrary.wiley.com/doi/abs/10.1046/j.1461-0248.2000.00165.x, 2000.

J. A. van Jaarsveld: The Operational Priority Substances model. Description and validation of OPS-Pro 4.1., RIVM, Bilthoven, Report 500045001, 2004.

Kim, Yeonuk and Johnson, Mark S. and Knox, Sara H. and Black, T. Andrew and Dalmagro, Higo J. and Kang, Minseok and Kim, Joon and Baldocchi, Dennis: Gap-filling approaches for eddy covariance methane fluxes: A comparison of three machine learning algorithms and a traditional method with principal component analysis, Global Change Biology, 26, 1499–1518, https://doi.org/10.1111/gcb.14845, https://onlinelibrary.wiley.com/doi/abs/10.1111/gcb.14845, 2020.

Loubet, Benjamin and Asman, Willem A.H. and Theobald, Mark and Hertel, Ole and Tang, Sim and Robin, Paul and Hassouna, Mélynda and Dämmgen, Ulrich and Génermont, Sophie and Cellier, Pierre and Sutton, Mark: Ammonia Deposition Near Hot Spots: Processes, Models and Monitoring Methods, pp. 205–267, https://doi.org/10.1007/978-1-4020-9121-6_15, 2009.

Manders, Astrid M. M. and Builtjes, Peter J. H. and Curier, Lyana and Denier van der Gon, Hugo A. C. and Hendriks, Carlijn and Jonkers, Sander and Kranenburg, Richard and Kuenen, J. J. P., Segers, A. J., Timmermans, R. M. A., Visschedijk, A. J. H., Wichink Kruit, R. J., van Pul, W. A. J., Sauter, F. J., van der Swaluw, E., Swart, D. P. J., Douros, J., Eskes, H., van Meijgaard, E., van Ulft, B., van Velthoven, P., Banzhaf, S., Mues, A. C., Stern, R., Fu, G., Lu, S., Heemink, A., van Velzen, N., and Schaap, M.: Curriculum vitae of the LOTOS–EUROS (v2.0) chemistry transport model, Geoscientific Model Development, 10, 4145–4173, https://doi.org/10.5194/gmd-10-4145-2017, https://www.geosci-model-dev.net/10/4145/2017/, 2017.

Meixner, F. X.: Surface exchange of odd nitrogen oxides, Nova Acta Leopoldina, 70, 299–348, 1994.

Rosenkranz, P. and Brüggemann, N. and Papen, H. and Xu, Z. and Seufert, G. and Butterbach-Bahl, K.: N_2O, NO and CH_4 exchange, and microbial N turnover over a Mediterranean pine forest soil, Biogeosciences, 3, 121–133, https://doi.org/10.5194/bg-3-121-2006, https://www.biogeosciences.net/3/121/2006/, 2006.

Schaap, M. and Timmermans, R. M. A. and Roemer, M. and Boersen, G. A. C. and Builtjes, P. J. H. and Sauter, F. J. and Velders, G. J. M. and Beck, J. P.: The LOTOS-EUROS model: description, validation and latest developments, International Journal of Environment and Pollution, 32, 270–290, https://doi.org/10.1504/Ijep.2008.017106, 2008.

Schaap, M. and Wichink Kruit, R. and Hendriks, C. and Kranenburg, R. and Segers, A. and Builtjes, P. and Banzhaf, S.: Modelling and assessment of acidifying and eutrophying atmospheric deposition to terrestrial ecosystems (PINETI-2): Part I: Atmospheric deposition to German natural and semi-natural ecosystems during 2009, 2010 and 2011, technical report, Umweltbundesamt, Dessau-Roßlau, Germany, https://www.umweltbundesamt.de/sites/default/files/medien/1410/publikationen/2017-08-15_texte_62-2017_pineti2-teil1.pdf, 2017.

Schrader, F. and Schaap, M. and Zöll, U. and Kranenburg, R. and Brümmer, C.: The hidden cost of using low-resolution concentration data in the estimation of NH_3 dry deposition fluxes, Scientific Reports, 8, 969, https://doi.org/10.1038/s41598-017-18021-6, https://www.ncbi.nlm.nih.gov/pubmed/29343777, 2018.

Schrader, Frederik and Erisman, Jan Willem and Brümmer, Christian: Towards a coupled paradigm of NH3-CO2 biosphere-atmosphere exchange modelling, Global Change Biology, https://doi.org/10.1111/geb.15184, https://onlinelibrary.wiley.com/doi/abs/10.1111/gcb.15184, 2020.

Staelens, J. and Houle, D.and De Schrijver, A. and Neirynck, J. and Verheyen, K.: Calculating Dry Deposition and Canopy Exchange with the Canopy Budget Model: Review of Assumptions and Application to Two Deciduous Forests, Water, Air, and Soil Pollution, 191, 149–169, https://doi.org/10.1007/s11270-008-9614-2, https://doi.org/10.1007/s11270-008-9614-2, 2008.

T. R. Moore: Winter-Time Litter Decomposition in A Subarctic Woodland, Arctic and Alpine Research, 15, 413–418, https://doi.org/10.1080/00040851.1983.12004366, https://www.tandfonline.com/doi/abs/10.1080/00040851.1983.12004366, 1983.

Taylor, Barry and Jones, H.: Litter decomposition under snow cover in a balsam fir forest, Canadian Journal of Botany, 68, 112–120, https://doi.org/10.1139/b90-016, 1990.

van der Graaf, S. C. and Kranenburg, R. and Segers, A. J. and Schaap, M. and Erisman, J. W.: Satellite-derived leaf area index and roughness length information for surface–atmosphere exchange modelling: a case study for reactive nitrogen deposition in north-western Europe using LOTOS-EUROS v2.0, Geoscientific Model Development, 13, 2451–2474, https://doi.org/10.5194/gmd-13-2451-2020, https://www.geosci-model-dev.net/13/2451/2020/, 2020.

Van Pul, W. A. J. and Jacobs, A. F. G.: The conductance of a maize crop and the underlying soil to ozone under various environmental conditions, Boundary-Layer Meteorology, 69, 83–99, https://doi.org/10.1007/BF00713296, https://doi.org/10.1007/BF00713296, 1994.

VDI: VDI-Guideline 3782 Part 5: Environmental meteorology – Atmospheric dispersion models – Deposition parameters, Tech. rep., Verein Deutscher Ingenieure, Düsseldorf, DE, 2006.

Vogt, Kristiina A. and Grier, Charles C. and Meier, Calvin E. and Keyes, Michael R.: Organic Matter and Nutrient Dynamics in Forest Floors of Young and Mature Abies amabilis Stands in Western Washington, as Affected by Fine-Root Input, Ecological Monographs, 53, 139–157, https://doi.org/10.2307/1942492, https://esajournals.onlinelibrary.wiley.com/doi/abs/10.2307/1942492, 1983.

Wang, W. and Ganzeveld, L. and Rossabi, S. and Hueber, J. and Helmig, D.: Measurement report: Leaf-scale gas exchange of atmospheric reactive trace species (NO_2, NO, O_3) at a northern hardwood forest in Michigan, Atmospheric Chemistry and Physics Discussions, 2020, 1–28, https://doi.org/10.5194/acp-2020-149, https://www.atmos-chem-phys-discuss.net/acp-2020-149/, in review, 2020.

Wichink Kruit, R. J. and Schaap, M. and Sauter, F. J. and van Zanten, M. C. and van Pul, W. A. J.: Modeling the distribution of ammonia across Europe including bi-directional surface–atmosphere exchange, Biogeosciences, 9, 5261–5277, https://doi.org/10.5194/bg-9-5261-2012, 2012.

Wutzler, T. and Lucas-Moffat, A. and Migliavacca, M. and Knauer, J. and Sickel, K. and Šigut, L. and Menzer, O. and Reichstein, M.: Basic and extensible post-processing of eddy covariance flux data with REddyProc, Biogeosciences, 15, 5015–5030, https://doi.org/10.5194/bg-15-5015-2018, https://www.biogeosciences.net/15/5015/2018/, 2018.

Delany, A. C., Fitzjarrald, D. R., Lenschow, D. H., Pearson, R., Wendel, G. J., and Woodrufl, B.: Direct measurements of nitrogen oxides and ozone fluxes over grassland, Journal of Atmospheric Chemistry, 4, 429–444, https://doi.org/10.1007/BF00053844, https://doi.org/10.1007/BF00053844, 1986.

Delaria, E. R., Vieira, M., Cremieux, J., and Cohen, R. C.: Measurements of NO and NO_2 exchange between the atmosphere and *Quercus agrifolia*, Atmospheric Chemistry and Physics, 18, 14 161–14 173, https://doi.org/10.5194/acp-18-14161-2018, https://www.atmos-chem-phys.net/18/14161/2018/, 2018.

Erisman, J. W., Van Pul, A., and Wyers, P.: Parametrization of surface resistance for the quantification of atmospheric deposition of acidifying pollutants and ozone, Atmospheric Environment, 28, 2595–2607, https://doi.org/10.1016/1352-2310(94)90433-2, http://www.sciencedirect.com/science/article/pii/1352231094904332, 1994.

Erisman, J. W., Galloway, J. N., Seitzinger, S., Bleeker, A., Dise, N. B., Petrescu, A. M., Leach, A. M., and de Vries, W.: Consequences of human modification of the global nitrogen cycle, Philosophical Transactions of the Royal Society London B: Biological Sciences, 368, 20130 116, https://doi.org/10.1098/rstb.2013.0116, https://royalsocietypublishing.org/doi/abs/10.1098/rstb.2013.0116, 2013.

Eugster, W. and Hesterberg, R.: Transfer resistances of NO_2 determined from eddy correlation flux measurements over a litter meadow at a rural site on the swiss plateau, Atmospheric Environment, 30, 307–311, https://doi.org/10.1016/1352-2310(95)00418-1, http://www.sciencedirect.com/science/article/pii/1352231095004181, 1996.

Falge, E., Baldocchi, D., Olson, R., Anthoni, P., Aubinet, M., Bernhofer, C., Burba, G., Ceulemans, R., Clement, R., Dolman, H., Granier, A., Gross, P., Grünwald, T., Hollinger, D., Jensen, N.-O., Katul, G., Keronen, P., Kowalski, A., Lai, C. T., Law, B. E., Meyers, T., Moncrieff, J., Moors, E., Munger, J., Pilegaard, K., Üllar Rannik, Rebmann, C., Suyker, A., Tenhunen, J., Tu, K., Verma, S., Vesala, T., Wilson, K., and Wofsy, S.: Gap filling strategies for defensible annual sums of net ecosystem exchange, Agricultural and Forest Meteorology, 107, 43–69, https://doi.org/10.1016/S0168-1923(00)00225-2, http://www.sciencedirect.com/science/article/pii/S0168192300002252, 2001.

Famulari, D., Fowler, D., Hargreaves, K., Milford, C., Nemitz, E., Sutton, M. A., and Weston, K.: Measuring Eddy Covariance Fluxes of Ammonia Using Tunable Diode Laser Absorption Spectroscopy, Water, Air, & Soil Pollution: Focus, 4, 151–158, https://doi.org/10.1007/s11267-004-3025-1, http://link.springer.com/10.1007/s11267-004-3025-1, 2004.

Farmer, D. K. and Cohen, R. C.: Observations of HNO_3, Σ AN, Σ PN and NO_2 fluxes: evidence for rapid HO_x chemistry within a pine forest canopy, Atmospheric Chemistry and Physics, 8, 3899–3917, https://doi.org/10.5194/acp-8-3899-2008, https://www.atmos-chem-phys.net/8/3899/2008/, 2008.

Farmer, D. K., Wooldridge, P. J., and Cohen, R. C.: Application of thermal-dissociation laser induced fluorescence (TD-LIF) to measurement of HNO_3, Σ alkyl nitrates, Σ peroxy nitrates, and NO_2 fluxes using eddy covariance, Atmospheric Chemistry and Physics, 6, 3471–3486, https://doi.org/10.5194/acp-6-3471-2006, https://www.atmos-chem-phys.net/6/3471/2006/, 2006.

Farmer, D. K., Kimmel, J. R., Phillips, G., Docherty, K. S., Worsnop, D. R., Sueper, D., Nemitz, E., and Jimenez, J. L.: Eddy covariance measurements with high-resolution time-of-flight aerosol mass spectrometry: a new approach to chemically resolved aerosol fluxes, Atmospheric Measurement Techniques, 4, 1275–1289, https://doi.org/10.5194/amt-4-1275-2011, https://www.atmos-meas-tech.net/4/1275/2011/, 2011.

Ferrara, R. M., Loubet, B., Di Tommasi, P., Bertolini, T., Magliulo, V., Cellier, P., Eugster, W., and Rana, G.: Eddy covariance measurement of ammonia fluxes: Comparison of high frequency correction methodologies, Agricultural and Forest Meteorology, 158-159, 30–42, https://doi.org/10.1016/j.agrformet.2012.02.001, https://doi.org/10.1016/j.agrformet.2012.02.001, 2012.

Finkelstein, P. L. and Sims, P. F.: Sampling error in eddy correlation flux measurements, Journal of Geophysical Research: Atmospheres, 106, 3503–3509, https://doi.org/10.1029/2000JD900731, https://agupubs.onlinelibrary.wiley.com/doi/abs/10.1029/2000JD900731, 2001.

Flechard, C. R., Nemitz, E., Smith, R. I., Fowler, D., Vermeulen, A. T., Bleeker, A., Erisman, J. W., Simpson, D., Zhang, L., Tang, Y. S., and Sutton, M. A.: Dry deposition of reactive nitrogen to European ecosystems: a comparison of inferential models across the NitroEurope network, Atmospheric Chemistry and Physics, 11, 2703–2728, https://doi.org/10.5194/acp-11-2703-2011, 2011.

Flechard, C. R., Massad, R. S., Loubet, B., Personne, E., Simpson, D., Bash, J. O., Cooter, E. J., Nemitz, E., and Sutton, M. A.: Advances in understanding, models and parameterizations of biosphere-atmosphere ammonia exchange, Biogeosciences, 10, 5183–5225, https://doi.org/10.5194/bg-10-5183-2013, https://www.biogeosciences.net/10/5183/2013/, 2013.

Flechard, C. R., Ibrom, A., Skiba, U. M., de Vries, W., van Oijen, M., Cameron, D. R., Dise, N. B., Korhonen, J. F. J., Buchmann, N., Legout, A., Simpson, D., Sanz, M. J., Aubinet, M., Loustau, D., Montagnani, L., Neirynck, J., Janssens, I. A., Pihlatie, M., Kiese, R., Siemens, J., Francez, A.-J., Augustin, J., Varlagin, A., Olejnik, J., Juszczak, R., Aurela, M., Berveiller, D., Chojnicki, B. H., Dämmgen, U., Delpierre, N., Djuricic, V., Drewer, J., Dufrêne, E., Eugster, W., Fauvel, Y., Fowler, D., Frumau, A., Granier, A., Gross, P., Hamon, Y., Helfter, C., Hensen, A., Horváth, L., Kitzler, B., Kruijt, B., Kutsch, W. L., Lobo-do Vale, R., Lohila, A., Longdoz, B., Marek, M. V., Matteucci, G., Mitosinkova, M., Moreaux, V., Neftel, A., Ourcival, J.-M., Pilegaard, K., Pita, G., Sanz, F., Schjoerring, J. K., Sebastià,

M.-T., Tang, Y. S., Uggerud, H., Urbaniak, M., van Dijk, N., Vesala, T., Vidic, S., Vincke, C., Weidinger, T., Zechmeister-Boltenstern, S., Butterbach-Bahl, K., Nemitz, E., and Sutton, M. A.: Carbon–nitrogen interactions in European forests and semi-natural vegetation – Part 1: Fluxes and budgets of carbon, nitrogen and greenhouse gases from ecosystem monitoring and modelling, Biogeosciences, 17, 1583–1620, https://doi.org/10.5194/bg-17-1583-2020, https://www.biogeosciences.net/17/1583/2020/, 2020.

Galloway, J. N., Aber, J. D., Erisman, J. W., Seitzinger, S. P., Howarth, R. W., Cowling, E. B., and Cosby, B. J.: The Nitrogen Cascade, BioScience, 53, 341–356, https://doi.org/10.1641/0006-3568(2003)053[0341:TNC]2.0.CO;2, https://doi.org/10.1641/0006-3568(2003)053[0341:TNC]2.0.CO;2, 2003.

Garland, J. A.: The Dry Deposition of Sulphur Dioxide to Land and Water Surfaces, Proceedings of the Royal Society A: Mathematical, Physical and Engineering Sciences, 354, 245–268, https://doi.org/10.1098/rspa.1977.0066, https://royalsocietypublishing.org/doi/abs/10.1098/rspa.1977.0066, 1977.

Geddes, J. A. and Murphy, J. G.: Observations of reactive nitrogen oxide fluxes by eddy covariance above two midlatitude North American mixed hardwood forests, Atmospheric Chemistry and Physics, 14, 2939–2957, https://doi.org/10.5194/acp-14-2939-2014, https://acp.copernicus.org/articles/14/2939/2014/, 2014.

Hansen, K., Pryor, S. C., Boegh, E., Hornsby, K. E., Jensen, B., and Sorensen, L. L.: Background concentrations and fluxes of atmospheric ammonia over a deciduous forest, Agricultural and Forest Meteorology, 214-215, 380–392, https://doi.org/10.1016/j.agrformet.2015.09.004, http://www.sciencedirect.com/science/article/pii/S0168192315007091, 2015.

Högberg, P.: Nitrogen impacts on forest carbon, Nature, 447, 781–782, https://doi.org/10.1038/447781a, https://doi.org/10.1038/447781a, 2007.

Horii, C. V., Munger, J. W., Wofsy, S. C., Zahniser, M., Nelson, D., and McManus, J. B.: Fluxes of nitrogen oxides over a temperate deciduous forest, Journal of Geophysical Research: Atmospheres, 109, https://doi.org/10.1029/2003JD004326, https://agupubs.onlinelibrary.wiley.com/doi/abs/10.1029/2003JD004326, 2004.

Horii, C. V., Munger, J. W., Wofsy, S. C., Zahniser, M., Nelson, D., and McManus, J. B.: Atmospheric reactive nitrogen concentration and flux budgets at a Northeastern US forest site, Agricultural and Forest Meteorology, 136, 159–174, https://doi.org/10.1016/j.agrformet.2006.03.005, http://www.sciencedirect.com/science/article/pii/S0168192306000888, 2006.

Jarraud, M.: Guide to meteorological instruments and methods of observation (WMO-No. 8), World Meteorological Organization, Geneva, Switzerland, 2008.

Jensen, N. and Hummelshøj, P.: Derivation of canopy resistance for water vapor fluxes over a spruce forest, using a new technique for the viscous sublayer resistance (correction to vol. 73, p. 339, 1995), Agricultural and Forest Meteorology, 85, 289, https://doi.org/10.1016/S0168-1923(97)00024-5, http://www.sciencedirect.com/science/article/pii/S0168192397000245, 1997.

Jensen, N. O. and Hummelshøj, P.: Derivation of canopy resistance for water-vapor fluxes over a spruce forest, using a new technique for the viscous sublayer resistance, Agricultural and Forest Meteorology, 73, 339–352, https://doi.org/10.1016/0168-1923(94)05083-I, http://www.sciencedirect.com/science/article/pii/016819239405083I, 1995.

Kolle, O. and Rebmann, C.: EddySoft Documentation of a Software Package to Acquire and Process Eddy Covariance Data, techreport, MPI-BGC, https://repository.publisso.de/resource/frl:4414276-1/data, 2007.

Krupa, S. V.: Effects of atmospheric ammonia (NH_3) on terrestrial vegetation: a review, Environmental Pollution, 124, 179–221, https://doi.org/10.1016/S0269-7491(02)00434-7, http://www.sciencedirect.com/science/article/pii/S0269749102004347, 2003.

Langford, B., Acton, W., Ammann, C., Valach, A., and Nemitz, E.: Eddy-covariance data with low signal-to-noise ratio: time-lag determination, uncertainties and limit of detection, Atmospheric Measurement Techniques, 8, 4197–4213, https://doi.org/10.5194/amt-8-4197-2015, https://www.atmos-meas-tech.net/8/4197/2015/, 2015.

Li, Y., Aneja, V. P., Arya, S. P., Rickman, J., Brittig, J., Roelle, P., and Kim, D. S.: Nitric oxide emission from intensively managed agricultural soil in North Carolina, Journal of Geophysical Research: Atmospheres, 104, 26 115–26 123, https://doi.org/10.1029/1999JD900336, https://agupubs.onlinelibrary.wiley.com/doi/abs/10.1029/1999JD900336, 1997.

LTER: Long Term Ecological Research (LTER) network, https://deims.org/993ed2fc-1cb0-4810-a619-8bcf78b6ecee, last access: 17 June 2020, 2020.

Magnani, F., Mencuccini, M., Borghetti, M., Berbigier, P., Berninger, F., Delzon, S., Grelle, A., Hari, P., Jarvis, P. G., Kolari, P., Kowalski, A. S., Lankreijer, H., Law, B. E., Lindroth, A., Loustau, D., Manca, G., Moncrieff, J. B., Rayment, M., Tedeschi, V., Valentini, R., and Grace, J.: The human footprint in the carbon cycle of temperate and boreal forests, Nature, 447, 848–50, https://doi.org/10.1038/nature05847, https://www.ncbi.nlm.nih.gov/pubmed/17568744, 2007.

Marx, O., Brümmer, C., Ammann, C., Wolff, V., and Freibauer, A.: TRANC – a novel fast-response converter to measure total reactive atmospheric nitrogen, Atmospheric Measurement Techniques, 5, 1045–1057, https://doi.org/10.5194/amt-5-1045-2012, http://www.atmos-meas-tech.net/5/1045/2012/, 2012.

Massad, R. S., Nemitz, E., and Sutton, M. A.: Review and parameterisation of bi-directional ammonia exchange between vegetation and the atmosphere, Atmospheric Chemistry and Physics, 10, 10 359–10 386, https://doi.org/10.5194/acp-10-10359-2010, https://www.atmos-chem-phys.net/10/10359/2010/, 2010.

Mauder, M. and Foken, T.: Impact of post-field data processing on eddy covariance flux estimates and energy balance closure, Meteorologische Zeitschrift, 15, 597–609, https://doi.org/10.1127/0941-2948/2006/0167, 2006.

Milford, C., Hargreaves, K. J., Sutton, M. A., Loubet, B., and Cellier, P.: Fluxes of NH_3 and CO_2 over upland moorland in the vicinity of agricultural land, Journal of Geophysical Research: Atmospheres, 106, 24 169–24 181, https://doi.org/10.1029/2001jd900082, http://doi.wiley.com/10.1029/2001JD900082, 2001.

Min, K.-E., Pusede, S. E., Browne, E. C., LaFranchi, B. W., Wooldridge, P. J., and Cohen, R. C.: Eddy covariance fluxes and vertical concentration gradient measurements of NO and NO_2 over a ponderosa pine ecosystem: observational evidence for within-canopy chemical removal of NO_x, Atmospheric Chemistry and Physics, 14, 5495–5512, https://doi.org/10.5194/acp-14-5495-2014, http://www.atmos-chem-phys.net/14/5495/2014/, 2014.

Moffat, A. M., Papale, D., Reichstein, M., Hollinger, D. Y., Richardson, A. D., Barr, A. G., Beckstein, C., Braswell, B. H., Churkina, G., Desai, A. R., Falge, E., Gove, J. H., Heimann, M., Hui, D. F., Jarvis, A. J., Kattge, J., Noormets, A., and Stauch, V. J.: Comprehensive comparison of gap-filling techniques for eddy covariance net carbon fluxes, Agricultural and Forest Meteorology, 147, 209–232, https://doi.org/10.1016/j.agrformet.2007.08.011, https://doi.org/10.1016/j.agrformet.2007.08.011, 2007.

Moncrieff, J., Clement, R., Finnigan, J., and Meyers, T.: Averaging, Detrending, and Filtering of Eddy Covariance Time Series, pp. 7–31, Kluwer Academic, Dordrecht, https://doi.org/10.1007/1-4020-2265-4_2, https://doi.org/10.1007/1-4020-2265-4_2, 2004.

Moravek, A., Singh, S., Pattey, E., Pelletier, L., and Murphy, J. G.: Measurements and quality control of ammonia eddy covariance fluxes: A new strategy for high frequency attenuation correction, Atmospheric Measurement Techniques, 12, 6059–6078, https://doi.org/10.5194/amt-12-6059-2019, https://www.atmos-meas-tech.net/12/6059/2019/, 2019.

Munger, J. W., Wofsy, S. C., Bakwin, P. S., Fan, S. M., Goulden, M. L., Daube, B. C., Goldstein, A. H., Moore, K. E., and Fitzjarrald, D. R.: Atmospheric deposition of reactive nitrogen oxides and ozone in a temperate deciduous forest and a subarctic woodland: 1.

Measurements and mechanisms, Journal of Geophysical Research-Atmospheres, 101, 12 639–12 657, https://doi.org/10.1029/96JD00230, https://agupubs.onlinelibrary.wiley.com/doi/abs/10.1029/96JD00230, 1996.

Nemitz, E., Sutton, M. A., Schjoerring, J. K., Husted, S., and Wyers, G. P.: Resistance modelling of ammonia exchange over oilseed rape, Agricultural and Forest Meteorology, 105, 405–425, https://doi.org/10.1016/S0168-1923(00)00206-9, http://www.sciencedirect.com/science/article/pii/S0168192300002069, 2000.

Nemitz, E., Milford, C., and Sutton, M. A.: A two-layer canopy compensation point model for describing bi-directional biosphere-atmosphere exchange of ammonia, Quarterly Journal of the Royal Meteorological Society, 127, 815–833, https://doi.org/10.1002/qj.49712757306, https://rmets.onlinelibrary.wiley.com/doi/abs/10.1002/qj.49712757306, 2001.

Nemitz, E., Sutton, M. A., Wyers, G. P., and Jongejan, P. A. C.: Gas-particle interactions above a Dutch heathland: I. Surface exchange fluxes of NH_3, SO_2, HNO_3 and HCl, Atmospheric Chemistry and Physics, 4, 989–1005, https://doi.org/10.5194/acp-4-989-2004, https://www.atmos-chem-phys.net/4/989/2004/, 2004.

Nemitz, E., Jimenez, J. L., Huffman, J. A., Ulbrich, I. M., Canagaratna, M. R., Worsnop, D. R., and Guenther, A. B.: An Eddy-Covariance System for the Measurement of Surface/Atmosphere Exchange Fluxes of Submicron Aerosol Chemical Species—First Application Above an Urban Areas, Aerosol Science and Technology, 42, 636–657, https://doi.org/10.1080/02786820802227352, https://doi.org/10.1080/02786820802227352, 2008.

Paulson, C. A.: The Mathematical Representation of Wind Speed and Temperature Profiles in the Unstable Atmospheric Surface Layer, Journal of Applied Meteorology, 9, 857–861, https://doi.org/10.1175/1520-0450(1970)009<0857:Tmrows>2.0.Co;2, 1970.

Reichstein, M., Falge, E., Baldocchi, D., Papale, D., Aubinet, M., Berbigier, P., Bernhofer, C., Buchmann, N., Gilmanov, T., Granier, A., Grünwald, T., Havránková, K., Ilvesniemi, H., Janous, D., Knohl, A., Laurila, T., Lohila, A., Loustau, D., Matteucci, G., Meyers, T., Miglietta, F., Ourcival, J.-M., Pumpanen, J., Rambal, S., Rotenberg, E., Sanz, M., Tenhunen, J., Seufert, G., Vaccari, F., Vesala, T., Yakir, D., and Valentini, R.: On the separation of net ecosystem exchange into assimilation and ecosystem respiration: review and improved algorithm, Global Change Biology, 11, 1424–1439, https://doi.org/10.1111/j.1365-2486.2005.001002.x, https://onlinelibrary.wiley.com/doi/abs/10.1111/j.1365-2486.2005.001002.x, 2005.

Rondon, A., Johansson, C., and Granat, L.: Dry Deposition of Nitrogen-Dioxide and Ozone to Coniferous Forests, Journal of Geophysical Research-Atmospheres, 98, 5159–5172, https://doi.org/Doi 10.1029/92jd02335, <GotoISI>://WOS:A1993KU06900024, 1993.

Rummel, U., Ammann, C., Gut, A., Meixner, F. X., and Andreae, M. O.: Eddy covariance measurements of nitric oxide flux within an Amazonian rain forest, Journal of Geophysical Research-Atmospheres, 107, LBA 17–1–LBA 17–9, https://doi.org/10.1029/2001JD000520, https://doi.org/10.1029/2001JD000520, 2002.

Schrader, F. and Brümmer, C.: Land Use Specific Ammonia Deposition Velocities: a Review of Recent Studies (2004–2013), Water, Air, and Soil Pollution, 225, 2114, https://doi.org/10.1007/s11270-014-2114-7, https://doi.org/10.1007/s11270-014-2114-7, 2014.

Schrader, F., Brümmer, C., Flechard, C. R., Wichink Kruit, R. J., van Zanten, M. C., Zöll, U., Hensen, A., and Erisman, J. W.: Non-stomatal exchange in ammonia dry deposition models: comparison of two state-of-the-art approaches, Atmospheric Chemistry and Physics, 16, 13 417–13 430, https://doi.org/10.5194/acp-16-13417-2016, https://www.atmos-chem-phys.net/16/13417/2016/, 2016.

Sparks, J. P., Monson, R. K., Sparks, K. L., and Lerdau, M.: Leaf uptake of nitrogen dioxide (NO2) in a tropical wet forest: implications for tropospheric chemistry, Oecologia, 127, 214–221, https://doi.org/10.1007/s004420000594, https://www.ncbi.nlm.nih.gov/pubmed/24577652, 2001.

Stella, P., Kortner, M., Ammann, C., Foken, T., Meixner, F. X., and Trebs, I.: Measurements of nitrogen oxides and ozone fluxes by eddy covariance at a meadow: evidence for an internal leaf resistance to NO_2, Biogeosciences, 10, 5997–6017, https://doi.org/10.5194/bg-10-5997-2013, http://www.biogeosciences.net/10/5997/2013/, 2013.

Sutton, M. A. and Fowler, D.: A Model for Inferring Bi-directional Fluxes of Ammonia Over Plant Canopies, in: Proceedings of the WMO conference on the measurement and modelling of atmospheric composition changes including pollutant transport, pp. 179–182, WMO/GAW(Gobal Atmosphere Watch)-91, Geneva, Switzerland, 1993.

Sutton, M. A., Tang, Y. S., Miners, B., and Fowler, D.: A New Diffusion Denuder System for Long-Term, Regional Monitoring of Atmospheric Ammonia and Ammonium, Water, Air and Soil Pollution: Focus, 1, 145–156, https://doi.org/10.1023/a:1013138601753, https://doi.org/10.1023/A:1013138601753, 2001.

Sutton, M. A., Simpson, D., Levy, P. E., Smith, R. I., Reis, S., van Oijen, M., and de Vries, W.: Uncertainties in the relationship between atmospheric nitrogen deposition and forest carbon sequestration, Global Change Biology, 14, 2057–2063, https://doi.org/10.1111/j.1365-2486.2008.01636.x, https://onlinelibrary.wiley.com/doi/abs/10.1111/j.1365-2486.2008.01636.x, 2008.

Sutton, M. A., Howard, C. M., Erisman, J. W., Billen, G., Bleeker, A., Grennfelt, P., van Grinsven, H., and Grizzetti, B., eds.: The European Nitrogen Assessment: sources, effects and policy perspectives, Cambridge University Press, Cambridge, UK, 2011.

Sutton, M. A., Reis, S., Riddick, S. N., Dragosits, U., Nemitz, E., Theobald, M. R., Tang, Y. S., Braban, C. F., Vieno, M., Dore, A. J., Mitchell, R. F., Wanless, S., Daunt, F., Fowler, D., Blackall, T. D., Milford, C., Flechard, C. R., Loubet, B., Massad, R., Cellier, P., Personne, E., Coheur, P. F., Clarisse, L., Van Damme, M., Ngadi, Y., Clerbaux, C., Skjoth, C. A., Geels, C., Hertel, O., Wichink Kruit, R. J., Pinder, R. W., Bash, J. O., Walker, J. T., Simpson, D., Horvath, L., Misselbrook, T. H., Bleeker, A., Dentener, F., and de Vries, W.: Towards a climate-dependent paradigm of ammonia emission and deposition, Philosophical Transactions of the Royal Society of London. Series B.: Biological Sciences, 368, 20130 166, https://doi.org/10.1098/rstb.2013.0166, https://www.ncbi.nlm.nih.gov/pubmed/23713128, 2013.

Tang, Y. S., Simmons, I., van Dijk, N., Di Marco, C., Nemitz, E., Dämmgen, U., Gilke, K., Djuricic, V., Vidic, S., Gliha, Z., Borovecki, D., Mitosinkova, M., Hanssen, J. E., Uggerud, T. H., Sanz, M. J., Sanz, P., Chorda, J. V., Flechard, C. R., Fauvel, Y., Ferm, M., Perrino, C., and Sutton, M. A.: European scale application of atmospheric reactive nitrogen measurements in a low-cost approach to infer dry deposition fluxes, Agriculture, Ecosystems and Environment, 133, 183–195, https://doi.org/10.1016/j.agee.2009.04.027, http://www.sciencedirect.com/science/article/pii/S0167880909001388, 2009.

Tang, Y. S., Flechard, C. R., Dämmgen, U., Vidic, S., Djuricic, V., Mitosinkova, M., Uggerud, H. T., Sanz, M. J., Simmons, I., Dragosits, U., Nemitz, E., Twigg, M., van Dijk, N., Fauvel, Y., Sanz-Sanchez, F., Ferm, M., Perrino, C., Catrambone, M., Leaver, D., Braban, C. F., Cape, J. N., Heal, M. R., and Sutton, M. A.: Pan-European rural atmospheric monitoring network shows dominance of NH_3 gas and NH_4NO_3 aerosol in inorganic pollution load, Atmospheric Chemistry and Physics Discussions, 2020, 1–61, https://doi.org/10.5194/acp-2020-275, https://acp.copernicus.org/preprints/acp-2020-275/, 2020.

Tarnay, L. W., Gertler, A., and Taylor, G. E.: The use of inferential models for estimating nitric acid vapor deposition to semi-arid coniferous forests, Atmospheric Environment, 36, 3277–3287, https://doi.org/10.1016/S1352-2310(02)00303-5, http://www.sciencedirect.com/science/article/pii/S1352231002003035, 2002.

UNECE: International Cooperative Program on Integrated Monitoring of Air pollution Effects on Ecosystems (ICP IM) within the framework of the Geneva Convention on Long-Range Transboundary, http://www.unece.org/env/lrtap/, last access: 17 June 2020, 2020.

Van Oss, R., Duyzer, J., and Wyers, P.: The influence of gas-to-particle conversion on measurements of ammonia exchange over forest, Atmospheric Environment, 32, 465 – 471, https://doi.org/https://doi.org/10.1016/S1352-2310(97)00280-X, http://www.sciencedirect.com/science/article/pii/S135223109700280X, 1998.

van Zanten, M. C., Sauter, F. J., Wichink Kruit, R. J., van Jaarsveld, J. A., and van Pul, W. A. J.: Description of the DEPAC module; Dry deposition modeling with DEPAC_GCN2010, Tech. rep., RIVM, Bilthoven, NL, 2010.

Vickers, D. and Mahrt, L.: Quality Control and Flux Sampling Problems for Tower and Aircraft Data, Journal of Atmospheric and Oceanic Technology, 14, 512–526, https://doi.org/10.1175/1520-0426(1997)014<0512:QCAFSP>2.0.CO;2, http://doi.org/10.1175/1520-0426(1997)014<0512:QCAFSP>2.0.CO;2, 1997.

Webb, E. K.: Profile relationships: The log-linear range, and extension to strong stability, Quarterly Journal of the Royal Meteorological Society, 96, 67–90, https://doi.org/10.1002/qj.49709640708, https://rmets.onlinelibrary.wiley.com/doi/abs/10.1002/qj.49709640708, 1970.

Wentworth, G. R., Murphy, J. G., Benedict, K. B., Bangs, E. J., and Collett Jr, J. L.: The role of dew as a nighttime reservoir and morning source for atmospheric ammonia, Atmospheric Chemistry and Physics Discussions, 16, 1–36, https://doi.org/10.5194/acp-2016-169, http://www.atmos-chem-phys-discuss.net/acp-2016-169/, 2016.

Wesely, M. L.: Parameterization of Surface Resistances to Gaseous Dry Deposition in Regional-Scale Numerical-Models, Atmospheric Environment, 23, 1293–1304, https://doi.org/Doi 10.1016/0004-6981(89)90153-4, http://www.sciencedirect.com/science/article/pii/0004698189901534, 1989.

Whitehead, J. D., Twigg, M., Famulari, D., Nemitz, E., Sutton, M. A., Gallagher, M. W., and Fowler, D.: Evaluation of laser absorption spectroscopic techniques for eddy covariance flux measurements of ammonia, Environ Sci Technol, 42, 2041–6, https://doi.org/10.1021/es071596u, https://www.ncbi.nlm.nih.gov/pubmed/18409634, 2008.

Wichink Kruit, R. J., van Pul, W. A. J., Sauter, F. J., van den Broek, M., Nemitz, E., Sutton, M. A., Krol, M., and Holtslag, A. A. M.: Modeling the surface–atmosphere exchange of ammonia, Atmospheric Environment, 44, 945–957, https://doi.org/10.1016/j.atmosenv.2009.11.049, http://www.sciencedirect.com/science/article/pii/S1352231009010346, 2010.

Wichink Kruit, R. J., Aben, J., de Vries, W., Sauter, F., van der Swaluw, E., van Zanten, M. C., and van Pul, W. A. J.: Modelling trends in ammonia in the Netherlands over the period 1990–2014, Atmospheric Environment, 154, 20–30, https://doi.org/10.1016/j.atmosenv.2017.01.031, https://www.sciencedirect.com/science/article/pii/S1352231017300316, 2017.

Wilczak, J. M., Oncley, S. P., and Stage, S. A.: Sonic Anemometer Tilt Correction Algorithms, Boundary-Layer Meteorology, 99, 127–150, https://doi.org/10.1023/A:1018966204465, https://doi.org/10.1023/A:1018966204465, 2001.

Wintjen, P., Ammann, C., Schrader, F., and Brümmer, C.: Correcting high-frequency losses of reactive nitrogen flux measurements, Atmospheric Measurement Techniques, 13, 2923–2948, https://doi.org/10.5194/amt-13-2923-2020, https://www.atmos-meas-tech.net/13/2923/2020/, 2020.

Wolff, V., Trebs, I., Foken, T., and Meixner, F. X.: Exchange of reactive nitrogen compounds: concentrations and fluxes of total ammonium and total nitrate above a spruce canopy, Biogeosciences, 7, 1729–1744, https://doi.org/10.5194/bg-7-1729-2010, https://www.biogeosciences.net/7/1729/2010/, 2010.

Wyers, G. and Duyzer, J.: Micrometeorological measurement of the dry deposition flux of sulphate and nitrate aerosols to coniferous forest, Atmospheric Environment, 31, 333 – 343, https://doi.org/https://doi.org/10.1016/S1352-2310(96)00188-4, http://www.sciencedirect.com/science/article/pii/S1352231096001884, 1997.

Wyers, G. P. and Erisman, J. W.: Ammonia exchange over coniferous forest, Atmospheric Environment, 32, 441–451, https://doi.org/10.1016/S1352-2310(97)00275-6, http://www.sciencedirect.com/science/article/pii/S1352231097002756, 1998.

Zöll, U., Brümmer, C., Schrader, F., Ammann, C., Ibrom, A., Flechard, C. R., Nelson, D. D., Zahniser, M., and Kutsch, W. L.: Surface–atmosphere exchange of ammonia over peatland using QCL-based eddy-covariance measurements and inferential modeling, At-

mospheric Chemistry and Physics, 16, 11 283–11 299, https://doi.org/10.5194/acp-16-11283-2016, http://www.atmos-chem-phys.net/16/11283/2016/, 2016.

Zöll, U., Lucas-Moffat, A. M., Wintjen, P., Schrader, F., Beudert, B., and Brümmer, C.: Is the biosphere-atmosphere exchange of total reactive nitrogen above forest driven by the same factors as carbon dioxide? An analysis using artificial neural networks, Atmospheric Environment, 206, 108–118, https://doi.org/10.1016/j.atmosenv.2019.02.042, http://www.sciencedirect.com/science/article/pii/S1352231019301463, 2019.